Methods for improved prediction of elastic, electrical and reservoir properties

Erling Hugo Jensen

Dissertation for the degree philosophiae doctor (PhD)

at the University of Bergen

2011

Preface

This thesis is submitted for the Philosophiae Doctor degree in Petroleum Geosciences at the Department of Earth Science, University of Bergen. Financial support for this study has been provided by the Research Council of Norway and Statoil through the PETROMAKS (Programme for the Optimal Management of Petroleum Resources) as a contribution to the project titled "Quantifying the Effects of Sediment Deposition, Compaction and Pore Fluid on Rock Properties and Seismic Signatures". This is a large project resulting from a meeting hosted by the Research Council of Norway in Washing DC on November 2, 2005. It has been a joint project between the University of Oslo, Norwegian Geotechnical Institute, Stanford University, Colorado School of Mines, Statoil and the University of Bergen.

The work presented in this thesis was initiated during the summary 2007 under a four year PhD contract with the University of Bergen. The majority of it was conducted in Bergen and during a six months stay as a visiting researcher at Stanford University in California. Furthermore, I have had occasional visits to the University of Oslo and participated in a laboratory experiment at the Norwegian Geotechnical Institute. In parallel, I have joined international conferences and seminars.

My principal supervisor for this study was Professor Tor Arne Johansen at the University of Bergen and my co-supervisor was Professor Leiv-J. Gelius at the University of Oslo.

The thesis is organised as follows. The overall objective of the study is stated before giving a general introduction to the field. The introduction contains a brief review of the most relevant parameters and rock physics models for this study. Afterwards follows a brief presentation of the inverse rock physics modelling philosophy and examples of possible ways of implementing it. Finally, a summary and the main conclusions of the papers and overall conclusion of the thesis are presented. The five research papers constitute the main scientific contributions and they can be found in their entirety in the appendix.

Erling Hugo Jensen

Bergen, July 21, 2011

"If you wish your merit to be known,

acknowledge that of other people."

Oriental Proverb

Acknowledgements

I would like to thank my supervisors Tor Arne Johansen and Leiv-J. Gelius for encouraging me to take this journey and for giving me both moral support and scientific advice along the way. This task would have been more difficult and less pleasant for me to do without you. You have shown patience and understanding with me for not having a background in geophysics.

I am grateful to those I have collaborated with on the scientific papers; Charlotte F. Andersen, Jack Dvorkin, Leiv-J. Gelius, Tor Arne Johansen, Gary Mavko, Bernardo Moyano and Zhong Wang. It has been very rewarding for me working together with you and learning from you. Hopefully it has been a good experience for you as well. I am also grateful to Magnus Løberg for suggesting and making the first implementation of the Newton-Raphson solver, as well as others who's **MATLAB** code I am using; Peter J. Acklam, Peder Axensten, Guillaume Flandin, Kevin Moerman, Eike Rietsch, RPHtools (Stanford), and Zhong Wang.

My colleagues at the Department of Earth Science at the University of Bergen and Department of Geophysics at Stanford University have also contributed towards me succeeding and filling these years with pleasant memories. Special thanks goes to Remy Agersborg for surviving six months being stuck with me in California, and to the lunch and gaming group for laughing at my jokes and letting me win (almost) all the time.

I would not have made it this far without my family and friends. I am in great debt to my mother Britt H. Jensen for always being there, supporting me and teaching me the value of consistency when it comes to studying. Unfortunately, she passed away in 2006, just before I started my PhD studies. My father, Edgar H. Jensen is of great inspiration to me, and he has challenged me in many discussions helping me develop a critical and rational mind. My sister, Henriette Lindqvist has taught me to be thorough and observant of details as well as defining a standard I can reach for. There are also many others, and I am grateful to you all.

Then there is the latest addition to the family and the pillar of my new family, my wife Francine Mbanza Jensen. You add colour to my life with your positive light-going nature and I am very grateful for you accepting me as I am with all my flaws and sometimes preoccupied mind. Also, I am very thankful that you stand by my side, even the time I left for my six months research stay at Stanford University, which was only one week after us moving in together.

”Writing is not necessarily something to be ashamed of,

but do it in private and wash your hands afterwards.”

Robert Heinlein

US science fiction author (1907 - 1988)

List of papers

Paper 1: Jensen E.H., Andersen C.H. and Johansen T.A. 2011. Estimation of elastic moduli of mixed porous clay composites. *Geophysics* **76**, E9-E20.

Paper 2: Jensen E.H., Gelius L.-J., Wang Z. and Johansen T.A. Consistent joint elastic-electrical differential effective medium modelling of compacting reservoir sandstones. *Submitted to Geophysical Prospecting, June 2011*.

Paper 3: Johansen T.A., Jensen E.H., Mavko G. and Dvorkin, J. Inverse rock physics modelling. *In preparation to be submitted to Geophysics, 2011.*

Paper 4: Moyano B., Jensen E.H. and Johansen T.A. Improved quantitative calibration of rock physics models. *Accepted for publication in Petroleum Geosciences, July 2011.*

Paper 5: Jensen E.H. and Johansen T.A. Conditioning of elastic and electrical parameters for use in reservoir characterization. *In preparation to be submitted to Geophysical Prospecting, 2011.*

”Do not go where the path may lead,

go instead where there is no path and leave a trail.”

Ralph Waldo Emerson

US essayist & poet (1803 - 1882)

Table of Contents

"If a man will begin with certainties, he shall end in doubts;

but if he will be content to begin with doubts he shall end in certainties."

Sir Francis Bacon

English author, courtier, & philosopher (1561 - 1626)

1 Objectives

The main objective of this study has been to develop strategies and methods for improved prediction of reservoir properties, e.g. porosity, lithology and fluid saturation from seismic and electromagnetic data. This should be achieved by:

- Improving methods for estimating the effective rock properties based on existing theories, e.g. by doing consistent joint elastic-electrical modelling.
- Improving methods for more direct, robust and precise reservoir characterization, e.g. through developing the inverse rock physics modelling approach.

Both synthetic and real data should be used to demonstrate the methods and to show that they have a practical application.

"Basic research is what I am doing when I don't know what I am doing."

Wernher von Braun

US (German-born) rocket engineer (1912 - 1977)

2 Introduction

Improved methods for reservoir characterization are crucial for both locating new hydrocarbon resources and maximizing the exploitation of discovered fields. The reservoir conditions are a result of geochemical and geological changes taking place over millions of years. However, during production the reservoir conditions may change rapidly on a geological timescale, and these changes affect the elastic and electrical properties of the rock. Well logging and various remote sensing tools provide us with a vast amount of data. Proper processing and analyses of this data allows us to create a detailed image of the subsurface. However, it is challenging to efficiently combine all the available information in an optimal way to e.g. give accurate and quantitative characterization of a reservoir. This requires a geological and geophysical understanding of processes in the upper regions of the Earth's crust. Also, we need to acquire knowledge about data processing and geophysical modelling. Following is a brief explanation of some basic terminology, properties and theories which are relevant for this study.

2.1 Hydrocarbon reservoirs

When animals and plants die, their organic materials are deposited on the Earth's surface and eventually buried under layers upon layers of sediments. With time, these sediments are exposed to high pressures and temperatures as they are buried deeper, and over a process of millions of years the organic materials are transformed into hydrocarbons. With time, these hydrocarbons migrate towards the surface through tiny cracks and pores in the rock. Rocks with high porosity and connected pore space permit easier flow of hydrocarbons than rocks with lower porosity and permeability. Hence, we can list three main requirements for successfully creating a hydrocarbon reservoir:

1. A source of organic materials which when exposed to the proper conditions over a longer period of time is transformed into hydrocarbons – **a source rock**.
2. A porous rock which can hold the hydrocarbons – **the reservoir**.
3. A ceiling rock with low porosity and permeability trapping the hydrocarbons – **the cap rock**.

When these three conditions are met there is a chance of accumulating enough oil and gas to create a hydrocarbon reservoir.

2.2 Reservoir parameters

Several parameters are used to characterize a reservoir. The most important are the fluid saturation, porosity, permeability, lithology, pressure and temperature.

Fluid saturation denotes the type and relative amount of fluid in a rock, i.e. potential of hydrocarbon resources. This can typically be quantified as a volume fraction satisfying the equation

$$\sum_{n=1}^{N} S_n = 1, \tag{2.2.1}$$

where S_n is the volume fraction of the n-th out of a total of N fluids. We have three main fluid types, namely brine, gas and oil.

Porosity describes the volume fraction of the rock which fluids may occupy, i.e. total reservoir volume. It is the space in a rock not occupied by solid materials. Porosity ϕ is quantified as

$$\phi = \frac{V_{\text{pore}}}{V_{\text{solid}} + V_{\text{pore}}}, \tag{2.2.2}$$

where V_{pore} and V_{solid} are the total volume of the pore space and the solid part of the rock, respectively.

Permeability describes how easily fluid flows through a rock, i.e. potential for extracting the hydrocarbons. Darcy's law (Darcy 1856) is an experimental relation for fluid flow in a porous media given by

$$Q_x = -A\frac{\kappa}{\eta}\frac{\partial P}{\partial x}, \tag{2.2.3}$$

where Q_x is the volumetric fluid flow rate in the x direction, A is the area of the cross section normal to the pressure gradient, κ is the permeability, η is the dynamic viscosity of the fluid and P is the pressure.

Lithology describes the types of minerals forming the rock. It can have an impact on reservoir quality, e.g. in siliciclastic rocks clay can result in reduced permeability. Similar to the fluid saturation, the lithology can be quantified as a volume fraction V_n of the n-th mineral. For a rock composed of N different minerals we have that

$$\sum_{n=1}^{N} V_n = 1. \qquad 2.2.4$$

Pressure and temperature are important for the effective properties of the rock and can induce geochemical processes in the reservoir. The effective pressure P_e is given by

$$P_e = P_c - nP_p, \qquad 2.2.5$$

where P_c and P_p are the confining and pore pressure, respectively, and n is the effective-stress coefficient taking into account structural effects. Typically, temperature increases with depth according to the geothermal gradient, which is approximately 20-30°C per kilometre (Turcotte and Schubert 2002, p.133). However, it can be higher, i.e. close to tectonic plate boundaries.

The reservoir properties change during production. For example, pressure and fluid saturation may change as hydrocarbon is replaced with other fluids. Also, temperature can change in this process if steam injection is used.

2.3 Elastic and electrical rock properties

The effective elastic and electrical rock properties are a result of the individual constituent properties, composition and the physical conditions imposed on it from its surroundings. That is, the pressure, temperature, porosity, lithology and fluid saturation have direct implications on the effective properties of the rock. We often study the average density, bulk and shear moduli, P- and S-wave velocities, Poisson's ratio and conductivity (or resistivity) to characterize a rock.

Average density is defined as the amount of mass within a volume segment. The mass of a rock is the summed mass of each of its constituents. Hence, the average density ρ for N constituents can be expressed as the volume weighted sum of density ρ_n for each constituent

$$\rho = \sum_{n=1}^{N} \rho_n V_n, \qquad 2.3.1$$

where V_n is the volume fraction of the n-th constituent.

Bulk modulus K is a measure of a medium's resistance to change in volume due to a change in pressure. For an isotropic medium it is defined as

$$K = \frac{\Delta P}{\Delta V / V}, \tag{2.3.2}$$

where ΔP is the pressure change resulting in the total volume V being increased or decreased with the value ΔV.

Shear modulus μ expresses the resistance to a shear type deformation, and for an isotropic medium it is given by

$$\mu = \frac{F}{A \tan \gamma}, \tag{2.3.3}$$

where F is the shear force applied to an area A resulting in a shear deformation with angle γ.

The speed with which a wave travels through a medium is for a pressure and shear wave given by the **P-** (V_p) and **S-wave** (V_s) **velocities**, respectively. For an isotropic medium they can be calculated from the density, bulk and shear moduli according to

$$V_p = \sqrt{\frac{K + 4/3\mu}{\rho}}, \tag{2.3.4}$$

$$V_s = \sqrt{\frac{\mu}{\rho}}. \tag{2.3.5}$$

Poisson's ratio for a medium exposed to uniaxial stress is the ratio of the transverse strain to the axial strain. For an isotropic material the Poisson's ratio ν is given by

$$\nu = \frac{3K - 2\mu}{2(3K + \mu)}. \tag{2.3.6}$$

Electric conductivity σ is a measure of how well a material conducts electricity. It is the reciprocal of electric resistivity. For materials behaving according to Ohm's law, we have that

$$\vec{J} = \sigma \vec{E}, \tag{2.3.7}$$

where $\vec{J}$ and $\vec{E}$ are the current density and electric field, respectively.

2.4 Remote sensing of hydrocarbon reservoirs

Hydrocarbon reservoirs are typically found a couple of kilometres under the Earth's surface which in turn can be several hundred meters under the sea surface. Drilling a well is

the only sure way to learn if the reservoir contains hydrocarbons. However, drilling wells are very expensive and we have several remote sensing tools, modelling and processing techniques available to reduce the risk of drilling a so-called dry well (Kearey, Brooks and Hill 2002). The work presented here is associated with two types of remote sensing techniques, namely seismic and marine controlled-source electromagnetic surveys.

In **seismic survey** a source e.g. an airgun, triggers pressure waves which travel through the water column and down into the upper crust of the Earth (Kearey *et al.* 2002). When the energy reaches an interface between layers in the Earth, parts of that energy propagates down into the next layer as transmitted waves and parts of the energy is reflected towards the surface (see Figure 2.1). In case of the wave hitting the interface at an angle, both pressure and shear waves are reflected and transmitted (Figure 2.1b). However, shear waves do not travel through the water column because water has no shear resistance. Therefore, receivers which are towed as streamers just below the sea surface will only record the energy from the reflected pressure waves. Alternatively, receivers can be placed on the seabed to record information about both the shear and pressure waves. In addition to the reflected energy from the subsurface the receivers record the direct wave from the airgun and the water surface reflected signal. Also, multiple arrivals from the same interface are recorded due to the signals being reflected back and forth between interfaces before returning to the surface. Hence, the recorded signal is a superposition of wave-energy containing information from several targets. We use various processing techniques to isolate the part of the signal which we are interested in. Afterwards, velocity models, cross-plotting and inversion can be utilized to estimate and evaluate the properties of the various layers in the subsurface. Typically, the aim is to identify geological formations which are associated with the presence of hydrocarbons. From seismic data it is easier to make predictions of the layers in the subsurface, rather than identifying the actual hydrocarbon resources.

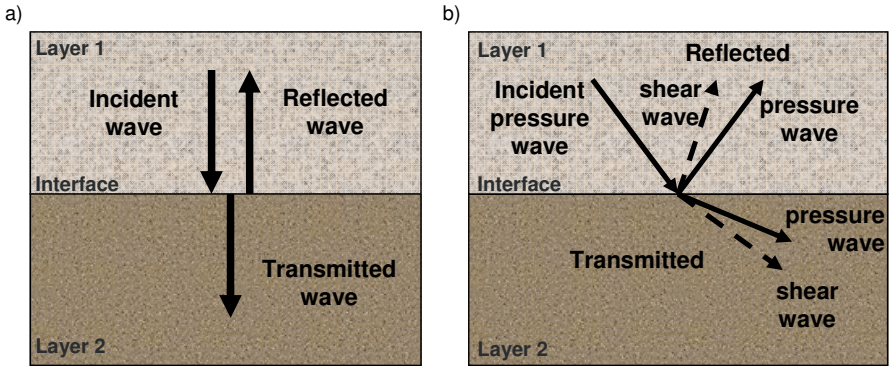

Figure 2.1 Reflected and transmitted waves at a layer interface for an incident wave arriving (a) at a normal angle and (b) at an oblique angle to the interface surface.

Marine controlled-source electromagnetic (CSEM) surveys or seabed logging (Eidesmo et al. 2002; Constable and Srnka 2007) is done in a similar way to seismic acquisition. Several methods exist, but typically a several hundred meters long horizontal electric dipole is towed behind a vessel generating an electric field which propagates down into the Earth (see Figure 2.2). Receivers placed on the seabed record the electric field. When the dipole is aligned with the receivers (inline configuration) refracted energy from a high resistive hydrocarbon reservoir can be recorded. This signal is mixed with the direct and surface-to-air refracted signals, which contains no information about the reservoir. At near offset, contributions from the direct field will dominate, and at far offset it is the surface-to-air refracted field which dominates. Because the electric field attenuates quickly in water and if the water depth is large enough, e.g. larger than 3-400 meters, the response from a hydrocarbon reservoir located at a sufficient depth will dominate at an intermediate offset. Resistivity predictions of the subsurface can be achieved through processing and inverse modelling of the CSEM data. Because brine is conductive and hydrocarbons are insulating CSEM has the potential of being an effective tool in locating hydrocarbon resources. However, it is not equally suited as seismic acquisition to use for mapping the subsurface layers. Hence, it works best when using seismic data to constrain the resistivity response to geological formations.

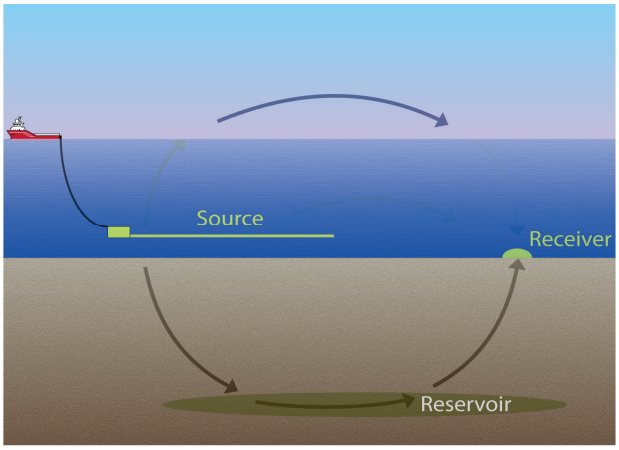

Figure 2.2 Schematics of a marine controlled-source electromagnetic survey (CSEM). (Adapted from Marine CSEM module in GeoCLASS, UniGEO 2011).

2.5 Rock physics models

In rock physics modelling we apply a theory to predict the effective properties of rocks, often referred to as **forward rock physics modelling**. Typical inputs to the modelling are the constituent properties and respective volume fractions, e.g. porosity, and details about lithology and fluid saturation. Many models also include other characteristics of the rock, such as pore and grain geometries, composition, cementation and anisotropy. Which theory is appropriate to use depends on the type of rock to be modelled. The first two papers in this thesis present research done on forward rock physics modelling against data from laboratory experiments. In paper 1 the effective elastic properties of mixed porous clay are calculated using an alternative method compared to the typical approach

which relies on the constituent properties. In Paper 2 we demonstrate consistent joint elastic-electrical modelling and we estimate porosity reduction from resistivity measurements on compacting reservoir sandstone core plugs. Rock physics models are however also vital for the remaining three papers, and in the following, a brief review of some of the common models used in this research is presented.

Bounds are often used as a first approximation. The lower and upper bounds for the elastic moduli of any isotropic or anisotropic media can be approximated with the **Reuss** (1929) and **Voigt** (1928) models, respectively. For N inclusions they are given as

$$C_{\mathrm{R}} = \left[\sum_{n=1}^{N} \frac{V_n}{C_n} \right]^{-1}, \tag{2.5.1}$$

$$C_{\mathrm{V}} = \sum_{n=1}^{N} V_n C_n , \tag{2.5.2}$$

where C_{R} and C_{V} are the effective elastic moduli according to Reuss and Voigt, respectively. The elastic moduli and volume fraction of the n-th constituent is respectively C_n and V_n. In case of a vertically applied force, a physical interpretation of these bounds are a horizontal or vertical layering of soft and stiff materials for the lower and upper bounds, respectively. Modelling according to the **Hill average** (Hill 1963) gives the mean of the Reuss and Voigt bounds, i.e. the effective elastic property C_{H} according to Hill is

$$C_{\mathrm{H}} = \frac{C_{\mathrm{R}} + C_{\mathrm{V}}}{2}. \tag{2.5.3}$$

Another bounding model is the **lower and upper Hashin-Shtrikman bounds** (Hashin and Shtrikman 1963)**.** A physical interpretation of the lower bound for a two phase composition is a spherical material with an inner stiffer core and an outer softer shell. The upper bound can be described in the same way, but interchanging the stiffer and softer constituents. The general version of these bounds is called the **Hashin-Shtrikman-Walpole bounds** (HSW), also known as the **modified Hashing-Shtrikman bounds**. The effective elastic moduli of the HSW bounds for a media with two components (Walpole 1966a,b) is

$$K_{\mathrm{HSW}} = K_1 + \frac{V_2}{(K_2 - K_1)^{-1} + V_1 \left(K_1 + \frac{4}{3}\mu_{\mathrm{m}} \right)^{-1}}, \tag{2.5.4}$$

$$\mu_{\mathrm{HSW}} = \mu_1 + \frac{V_2}{(\mu_2 - \mu_1)^{-1} + V_1\left[\mu_1 + \frac{\mu_{\mathrm{m}}}{6}\left(\frac{9K_{\mathrm{m}} + 8\mu_{\mathrm{m}}}{K_{\mathrm{m}} + 2\mu_{\mathrm{m}}}\right)\right]^{-1}}, \qquad 2.5.5$$

where the indexes 1 and 2 refer to the two components, and V, K and μ are the volume fraction, bulk and shear moduli, respectively. The equations give the upper bound when the largest bulk and shear moduli values of the two components are used for K_{m} and μ_{m}, respectively. The lower bound is found when the minimum moduli values are used for these parameters.

Physical interpretations of the above theories can be linked to the composition of the rock. Other theories integrate more details about the structure of the rock, such as grain and pore shapes, number of contact points between grains, roughness of the grains, cementation, etc. For example, the elastic moduli of unconsolidated dry random packing of non-frictionless spherical grains can be calculated according to the **Hertz-Mindlin theory** (Mindlin 1949)

$$K_{\mathrm{HM}} = \left[\frac{C_0^2(1-\phi_0)^2\mu_{\mathrm{s}}^2}{18\pi^2(1-\nu_{\mathrm{s}})^2}P_{\mathrm{c}}\right]^{1/3}, \qquad 2.5.6$$

$$\mu_{\mathrm{HM}} = \frac{3(5-4\nu_{\mathrm{s}})}{5(2-\nu_{\mathrm{s}})}\left[\frac{C_0^2(1-\phi_0)^2\mu_{\mathrm{s}}^2}{18\pi^2(1-\nu_{\mathrm{s}})^2}P_{\mathrm{c}}\right]^{1/3}, \qquad 2.5.7$$

where K_{HM}, μ_{HM}, μ_{s}, ν_{s} and P_{c} are the effective bulk and shear moduli, shear moduli and Poisson's ratio of the grains and hydrostatic confining pressure, respectively. The coordination number C_0 is the average number of contact points between the grains at the critical porosity ϕ_0.

For consolidated rocks, one can for example use the **self consistent approximation (SCA) theory** (Berryman 1980a, b; Berryman 1995). This inclusion based model takes into account interaction between the inclusions by considered them to be embedded into a host material with yet unknown elastic properties. The elastic properties of the host medium are perturbed until the net effects of all inclusions vanish. The bulk K_{SCA} and shear moduli μ_{SCA} according to the self consistent approximation can be derived from solving the equations

$$0 = \sum_{i=1}^{N}\sum_{j=1}^{M} V_{ij}\left(K_j - K_{\mathrm{SCA}}\right)P_{ij}, \qquad 2.5.8$$

$$0 = \sum_{i=1}^{N}\sum_{j=1}^{M} V_{ij}\left(\mu_j - \mu_{\mathrm{SCA}}\right)Q_{ij}\,, \qquad 2.5.9$$

where K_j and μ_j are the bulk and shear moduli of the j-th inclusion, respectively, V_{ij} is the volume fraction of the j-th inclusion with the i-th aspect ratio, and P_{ij} and Q_{ij} are geometrical factors associated with the inclusion material.

The **differential effective medium (DEM)** theory (Bruggeman 1935) is another inclusion based theory which takes into account higher order interactions. For a two phase composition, one of the constituents is embedded into the other material, which acts as the host medium. This is an asymmetric model because given the same volume fractions of the constituents, interchanging the host with one of the embedding components results in different elastic moduli. The elastic moduli can, according to the differential effective medium theory, be solved from the coupled differential equations (Berryman 1992; Berryman 1995)

$$(1-y)\frac{d}{dy}\left[K^*(y)\right] = \left(K_2 - K^*(y)\right)P_2^*(y)\,, \qquad 2.5.10$$

$$(1-y)\frac{d}{dy}\left[\mu^*(y)\right] = \left(\mu_2 - \mu^*(y)\right)Q_2^*(y)\,. \qquad 2.5.11$$

Phase one acts as the host material with bulk moduli $K_1 = K^*(y{=}0)$ and shear moduli $\mu_1 = \mu^*(y{=}0)$, while the bulk and shear moduli of phase two is K_2 and μ_2, respectively, and y is the volume fraction of phase two. The geometrical factors $P_2^*(y)$ and $Q_2^*(y)$ are calculated having phase two as the inclusion material in a host with effective moduli K^* and μ^*.

Counterparts to the above theories exist for calculating the conductivity. However, in this thesis we only make use of the differential effective medium model of Gelius and Wang (2008) where the conductivity σ is given by

$$\sigma(s,p,T,S_{\mathrm{w}}) = \left[\sigma_{\mathrm{w}}(s_0,T_0) + \Delta\sigma_{\mathrm{w}}\right]\left[S_{\mathrm{w}0} + \Delta S_{\mathrm{w}}\right]^m\left[\phi(p_0) + \Delta\phi\right]^m \cdot \left(\frac{B(s_0,T_0) + lB(s,T)\sigma_{\mathrm{c}}(s_0,T_0)/\sigma(s,p,T,S_{\mathrm{w}})}{B(s_0,T) + lB(s,T)\sigma_{\mathrm{c}}(s_0,T_0)/(\sigma_{\mathrm{w}}(s_0,T_0) + \Delta\sigma_{\mathrm{w}})}\right)^n, \qquad 2.5.12$$

where s, p, T, S_{w}, ϕ, σ_{w} and σ_{c} are the brine salinity, differential pressure, temperature, water saturation, porosity, water and solid conductivity, respectively. These parameters are index edwith a zero for the initial or reference value. The delta values reflect the variation from the reference state. The ease of which cations move along the clay surface is given by the equivalent electrical conductance parameter B. The geometrical parameters l, m and n are

functions of the porosity, water saturation and clay volume fraction, as well as the grain alignment factors.

2.6 Reservoir characterization with rock physics modelling

In forward rock physics modelling the characteristics of the reservoir are used as input to make predictions of the effective elastic properties. When mapping the subsurface, e.g. in search of hydrocarbon resources or CO_2 sequestration, it is the reservoir properties which we are interested to determine. Hence, we have the unfavourable situation where what we want to calculate is the input and what we measure is the output of the modelling.

A typical workflow in reservoir characterization using **forward rock physics modelling** is first to make some initial assumptions about the reservoir. That is, to make a qualified guess of the geology and reservoir properties in order to choose representative rock physics theories to apply for predicting the effective elastic properties. The modelling results are compared with the observations, and the initial parameters are modified to create a better match between modelled and observed data. This process is repeated until a adequate match is achieved. This can obviously be a tedious task, and a direct prediction of the reservoir parameters from the rock physics properties is preferred. Such an approach is referred to as inversion.

Inversion of reservoir parameters from seismic and electromagnetic properties is challenging from a mathematical and physical point of view. Many theories for modelling rocks and trying to capture their complexity exist. However, no matter how complex the models are they are still only simplifications of the actual rock. Still, many of the theories produce good predictions under given circumstances. However, because measurements are uncertain we are not guaranteed that the inversion has a solution. The problem is typically ill posed with non-unique solutions, making it practically impossible to find an analytical inverse function.

"There is nothing like returning to a place that remains unchanged to find the ways in which you yourself have altered."

Nelson Mandela, *'A Long Walk to Freedom'*

S. African black civil rights leader (1918 -)

3 Inverse rock physics modelling

Inverse rock physics modelling (IRPM) is an approach to systematically test observations against the results of forward modelled predictions from various rock physics models. Hence, it allows capturing all possible solutions which exists within the tested models, and it can also take into account uncertainties.

3.1 Constraint cubes

The IRPM approach relies on a library of forward rock physics model constraints between the effective elastic and electrical rock properties and the reservoir or model parameters. We denote these forward models **constraint cubes**.

Figure 3.1 gives an overview of how constraint cubes are created. In each cube we perturb over up to three reservoir or model parameters, which are related to the *x*-, *y*- and *z*-axis in a 3D coordinate system. More model parameters can be handled by creating multiple constraint cubes, e.g. introducing several aspect ratios of the inclusion material.

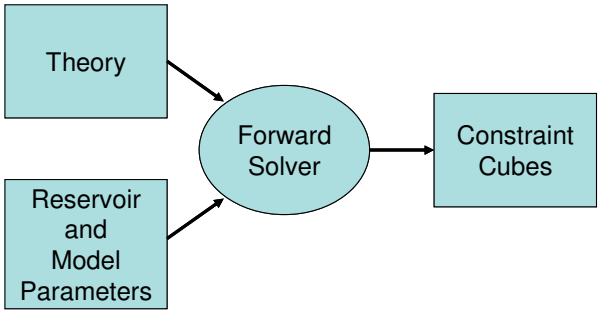

Figure 3.1 Flowchart for creating constraint cubes.

In the following examples we focus on **porosity** ϕ, **lithology** C and **fluid saturation** S (**PLF**), which we relate to the *x*-, *y*- and *z*-axis, respectively. Here, the lithology is quantified as the volume fraction of clay in the solid phase, and the fluid saturation is the volume fraction of brine in the fluid phase.

The **minimum and maximum values** of the reservoir parameters make up the corners of the constraint cube; e.g. one corner for (ϕ_{min}, C_{min}, S_{min}) coincides with origin and the corner diagonally to it is defined by (ϕ_{max}, C_{max}, S_{max}). The cube is divided into a **grid** with NxNxN equidistant nodes. We calculate effective elastic and electrical property values for each node according to the chosen theory and model specifications. For a rock property d we have that the discretely **sampled constraint cube** R is

$$R(\phi,C,S)=d,\ \ \forall\ \phi\in\left(\phi_{\min},\phi_{\min}+\Delta\phi,\phi_{\min}+2\Delta\phi,...,\phi_{\min}+(N-1)\Delta\phi,\phi_{\max}\right),$$
$$C\in\left(C_{\min},C_{\min}+\Delta C,C_{\min}+2\Delta C,...,C_{\min}+(N-1)\Delta C,C_{\max}\right),$$
$$S\in\left(S_{\min},S_{\min}+\Delta S,S_{\min}+2\Delta S,...,S_{\min}+(N-1)\Delta S,S_{\max}\right).\qquad 3.1.1$$

Interpolation between the nodes in *R* gives the continuous **scalar field function** *D*

$$D(\phi,C,S)=d,\ \ \forall\ \phi\in\left[\phi_{\min},\phi_{\max}\right]\wedge C\in\left[C_{\min},C_{\max}\right]\wedge S\in\left[S_{\min},S_{\max}\right].\qquad 3.1.2$$

Figure 3.2 shows an **example of a density constraint cube** for a rock made up of a mixture of quartz and clay, and which is saturated with brine and gas. The colour gradient corresponds to the density.

Where as one set of PLF values corresponds to only one density value, one density value typically corresponds to more than one set of PLF values. All sets $F_d\left(\hat{d}\right)$ of PLF values for a rock property *d* with value $\hat{d}$ can for example be extracted using a marching cubes algorithm (Lorensen and Cline 1987). Connecting these sets leads to a surface in the PLF domain (see Figure 3.3). We denote it an **isosurface** because each point on the surface has the same value of the inspected property, and we denote $F_d\left(\hat{d}\right)$ the isosurface relation of the elastic or electrical property *d*.

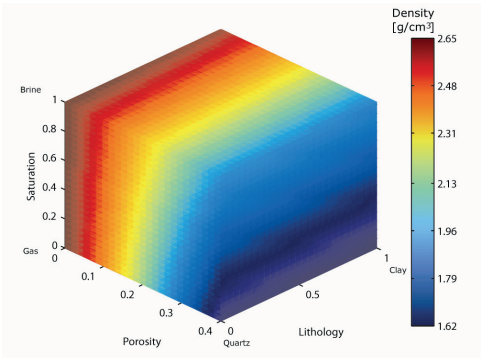

Figure 3.2 Density constraint cube.

The **topology of the isosurface** relates the constraints which that property value has on the porosity, lithology and fluid saturation. In the example in Figure 3.3, we can see that this density value constrains the porosity quite well, but not the lithology and fluid saturation. An inspection of the density constraint cube shows that this is a general trend. This is also logical, because the contrast in density between the two solid components is small and the same applies to the two fluid components. However, the porosity reflects the large density contrast of the solid and fluid.

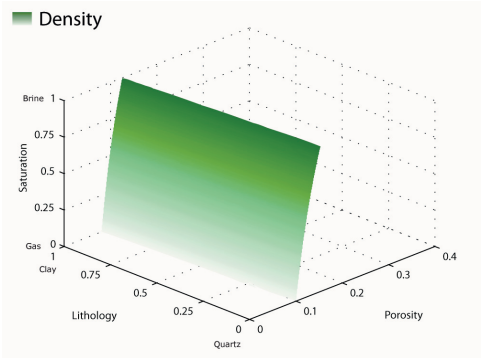

Figure 3.3 Isosurface for a density = 2.4 g/cm^3. The colour gradient corresponds to the saturation.

3.2 Modelling strategy

Figure 3.4 gives an overview of the inverse rock physics modelling strategy. The IRPM solver can test the data against several models. The solutions contain the possible sets of reservoir and model parameters, e.g. porosity, lithology, fluid saturation, pore geometry, etc. The applied rock physics models can have a geological interpretation which can be used when analyzing the solutions.

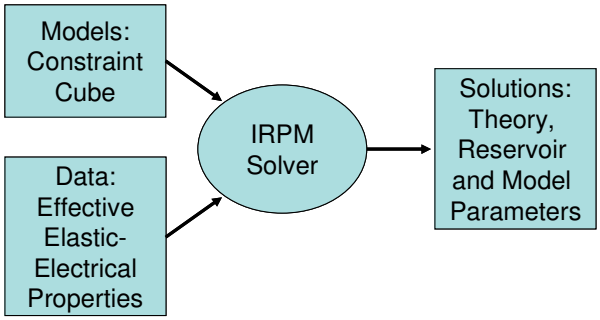

Figure 3.4 Flowchart for the inverse rock physics modelling.

The **solutions of an IRPM** using only one rock physics model and the measurement of only one rock physics property is the set of PLF values which makes up the corresponding isosurface. As shown in Figure 3.3, $F_\rho(\hat{\rho})$ for an observed density value $\hat{\rho}$ does not only give non-unique PLF solutions, but the solutions span over a wide range of values. The range can be reduced by utilizing the observation from a second property, e.g. the bulk modulus K with an observed value $\hat{K}$. The isosurfaces of a bulk modulus and density value corresponding to the same rock volume is plotted in Figure 3.5. Now, the solution of the IRPM is constrained to the intersecting line between these two surfaces, i.e. $F_\rho(\hat{\rho}) \cap F_K(\hat{K})$.

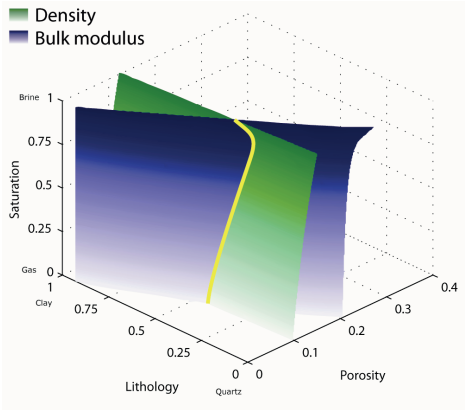

Figure 3.5 Isosurfaces for a density = 2.4 g/cm^3 and bulk modulus = 22 GPa for the same rock volume. The colour gradients correspond to saturation. The IRPM solution highlighted with a yellow line is constrained to the intersection between the two surfaces.

In Figure 3.6, a third isosurface is plotted, namely for the shear modulus μ with observed value $\hat{\mu}$. In this example, making use of all three observations of the same rock volume gives a single PLF solution defined by the point where all three surfaces intersect, i.e. $F_\rho(\hat{\rho}) \cap F_K(\hat{K}) \cap F_\mu(\hat{\mu})$.

Because the rock physics models are nonlinear using measurements from three properties does not necessarily give a unique solution; often we will find two points where the three surfaces intersect. But even when the surfaces intersect in only one point, it does not necessarily mean that this is the only possible solution. In fact, here only one rock physics model has been considered. It is likely that more than one model will match the data, leading to **several possible PLF solutions**. Finally, uncertainties in the input parameters increase the number of possible PLF solutions even further.

For more details on the inverse rock physics modelling strategy, the reader is referred to Paper 3.

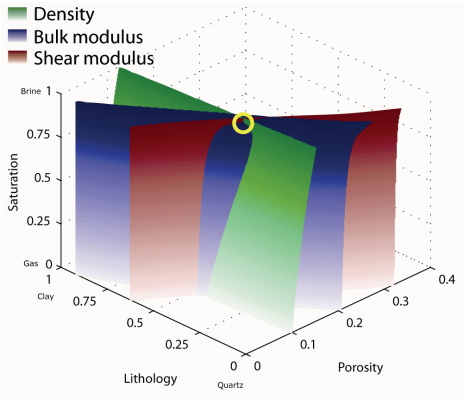

Figure 3.6 Isosurfaces for a density = 2.4 g/cm^3, bulk and shear modulus of respectively 22 and 15.5 GPa for the same rock volume. The colour gradients correspond to the saturation. The IRPM solution highlighted with a yellow circle is constrained to the intersection between all three surfaces.

3.3 Solvers

The **physics** in the inverse rock physics modelling (IRPM) strategy is in analysing the problem, generating new or selecting previously created constraint cubes and interpreting the results of the modelling. Solving the stated problem according to the IRPM approach is a **mathematical** exercise which in practice requires a **computer science** implementation. In the research presented in this thesis, two complementing solvers are used, which we refer to as the Newton-Raphson and the proximity detection solvers.

Results of IRPM using the two solvers with two and three input properties are shown in Figure 3.7. The **Newton-Raphson** solver based on Newton-Raphson's method (Kelley 2003) gives the coordinates of the intersecting points between two or three isosurfaces within a certain amount of precision. The **proximity detection** solver identifies points on each isosurface which are within a specified Euclidian distance in the PLF domain of points on either the other two or three isosurfaces. Hence, solutions are not necessarily constrained to where all surfaces intersect, but it also allows them to be within a maximum distance of each other. To cover the PLF volume of possible solutions we create a spherical cloud of points around the identified solutions.

An obvious difference between the two solvers is that the Newton-Raphson gives "**exact**" solutions, while **uncertainty** is implicit in the proximity detection solver.

Uncertainty can be handled in the Newton-Raphson solver by repeating the modelling over perturbed input values. However, that is a more tedious task and requires an extra iteration per perturbation.

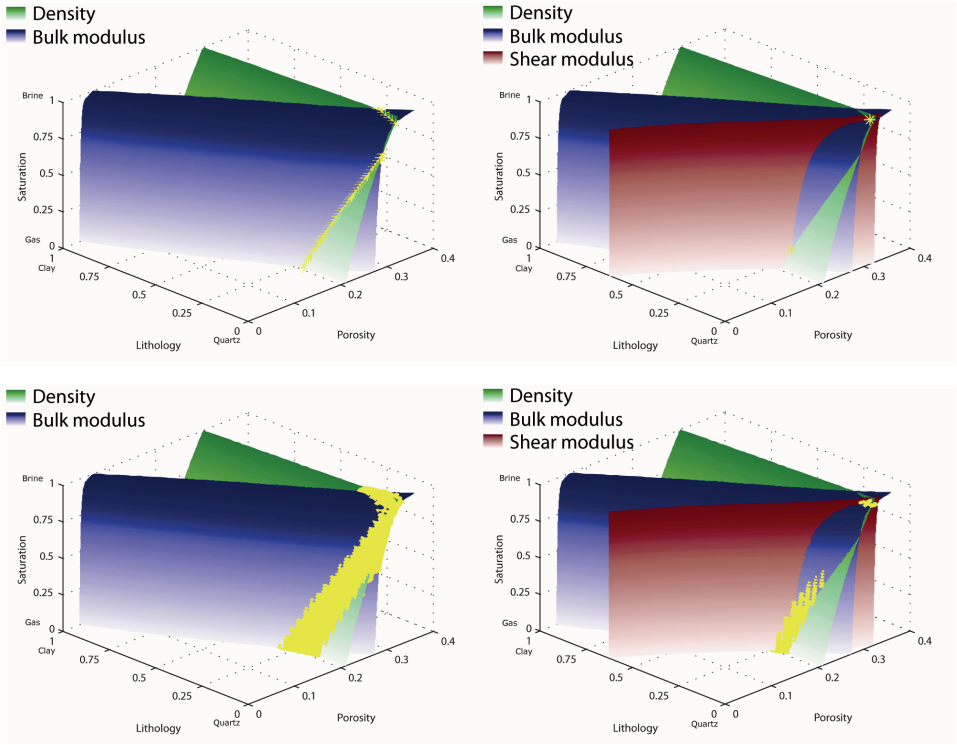

Figure 3.7 Examples of IRPM solutions produced using the Netwon-Raphson based solver (top) and proximity based solver (bottom), with two (left) or three input parameters (right). The identified solutions are marked in yellow.

3.3.1 Workflow of Newton-Raphson solver

The Newton-Raphson solver consists of four main steps (see Figure 2.8).

1. **Calculate gradient functions**

In addition to the scalar field functions of the various elastic or electrical properties (eq. 3.1.2) the Newton-Raphson solver also requires the gradient of the scalar field. We calculate the gradient of the discretely sampled property cubes (eq. 3.1.1) and interpolate the result according to the same procedure as for the scalar field function (eq. 3.1.2) to acquire a continuous gradient function of the scalar field.

2. **Sub-cube segmentation**

To create the discrete constraint cubes a grid with 26x26x26 nodes is defined. Each node forms the corners of cells for a total of 25x25x25 sub-cubes. The number of sub-cubes must be sufficiently large to capture the topological variations of the elastic or electrical properties in the PLF domain.

3. **Discard sub-cubes**

A requirement for an intersection inside a sub-cube between elastic and/or electrical properties used in the inverse modelling is that the respective property values exist inside that volume. Applying a check for this allows us to eliminate sub-cubes which do not contain solutions before initiating the more time-consuming Newton-Raphson algorithm. Hence, sub-cubes where the property value is outside the range of the sub-cube's minimum and maximum values are discarded.

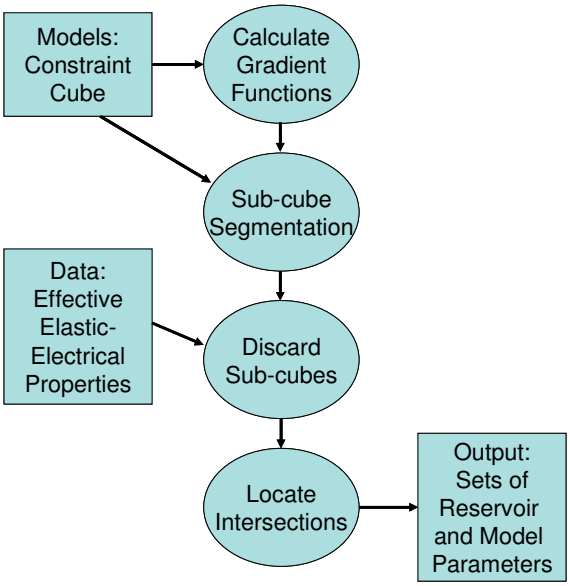

Figure 2.8 Flowchart of the Netwon-Raphson solver.

4. **Locate intersections**

Newton-Raphson's method (Kelley 2003) is used on each remaining sub-cube to locate possible intersecting solutions. The value in the centre of each sub-cube is used as the initial value. In addition, when using only two input properties in the inverse modelling, each side of the cube is tested for an intersection, with the value at the centre of the sides as the initial values. This is because a solution between two properties will typically be an intersecting line between the isosurfaces of the two properties. Testing each side allows connecting the dots making up the line in addition to a denser sampling of the line. Figure 3.9 shows an example where the Newton-Raphson solver successfully identifies the intersection between two isosurfaces along two separate line segments.

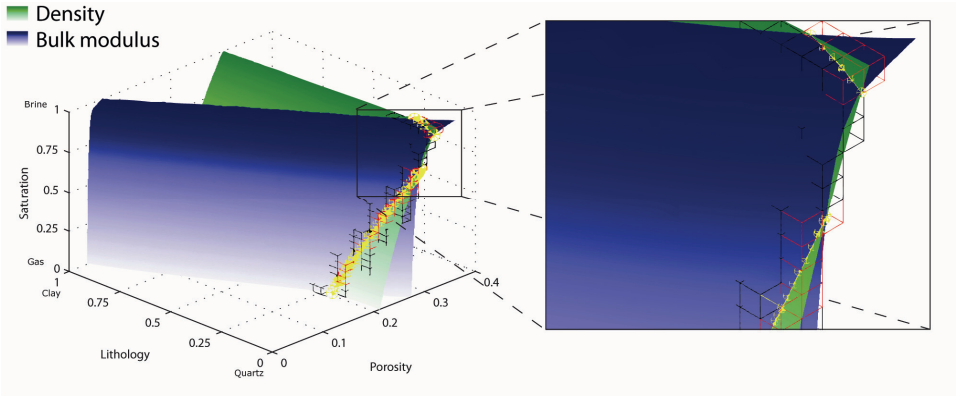

Figure 3.9 Intersection between the density and bulk modulus isosurfaces. The top right corner on the figure to the left has been zoomed in and displayed in the figure to the right. The boxes are the sub-cubes with possible solutions which were not discarded, and the red and black highlights those were a solution and no solution were found, respectively. The yellow circles with stars are the identified solutions and a yellow line is drawn through the solutions which are identified to be connected. Here two line segments have been identified.

3.3.2 Workflow of proximity detection solver

The proximity detection solver consists of four main steps (see Figure 3.10).

1. **Resampling**

The isosurface relation are used to resample to a higher resolution than the one we have in the original cubes; e.g. from cubes with a grid made up of 26x26x26 nodes to a grid made up of 50x50x50 nodes.

2. **Isosurface extractions**

Isosurfaces are extracted, e.g. using a marching cubes algorithm (Lorensen and Cline 1987) or in MATLAB we can use the native ISOSURFACE. The points making up the resampled constraint cubes must have sufficiently high resolution to capture the varying non-linear topology of the isosurfaces.

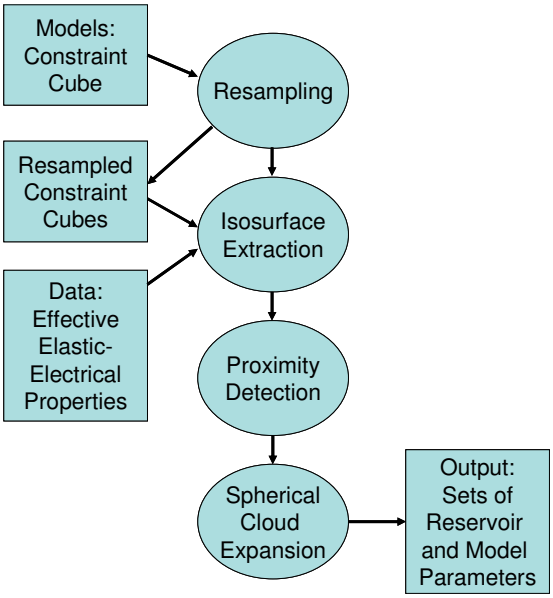

Figure 3.10 Flowchart of the proximity detection solver.

3. **Proximity detection**

Points on each surface within a maximum pre-defined distance δ from each other are identified as solutions. Hence, for three input properties, a point on one surface must be within a distance δ of a point on the other two surfaces and those points must also be within a distance δ of each other.

4. **Spherical cloud expansion**

For each identified solution, a sphere of points within a radius $\delta/2$ and a spacing $\delta/4$ are also considered possible solutions.

The output is a list of discrete points with PLF coordinates, but the actual solutions should be continuous regions. If the resolution is large enough in the resampled constraint cubes the list of discrete points can be interpreted as continuous in those regions.

3.3.3 Run-time performances

The run-time performances of the two solvers can be expressed according to

$$T = m \cdot \left(pt_{\mathrm{s}} + pt_{\mathrm{g}} + dt_{\mathrm{d}} \right), \tag{2.3.1}$$

where T is the total run-time, m, p and d are respectively the number of rock physics models, number of input elastic and electrical properties and number of data samples, and t_{s}, t_{g} and t_{d} are the times it takes to create one isosurface relation and one gradient scalar field function for one property and process one data sample, respectively. The gradient scalar field functions are only required for the Newton-Raphson solver, therefore that term is zero in case of the proximity detection solver.

On a Dell OptiPlex workstation with an Intel Core 2 Quad Q9400 2.66GHz and 4GB ram running Windows Vista and **MATLAB R2010A** approximate values for t_{s} and t_{g} are 5 seconds, and $t_{\mathrm{d}} \approx 5$ seconds in case of Newton-Raphson when using only two input properties, and $t_{\mathrm{d}} \approx 0.5$ seconds when using three input properties or in case of using the proximity detection solver for two or three properties. However, these times depend on the number of identified solutions.

The large difference in t_{d} is because the Newton-Raphson method is very time consuming and using two instead of three elastic and/or electrical properties as input to the inverse modelling, results in more identified solutions. In all cases, once the isosurface relation and gradient scalar field functions have been found the calculations for each model m are independent as well as for each data parameter d. Hence, a parallel implementation can be used to increase the efficiency of the algorithms.

3.4 Applications

There are several applications for inverse rock physics modelling (IRPM). In paper 3 and 4 we use this strategy to do a **quantitative calibration** of rock physics models and property values to fit a given data set. Because the strategy allows us to capture all possible solutions for a given model, it gives us a quantitative basis to evaluate and compare the performance of various rock physics models. Fine-tuning can be done by perturbing the various unknown parameters after discarding the least promising models.

When we are finished calibrating models to various geological facies, e.g. using information from well log data, the IRPM can be utilized in **reservoir characterization**, e.g. between well locations. Using the IRPM to test the various models performance against e.g. data derived from seismic acquisition, one can identify these formations. By testing different realizations of the models for different fluid saturations the IRPM can be used in **reservoir monitoring**.

In paper 5 we show how the constraint cubes, which are the basis for the IRPM can be used in **conditioning of elastic and electrical properties** for use in reservoir characterization. Such a **sensitivity study** can help us to identify the optimal parameter combination to characterize a specific reservoir or indicate possible ambiguities associated with solutions for particular parameter combinations.

As explained earlier, once a problem has been stated the physics of the IRPM is not in solving it. This means that the IRPM strategy and solvers has a **scope beyond rock physics**. It should be applicable to other multivariable problems which proves difficult to find the inverse solution to, e.g. within meteorology, economics, physics, mathematics, etc.

"The worthwhile problems are the ones you can really solve or help solve, the ones you can really contribute something to."

Richard Feynman, *Letter to Koichi Mano, February 3, 1966*

US educator & physicist (1918 - 1988)

4 Main scientific contributions

The main scientific contributions of this thesis are presented in five research papers which have either been published, are in review, submitted or in preparation of being submitted to an international journal. Preliminary results of this research have been presented at several international conferences during the time span of the work (Jensen and Wang 2010; Moyano, Jensen and Johansen 2010; Andersen, Jensen and Johansen 2009; Jensen and Johansen 2009; Johansen and Jensen 2008). In Paper 1 we present an alternative to more typical methods for **calculating the effective elastic properties of clay composites** tested on measurements from a laboratory experiment on mixtures of smectite and kaolinite. In Paper 2 we demonstrate **consistent modelling of elastic and electrical properties** compared with measurements on compacting reservoir sandstone core plugs. A methodology for doing **inverse rock physics modelling** is presented in Paper 3 and it is tested both against synthetic data and a well log from the Glitne field in the North Sea. The methodology from Paper 3 is used in Paper 4 as a tool to **calibrate rock physics models** against real data. Finally, in Paper 5 the inverse rock physics modelling is complemented with a method for **confining elastic and electrical parameters for use in reservoir characterization**.

Following is a brief presentation of the objective and the main conclusions of each research paper. The papers in their entirety can be found in the appendix.

4.1 Paper 1: Estimation of elastic moduli of mixed porous clay composites

Erling Hugo Jensen, Charlotte Faust Andersen and Tor Arne Johansen.

Geophysics **76**, E9-E20, 2011.

Calculating the effective elastic properties is vital in rock physics modelling. Normally, rock physics models are applied to calculate the effective elastic properties from the constituent properties with their respective volume fractions and possibly some specifications of the texture and composition.

In this paper we test an alternative methodology for calculating the effective elastic properties of mixtures of smectite and kaolinite. The elastic properties of clay are ambiguous and any modelling based on these constituent properties is hefted with uncertainty. We avoid introducing this uncertainty by using measured effective elastic properties of pure clay samples to calculate the effective elastic properties of mixed clay

samples. The modelling is tested against published laboratory data on six different samples with various volume fractions of smectite and kaolinite, and at various confining pressures between 1 MPa to 50 MPa. The main findings of this study are:

- In the modelling, we assumed the mixed clay samples to be composed of spherical clusters consisting of pure smectite and kaolinite grains and associated pore spaces. In addition to achieving good results in our modelling, we found support for this assumption in form of a heterogeneous mixture in the observed linear increase in porosity for the same applied stress, between the pure kaolinite, through the kaolinite-smectite mixtures to the pure smectite sample. A more homogeneous mixture should have lead to a V-shaped drop in porosity due to the smaller smectite grains filling the pore space associated with the larger kaolinite grains.

- The difference in porosity for the two pure clay samples when exposed to the same external stress means that the pore space associated with the two clays compact differently. This has possible implications for our clustered based modelling, which is why we also test a correction to the volume fractions of the clay clusters in the presented modelling.

- In the study we tested three different strategies for selecting the pure clay end-members:

  Iso-porosity: The pure clay end-members were assumed to have the same porosity.

  Iso-pressure: The same confining pressure was assumed for the two pure clay end-members.

  Average: The end-members were assumed to be half-way between the previous two (with respect to porosity).

  The best predictions where achieved using the iso-pressure strategy for selecting the end-members and applying the correction to the cluster volume fractions.

- We found the various tested mixing models to have less impact on the modelling compared to the choice of strategy for selecting the end-members. In fact, when following the iso-pressure strategy all mixing models gave almost equally good predictions, with the Hashin-Shtrikman upper bound giving slightly better results for the shear modulus.

- The study shows that the presented method can be a viable alternative to more typical modelling approaches which relies on the constituent properties.

4.2 Paper 2: Consistent joint elastic-electrical differential effective medium modelling of compacting reservoir sandstones

Erling Hugo Jensen, Leiv-J Gelius, Tor Arne Johansen and Zhong Wang.

Submitted to Geophysical Prospecting, June 2011.

The development of coherent rock physics descriptions for elastic and electrical properties is required to be able model on combined seismic and controlled-sourced electromagnetic (CSEM) data. The information retrieved from CSEM is suitable for fluid predictions, and the data from seismic exploration is better suited for predicting structure and lithology. Therefore, the two types of data are complementing and using both has the potential of achieving improved reservoir characterization and monitoring.

In this paper we demonstrate consistent joint elastic-electrical modelling using a differential effective medium scheme. We test the modelled results against measurements on eleven compacting reservoir sandstones. All samples were brine saturated and consisted mainly of quartz and kaolinite. Our main findings of this study are:

- We did a sensitivity analysis to examine the effect of variance for the various properties to be used in the modelling. We found that for the given samples, we can safely assume the quartz grains to be spherical and the clay grains to have a conductivity of 0.02 S/m.

- We used the measured resistivities to calibrate the aspect ratio of the oblate clay grains for the various samples. In addition, they were used to estimate the porosity reduction due to compaction of the samples.

- The calibrated clay aspect ratios and estimated porosities were used in modelling of the effective elastic properties. Both the elastic and electrical modelling were done according to a differential effective medium approach. Here, the high porosity end-member constitutes the host material, while the solid minerals were gradually added as inclusions.

- Due to the large variance in reported elastic moduli values for kaolinite, we decided to treat them as unknowns. However, because all samples came from the same well location we constrained the elastic moduli of kaolinite to be the same for all of them. We used a constrained multivariable non-linear regression approach to calibrate these moduli and to predict the critical porosity and corresponding elastic moduli for the various samples.

- We achieved an overall good fit between the modelled and corresponding measurements supporting the basic idea of joint modelling of elastic and electrical properties.

4.3 Paper 3: Inverse rock physics modelling

Tor Arne Johansen, Erling Hugo Jensen, Gary Mavko and Jack Dvorkin.

In preparation to be submitted to Geophysics, 2011.

Prediction of reservoir and model parameters from seismic data is essential in reservoir characterization and monitoring. However, this task is challenging due to the number of possible rock physics models with various geological and geophysical interpretations, the number of unknown parameters and the non-linear dependency of the parameters.

In this paper we propose a method based on a new philosophy for doing this type of inverse rock physics modelling, where all possible solutions of the model and reservoir parameters from seismic parameters are identified. The method permits systematic testing of various rock physics models, giving geophysicists a robust basis for doing quantitative reservoir characterization. The approach is tested both on a synthetic data set as well as on well log data from the Glitne field. Our main findings of this study are:

- The rock physics model relations were reformulated in order for elastic and electrical properties to be used as input, while the reservoir parameters are the output of the modelling. Therefore, the approach permits efficient testing of observations against various rock physics models in order to do reservoir characterization.

- The suggested approach is flexible with respect to the type and number of properties to use as input and output as well as the applied theories. Furthermore, it is also able to handle the nonlinear relations of the rock physics properties.

- The systematic testing of all selected models ensures the identification of all possible solutions, and the modelling provides a simple way for displaying the non-unique solutions.

- The suggested approach can incorporate uncertainties in a number of ways; 1) perturbing the input data, 2) probability distribution estimations from error distributions attached to the input parameters, 3) using the proximity detection based solver which inherently accepts less constrained solutions.

- We successfully predicted the porosity, lithology and fluid saturation of samples in a synthetic data set using the proposed approach. We demonstrated the clear reduction in the number of non-unique solutions, when using three instead of two elastic properties as input to the modelling. Furthermore, we were able to obtain a consistent rock physics model for the well log data from the Glitne field using the inverse rock physics modelling.

4.4 Paper 4: Improved quantitative calibration of rock physics models

Bernardo Moyano, Erling Hugo Jensen and Tor Arne Johansen.

Accepted for publication in Petroleum Geosciences, July 2011.

Reservoir characterization and monitoring can be an iterative process where models are recalibrated based on newly acquired information. Initially, there might not be much data to work with, but e.g. after a test well has been drilled, more detailed information about the lithology, porosity, fluid saturations and other properties become available. This can improve the accuracy in the rock physics modeling and allow the geophysicist to make more correct predictions further away from the wells, e.g. from modelling on seismic data.

In this paper we use the inverse rock physics modelling approach as a tool to calibrate rock physics models against real data. We compare the results with those found from more traditional calibration techniques. The approach is tested on various models and data sets. Our main findings of this study are:

- We compared using the inverse rock physics modelling, presented in Paper 3, against a traditional technique for calibrating rock physics models. When we applied the traditional technique on data which previously has been used as an example to illustrate the effect of pore-filling clay on porosity and velocity, we found no contradiction to this perception. However, using the inverse rock physics modelling revealed more robust predictions of both lithology and porosity when applying a structural instead of a dispersed clay model.

- Also, the inverse rock physics modelling approach gives a more quantitative basis for doing calibration, which allows us to evaluate the goodness of fit for the model considering all the available data in a consistent manner.

- Furthermore, we demonstrate a more complete workflow using the quantitative inverse rock physics modelling calibration technique on a larger data set. First, we do

an initial screening of plausible models, before continuing more detailed calibration on the most promising candidates.

- The study shows that using the inverse rock physics modelling approach gives a quantitative basis for doing the calibration. This makes it possible to formulate more robust models which give better fits to the observations.

4.5 Paper 5: Conditioning of elastic and electrical parameters for use in reservoir characterization

Erling Hugo Jensen and Tor Arne Johansen.

In preparation to be submitted to Geophysical Prospecting, 2011.

In reservoir characterization, we typically have an imbalance in number of parameters derived from observations and the number of reservoir parameters to be estimated. This imbalance as well as the many different rock physics models and the nonlinear relations between the rock physics properties lead to non-unique solutions when attempting to determine the reservoir quality.

In this paper we study the conditioning of elastic and electrical parameters to use in prediction of the reservoir properties. We present a method which helps us identify the combinations which gives the most precise and robust predictions. The method can also be used to acquire an opinion about the expected performance of a particular parameter combination. Our main findings of this study are:

- We make use of the constraint cubes from the inverse rock physics modelling (see Paper 3) to calculate an average sensitivity value for the elastic and electrical parameters with respect to the various reservoir properties. We also calculated the variance in the sensitivity values for the studied rock physics models and we combined the reservoir property sensitivity values.

- Using this information we can identify elastic and electrical properties, which on average are more sensitive to one reservoir property than the others. We can achieve the most precise and robust prediction by using parameters which singles out a respective reservoir property which they are sensitive to.

- We tested our analysis by doing an inverse rock physics modelling on various combinations of elastic properties. Our predictions of which combinations would do well and which would do badly were confirmed in this modelling on a controlled synthetic data set.

- The method was also applied to eleven rock physics models which had been calibrated against joint elastic-electrical measurements on compacting reservoir sandstone core plugs. Our findings could be used in future modelling based on seismic and controlled-source electromagnetic data acquired in the vicinity of the well where the plugs had been retrieved from.
- The method is flexible with respect to rock physics properties and models to be tested. However, one must be careful to generalise the results as they depend on the applied rock physics models.

”People do not like to think. If one thinks, one must reach conclusions. Conclusions are not always pleasant.”

Helen Keller

US blind & deaf educator (1880 - 1968)

5 Conclusions

Improved reservoir characterization and monitoring can increase our understanding of hydrocarbon reservoirs. This can allow us to locate new hydrocarbon resources as well as extending the lifetime and increase the recovery from existing fields. The research presented in this thesis demonstrates various methods for improving the modelling of rock physics properties and estimating the reservoir quality from elastic and electrical data. The main conclusions of this study are:

- Estimation of effective elastic properties of mixed composites can be done based on the effective elastic properties for rocks made up of the individual components. This modelling approach is advantageous when the rocks are made up of minerals with uncertain elastic properties, such as clay.

- Consistent joint elastic-electrical modelling using a differential effective medium scheme was successfully demonstrated on compaction measurements on eleven core samples. Both the elastic and electrical modelling used the same property specifications and treated the solid components as inclusion material and the high porous end-member as the host medium.

- An inverse rock physics modelling approach was demonstrated, giving a robust platform for conducting reservoir characterization based on seismic and controlled-source electromagnetic observations. The method handles the non-uniqueness of the inverse problem, i.e. it can identify and present all possible solutions of the tested models.

- The inverse rock physics modelling approach provides a basis for doing quantitative calibration of rock physics models. It is demonstrated on two different data sets, and it shows improvements in the calibration compared with using more traditional cross-plot based approaches.

- The method for evaluating the conditioning of elastic and electrical parameters allows us to predict the performance of parameter combinations to use in reservoir characterization. It can be used to identify the combinations which on average will give the most precise and robust solutions before inverting the reservoir properties from our acquired data.

”Our test of truth is a reference to either a present or imagined future majority in favour of our view.”

Oliver Wendell Holmes Jr.

US jurist (1841 - 1935)

6 References

Andersen C.F., Jensen E.H. and Johansen, T.A. 2009. Evaluation of Effective Medium Models for Estimating Effective Elastic Properties of Clay Mineral Mixtures. Sounds of Geology, Bergen, Norway, Extended Abstract.

Berryman J.G. 1980a. Long-wavelength propagation in composite elastic media I. Spherical inclusions. *The Journal of the Acoustical Society of America* **68**, 1809-1819.

Berryman J.G. 1980b. Long-wavelength propagation in composite elastic media II. Ellipsoidal inclusions. *The Journal of the Acoustical Society of America* **68**, 1820-1831.

Berryman J.G. 1992. Single-scattering approximations for coefficients in Biot's equations of poroelasticity. *The Journal of the Acoustical Society of America* **91**, 551-571.

Berryman J.G. 1995. Mixture Theories for Rock Properties. In: *Physics and Phase Relations, A Handbook of Physical Constants* (ed. T.J. Ahrens), pp. 205-228. American Geophysical Union, ISBN 0-87590-853-5.

Bruggeman D.A.G. 1935. Berechnung verschiedener physikalischer Konstanten von heterogenen Substanzen. I. Dielektrizitätskonstanten und Leitfähigkeiten der Mischkörper aus isotropen Substanzen. *Annalen der Physik* **416**, 636-664.

Constable S. and Srnka L.J. 2007. An introduction to marine controlled-source electromagnetic methods for hydrocarbon exploration. *Geophysics* **72**, WA3-WA12.

Darcy H. 1856. *Les Fontaines Publiques de la Ville de Dijon.* Dalmont.

Eidesmo T., Ellingsrud S., MacGregor L.M., Constable S., Sinha M.C., Johansen S.E., Kong F.N. and Westerdahl H. 2002. Sea Bed Logging (SBL), a new method for remote and direct identification of hydrocarbon filled layers in deepwater areas. *First Break* **20**, 144-152.

Gelius L.-J. and Wang Z. 2008. Modelling production caused changes in conductivity for a siliciclastic reservoir: a differential effective medium approach. *Geophysical Prospecting* **56**, 677-691.

Hashin Z. and Shtrikman S. 1963. A variational approach to the theory of the elastic behaviour of multiphase materials. *Journal of the Mechanics and Physics of Solids* **11**, 127-140.

Hill R. 1963. Elastic properties of reinforced solids: Some theoretical principles. *Journal of the Mechanics and Physics of Solids* **11**, 357-372.

Jensen E.H. and Johansen T.A. 2009. On Choice of Seismic Parameters to Use in Estimation of Porosity, Lithology and Pore Fluid. 71st EAGE Conference & Exhibition, Amsterdam, The Netherlands, Extended Abstract..

Jensen E.H. and Wang Z. 2010. Sensitivity analysis of seismic and electromagnetic properties. Lofoten Seminar, Lofoten, Norway, Extended Abstract.

Johansen T.A. and Jensen E.H. 2008. Pitfalls in estimation of reservoir quality from seismic data. SEG Summer Research Workshop, Galway, Ireland, Extended Abstract.

Kearey P., Brooks M. and Hill I. 2002. *An introduction to geophysical exploration.* Blackwell Science, ISBN 9780632049295.

Kelley C.T. 2003. *Solving nonlinear equations with Newton's method.* Society for Industrial and Applied Mathematics, ISBN 9780898715460.

Lorensen W.E. and Cline H.E. 1987. Marching cubes: A high resolution 3D surface construction algorithm. *SIGGRAPH Comput. Graph.* **21**, 163-169.

Mindlin G.W. 1949. Compliance of elastic bodies in contact. *J. Appl. Mech.* **16**, 259-268.

Moyano B., Jensen E.H. and Johansen T.A. 2010. Quantitative calibration of rock-physics models. *SEG Technical Program Expanded Abstracts* **29**, 2496-2500.

Reuss A. 1929. Berechnung der Fließgrenze von Mischkristallen auf Grund der Plastizitätsbedingung für Einkristalle. *ZAMM - Journal of Applied Mathematics and Mechanics / Zeitschrift für Angewandte Mathematik und Mechanik* **9**, 49-58.

Turcotte D.L. and Schubert G. 2002. *Geodynamics.* Cambridge University Press, ISBN 9780521666244.

Voigt W. 1928. *Lehrbuch der Kristallphysik (mit Ausschluss der Kristalloptik).* B.G. Teubner J.W. Edwards.

Walpole L.J. 1966a. On bounds for the overall elastic moduli of inhomogeneous systems--I. *Journal of the Mechanics and Physics of Solids* **14**, 151-162.

Walpole L.J. 1966b. On bounds for the overall elastic moduli of inhomogeneous systems--II. *Journal of the Mechanics and Physics of Solids* **14**, 289-301.

"Doubt is not a pleasant condition, but certainty is absurd."

Voltaire

French author, humanist, rationalist, & satirist (1694 - 1778)

APPENDIX I: PAPER 1

Estimation of elastic moduli of mixed porous clay composites

Erling Hugo Jensen, Charlotte Faust Andersen and Tor Arne Johansen.

Geophysics **76,** E9-E20, 2011.

GEOPHYSICS, VOL. 76, NO. 1 (JANUARY-FEBRUARY 2011); P. E9–E20, 9 FIGS., 3 TABLES.
10.1190/1.3511351

PRACTICING GEOPHYSICS

Estimation of elastic moduli of mixed porous clay composites

Erling Hugo Jensen[1], Charlotte Faust Andersen[2], and Tor Arne Johansen[3]

ABSTRACT

We have developed a procedure for estimating the effective elastic properties of various mixtures of smectite and kaolinite over a range of confining pressures, based on the individual effective elastic properties of pure porous smectite and kaolinite. Experimental data for the pure samples are used as input to various rock physics models, and the predictions are compared with experimental data for the mixed samples. We have evaluated three strategies for choosing the initial properties in various rock physics models: (1) input values have the same porosity, (2) input values have the same pressure, and (3) an average of (1) and (2). The best results are obtained when the elastic moduli of the two porous constituents are defined at the same pressure and when their volumetric fractions are adjusted based on different compaction rates with pressure. Furthermore, our strategy makes the modeling results less sensitive to the actual rock physics model. The method can help obtain the elastic properties of mixed unconsolidated clays as a function of mechanical compaction. The more common procedure for estimating effective elastic properties requires knowledge about volume fractions, elastic properties of individual constituents, and geometric details of the composition. However, these data are often uncertain, e.g., large variations in the mineral elastic properties of clays have been reported in the literature, which makes our procedure a viable alternative.

INTRODUCTION

Lithology prediction from seismically derived properties (such as velocity, impedance, and velocity ratio) is important in seismic exploration and reservoir characterization. In siliciclastic rocks, for instance, elastic properties and permeability are known to be strongly influenced by the clay/sand ratio (Castagna et al., 1985; Best and Katsube, 1995). Usually, we need to estimate the so-called effective solid and fluid properties to calculate the impact of lithology and fluid variations on seismic properties. Knowing the effective properties of the solid grains is necessary when, for instance, using the Gassmann equation (Gassmann, 1951) to study pore fluid effects. A common strategy is to use the Hill average (Hill, 1963) to obtain the effective solid properties before applying the Gassmann equation to predict the fluid effects.

In this study, we investigate an alternative approach for modeling the effective properties of mixed clay composites. The basis for the study is a set of experimental data published by Mondol et al. (2007). Here, dry and brine-saturated smectite and kaolinite have been mixed and subsequently subjected to increasing (confining) pressure while P- and S-wave velocities were measured. We consider the mineral heterogeneity not to be on a mineral grain scale (see Figure 1a for illustration of mineral grain scale heterogeneity) but instead to be composed of clusters of each mineral, i.e., as a mixture of porous smectite and porous kaolinite (see Figure 1b). Therefore, we apply the effective elastic properties of the pure samples to define end members, which we then use to study the relevance of various rock physics models without specifying the grain, fluid, or pore properties.

The elastic properties of smectite and kaolinite mineral clusters differ, so we need to take into account the effects of different compaction of the two components, altering the relative volume fractions as pressure is increased. We compare results obtained when the end members are defined at isopressure, at isoporosity, or as an average between these two conditions.

Our approach is somewhat analogous to the one discussed by Gurevich and Carcione (2000) for deriving the elasticity effects resulting from pore fluid alterations in heterogeneous sand/clay mixtures. They propose a composite Gassmann model whereby fluid substitution is performed for each constituent, subsequently using an

Manuscript received by the Editor 9 December 2009; revised manuscript received 23 July 2010; published online 13 January 2011; corrected version published online 19 January 2011.
[1]University of Bergen, Department of Earth Science, Bergen, Norway. E-mail: erling.jensen@geo.uib.no.
[2]On leave from Statoil, Bergen, Norway; presently University of Bergen, Department of Earth Science, Bergen, Norway. E-mail: charlotte.andersen@geo.uib.no.
[3]University of Bergen, Department of Earth Science, Bergen, Norway and NORSAR, Bergen, Norway. E-mail: torarne.johansen@geo.uib.no.

appropriate mixing law to calculate the total effective properties. In our case, we use the experimental data of the effective elastic properties of pure dry and saturated smectite and kaolinite clusters directly in modeling the mixtures.

Our paper is organized as follows. We start by examining the data set of the pure and mixed samples of smectite and kaolinite. Then we define three strategies for selecting pairs of end members from data characterizing the pure samples. For two of the strategies, we specify a correction to the volume fractions of the constituents because of their different compaction. Finally, we examine commonly used rock physics models, with the end members and volume fractions as input, to estimate the elastic properties of the mixed clay composites. We make a statistical comparison between the predicted and measured data for the mixed samples.

DATA SET

We use data from a mechanical compaction experiment reported by Mondol et al. (2007). Six dry and six brine-saturated samples with mixtures of smectite and kaolinite, ranging from 100% smectite to 100% kaolinite in steps of 20% matrix volume fractions, were prepared in the laboratory and exposed to uniaxial (vertical) compression using an oedometer cell. The P- and S-wave velocities and changes in sample heights were measured at pressure intervals of approximately 5 MPa, from 1 to 50 MPa, using the transmission technique (Birch, 1960). Changes in volume were deduced from the measured decrease in the heights of the specimens and were used to compute the porosities and densities. Dynamic bulk and shear moduli were calculated from the velocities and density.

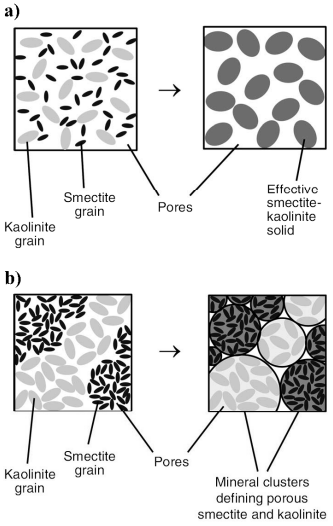

Figure 1. Two ways of modeling the effects of mixed minerals. (a) Homogeneous mixing can be modeled as a composite of single minerals, defining a set of effective (mixed) grain properties. (b) Heterogeneous mixing can be modeled as a composite of mineral clusters, defining effective properties of porous clusters of each mineral.

Figure 2 shows the bulk and shear moduli of the various dry and wet samples measured at 11 different pressures (and porosities), plotted as circles. Because our modeling typically requires input for other porosities or pressures than those which have been measured, we find third-order polynomial fitted functions for these observations and use them to calculate the input values we need.

MODELING APPROACH

The use of effective medium models to obtain the elastic properties of porous composites typically requires knowledge of the corresponding properties of the individual constituents. A general procedure (e.g., Mavko et al., 1998) is first to model the two sets of effective parameters, one for the solid phase and one for the fluid phase, and their respective volume fractions (Figure 1a). Subsequently, the effect of porosity and pore texture is modeled. However, the elastic properties of clay minerals are poorly known and may also depend on the geochemical interaction with the pore fluid (Meade, 1966), which makes the general procedure unsuitable.

We propose an alternative procedure wherein we consider the smectite-kaolinite mixtures to have two phases: one cluster of porous smectite and one cluster of porous kaolinite (Figure 1b). Thus, the effects of mineral and fluid properties, grain geometries, pore space, and structure are embedded implicitly in the effective elastic properties of the two phases. For these properties, we use the measured data of the pure porous smectite and kaolinite samples as end members and input to the effective medium models.

Figure 2 shows that the variation in elastic moduli versus porosity and pressure differs for the pure smectite and kaolinite samples. We will demonstrate how to use these curves to predict the properties of any mixture of smectite and kaolinite.

The mixed samples initially are very loose. As confining pressure increases, the porosity decreases and the bulk and shear moduli increase. We assume that within the pressure range of this experiment (pressure < 50 MPa), the reduction in sample volume is dominated by a reduction of the pore volume; we also assume that alteration of the solid minerals is negligible. The porosity variations seen in Figure 2 should then be a result of mechanical compaction only. The elastic properties of the various mineral mixtures are different, so their compaction rates and porosity reductions are different. As seen in Figure 2c, the porosity in the wet samples reduces with confining pressure from approximately 41% to 11% in the pure kaolinite sample, whereas the range for smectite is 57%–36%. Figure 3 shows schematically the compaction trends and the expected differences in compaction of smectite and kaolinite mineral clusters.

Strategies for selecting modeling end members

To base the modeling on observed data, we avoid using extrapolated values, but we use best-fit values within a porosity range limited by the observations and the approach for selecting end members for the modeling. We consider the following three strategies for defining which end members to use as input to the effective medium models.

Isoporosity

In this strategy, we assume an equal compaction of the pore volumes of the smectite and kaolinite mineral clusters. Hence, both end members and the mixed sample have the same porosity (Figure 4a):

$$\phi_S = \phi_{mix} = \phi_K, \quad (1)$$

where ϕ_S, ϕ_K, and ϕ_{mix} are the porosities in the pure smectite, pure kaolinite, and mixed samples, respectively. Then, in our modeling, the pressures for the pure end members P_S and P_K respectively, and the mixture P_{mix}, are different:

$$P_S \neq P_{mix} \neq P_K \neq P_S. \quad (2)$$

This limits our studied porosity interval to where we have observations for the pure smectite and kaolinite. The porosity values are sampled with a 0.02 increment in the range [0.45, 0.59] for the dry samples and [0.35, 0.41] for the wet samples.

Isopressure

Here, we assume that during compaction the same pressure is applied on the individual clusters in the mixed samples as we observe for the pure samples. Hence, the end members and mixed sample have the same pressure (Figure 4b):

$$P_S = P_{mix} = P_K. \quad (3)$$

However, in our modeling, the porosities are now different:

$$\phi_S \neq \phi_{mix} \neq \phi_K \neq \phi_S. \quad (4)$$

The pressure range is nearly equal for all samples, which gives the largest porosity range of the three approaches. The pressures are calculated from the best-fit function of the pure kaolinite $P_K(\phi)$, with a 0.02 increment in porosity sampling in the range [0.29, 0.59] for the dry samples and [0.11, 0.41] for the wet samples. These pressures are in turn used in the porosity best-fit functions to calculate the porosities of the end members and the mixed samples.

Average

The two previous strategies form extreme bounds in our modeling. The average strategy examines the use of average properties between these two bounds (Figure 4c). In this case, neither the pressure nor the porosity is the same for the end members and the mixed sample:

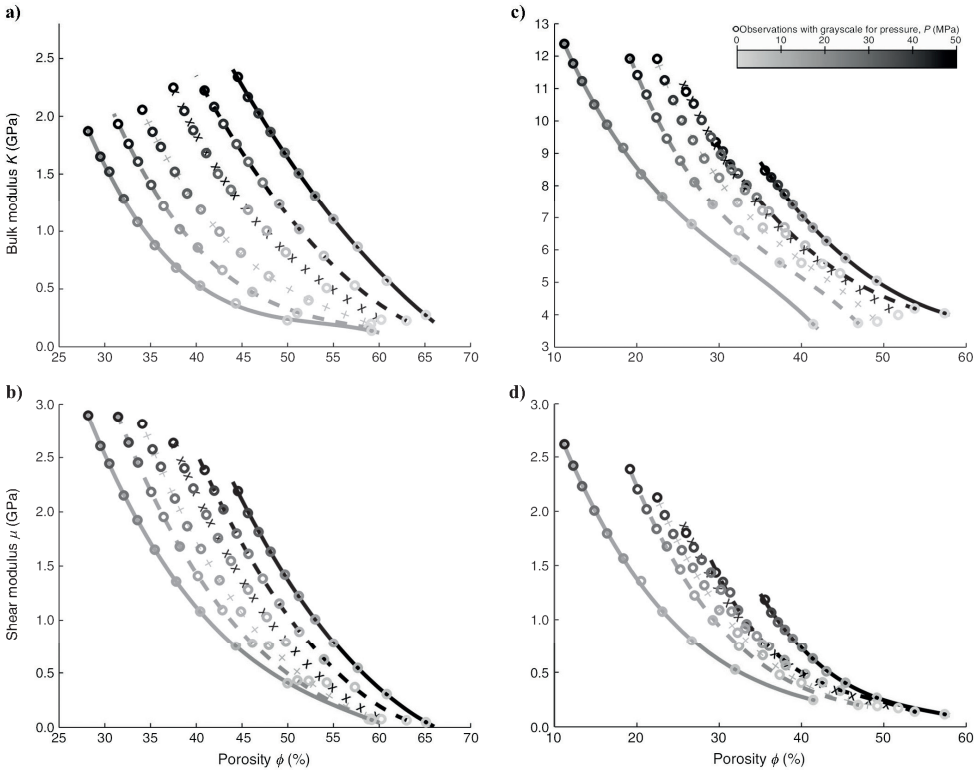

Figure 2. Measured bulk and shear moduli versus porosity for (a, b) dry and (c, d) wet samples. Circles denote moduli calculated from measured P- and S-wave velocities and density. Increased pressure P decreases porosity, as indicated by the gray gradient applied on the circles. Lines are best-fit curves for various smectite-kaolinite mixtures, where S is smectite and K is kaolinite: black solid line (smectite — S100/K0); black dashed line (S80/K20); black x's (S60/K40); gray plus signs (S40/K60); gray dashed line (S20/K80); gray solid line (kaolinite — S0/K100).

$$P_S \neq P_{mix} \neq P_K \neq P_S, \quad (5)$$

$$\phi_S \neq \phi_{mix} \neq \phi_K \neq \phi_S. \quad (6)$$

Porosities in the range [0.37, 0.59] for the dry samples and [0.26, 0.42] for the wet samples are utilized to identify the kaolinite end members and to calculate the corresponding pressure-porosity relation $P_K(\phi)$. Then the average of these porosities and the calculated porosities $\phi(P = P_K)$ for the pure smectite and mixed samples are input into the model.

For the three strategies, the modeling end members are calculated using the obtained porosities as input in the bulk and shear moduli best-fit functions $K(\phi)$ and $\mu(\phi)$, respectively. The porosities and corresponding moduli of the end members can be found in Appendix A.

Volume fraction correction from varying pressure

The initial volume fractions of smectite V_S and kaolinite V_K in the mixed samples refer to the relative matrix fractions. Because we model mixtures of porous smectite and kaolinite, the volume fractions must also capture the relative pore volumes of the constituents. Hence, the volume fraction for smectite L_S is given by

$$L_S = \frac{(\text{smectite mineral volume}) + (\text{smectite pore volume})}{\text{total volume}}. \quad (7)$$

A similar relation can be written for the volume fraction of kaolinite L_K; these fractions must satisfy the equation

$$L_S + L_K = 1. \quad (8)$$

For the isoporosity strategy, we consider the volume fractions of the porous constituents to remain constant and thus resemble the initial volume fractions. For smectite, this means that

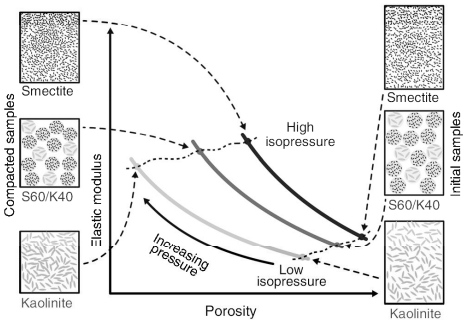

Figure 3. Illustration of how elastic modulus and porosity of pure smectite (black) and kaolinite (light gray) samples with a 60% smectite (S60) and 40% kaolinite (K40) mixture (dark gray) are controlled by confining pressure. The mixture of smectite and kaolinite is illustrated to take place as clusters of the constituents. The pore space of the mineral clusters reduces with increasing compaction, from initial conditions on the right side to final ones on the left side.

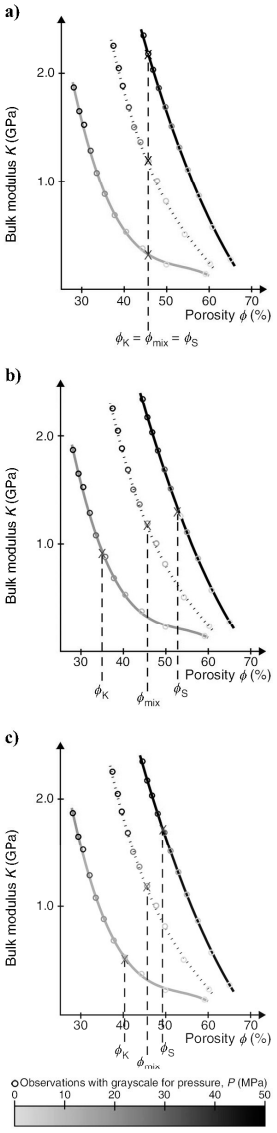

Figure 4. Schematics of the various strategies to model the mixed smectite-kaolinite composites. End members of elastic properties, marked with X, are defined at (a) the same porosity, (b) the same pressure, or (c) the average between (a) and (b). Associated pressures to the measured seismic property are represented in the legend. Black solid line is smectite, dotted line is S40/K40 mixture, and gray line is kaolinite.

$$L_S = V_S. \tag{9}$$

For the isopressure and the average strategies, we perform one set of modeling whereby the volume fractions remain constant, as explained above, and another where the volume fractions change as a result of the relative difference in compaction of the smectite and kaolinite pore space. Then the smectite volume fraction is adjusted by

$$L_S = V_S \frac{1-\phi}{1-\phi_S}, \tag{10}$$

where ϕ and ϕ_S are the porosities that depend on the selected end members of the mixed and pure smectite samples, respectively. (See Appendix B for details about the volume fraction correction.)

Figure 5 shows the predicted porosity effects from compaction given by equation 10 for the isopressure and average strategies, compared with constant volume fractions (equation 9). The largest corrections are clearly seen subsequent to initial compaction; the porosity correction vanishes as the pore space becomes relatively small compared to the total volume.

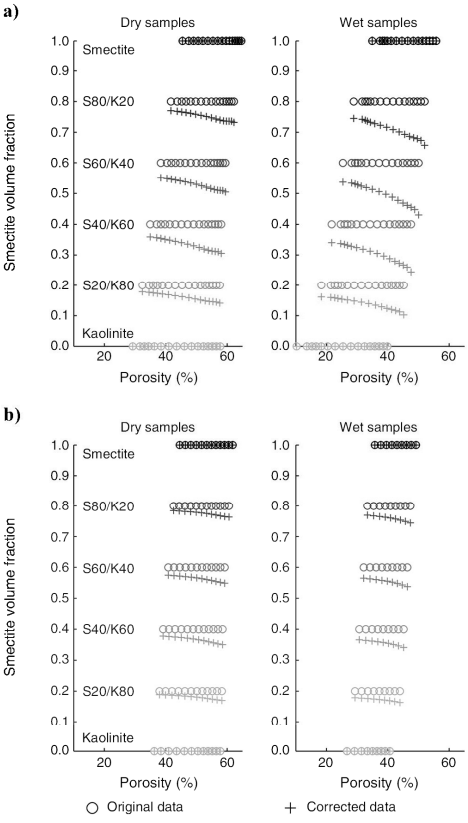

Figure 5. Effect of lithology correction on smectite fraction as a function of porosity when following (a) the isopressure and (b) the average strategy. For the observed porosities the circles denote uncorrected data as given by equation 9 and the crosses denote the corrected data as given by equation 10. The gray gradient refers to the different smectite and kaolinite fractions.

Models used in calculating effective moduli

Eight models are used and compared for predicting the observed elastic moduli of the various mixtures. Reuss (1929), Voigt (1928), Hill (1963), and Hashin-Shtrikman upper and lower bounds (HSUB, HSLB) (Hashin and Shtrikman, 1963) are multipurpose models used for deriving the elastic moduli for any mixture of minerals from the elastic moduli of the individual constituents. Differential effective medium (DEM) modeling (Sheng, 1990) and self-consistent approximation (SCA) (Berryman, 1980a, 1980b) are inclusion-based models that consider the shapes of the inclusions and their respective concentration. Normally, these shapes relate to the shape of the grains or the pore space. But because we model mixing porous clusters of pure smectite and kaolinite, the inclusions in our modeling are not bound by these dependencies. So the spherical inclusions we use do not denote the shape of the individual minerals but the shape of the aggregate of minerals, representing the porous clay constituents.

In the case of DEM, we consider two versions: one where the kaolinite is the host medium (DEM_K) and another where smectite is the host medium (DEM_S). More details of the various models can be found in Appendix C. Predicted bulk modulus versus porosity for these models are shown in Figure 6. The two end members used as input in the modeling are the bulk modulus of the porous material and of the mineral. This is equivalent to considering a plot between two porous materials — one being relatively soft and the other being relatively stiff, where the x-axis denotes volume fractions of the two.

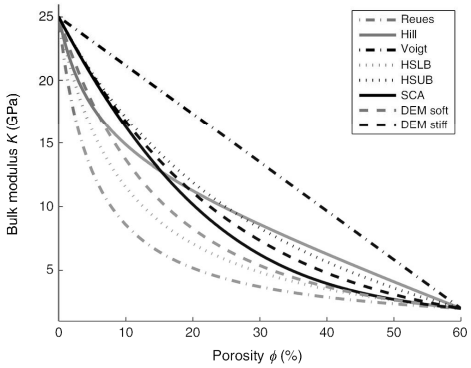

Figure 6. Examples of the estimated bulk modulus as a function of mineral fractions when the difference in bulk modulus of the two constituents (end members) is large. Models: Reuss (dotted-dashed gray curve), Hill (solid gray curve), Voigt (dotted-dashed black curve), Hashin-Shtrikman lower bound (dotted gray curve), Hashin-Shtrikman upper bound (dotted black curve), self-consistent approximation (solid black curve), differential effective medium with the soft material as the host medium (dashed gray curve), and differential effective medium with the stiff material as the host medium (dashed black line).

MODELING RESULTS

To evaluate the results of the modeled versus observed data, we use the rms deviation normalized to the mean of the observed values. This is also referred to as the coefficient of variation of the rms deviation (CVRMSD).

Figure 7 shows the CVRMSD for the bulk and shear moduli, based on isoporosity, isopressure, and average approaches and subsequently used in the eight prediction models. We see that the match between modeled and observed data for the wet samples is better than for the dry samples. The best results for the dry samples have a CVRMSD smaller than 10%, whereas for the wet samples it is less than 5%.

The modeling results generally are more sensitive to the choice of strategy for defining the elastic properties of the end members than the particular rock physics model being used. Thus, isopressure gives a better prediction of the effective elastic properties of the mixed samples than does isoporosity. Of the three approaches, isoporosity implies the largest difference between the elastic properties of the two end members, leading to a stronger rock physics model dependency than for the other two approaches, as revealed in Figure 6. The average gives results almost as good as when considering isopressure.

In general, the volume correction clearly improves the predictions for the isopressure approach. The two exceptions are for modeling the bulk modulus of the dry samples and when applying the Voigt model to calculate the shear modulus of the wet samples. But for the average strategy, this correction only improves the results when the Voigt model is used to calculate the bulk modulus of the dry samples.

Individually, the best results for the bulk and shear moduli of the dry samples are obtained with the Voigt model with end members from the isopressure or average strategy, respectively, both without applying correction to the bulk volume fraction. Overall, the best model to predict both moduli is the HSUB, defining end members by the average strategy and with no volume fraction correction.

The bulk and shear moduli of the wet samples are best predicted

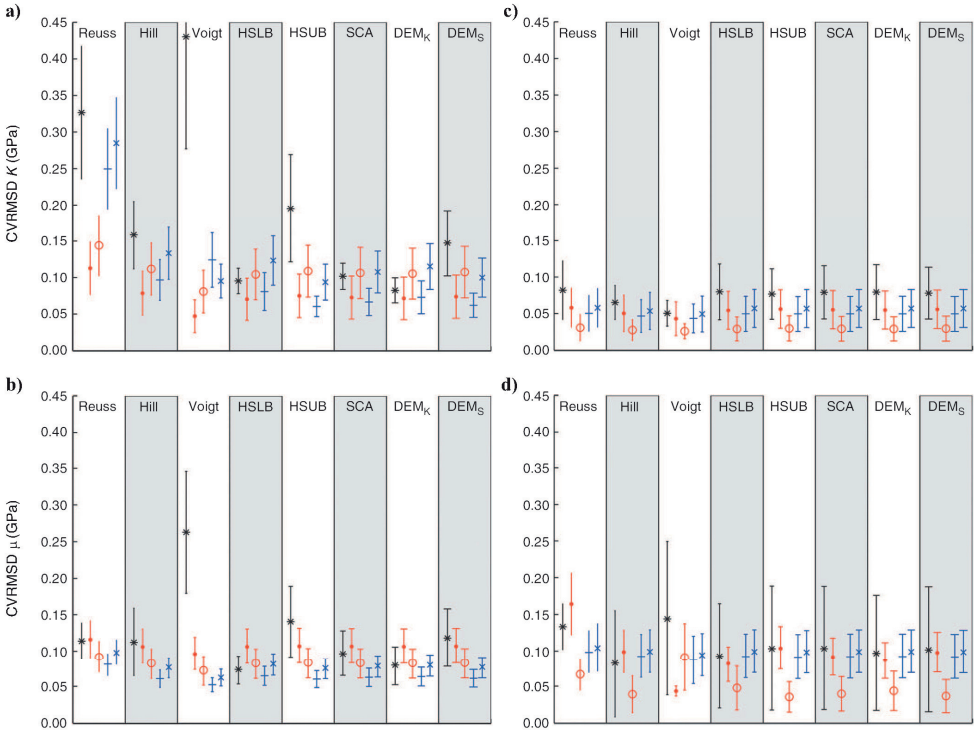

Figure 7. The mean and standard deviation of the coefficient of variation of the rms deviation versus model for the (a) dry bulk modulus, (b) dry shear modulus, (c) wet bulk modulus, and (d) wet shear modulus. The results are grouped for each model: Reuss, Hill, Voigt, Hashin-Shtrikman lower bounds (HSLB), Hashin-Shtrikman upper bounds (HSUB), self-consistent approximation (SCA), differential effective medium with kaolinite as host medium (DEM_K), and differential effective medium with smectite as host medium (DEM_S). The mean values for the various modeling are black asterisk (isoporosity), red dot (isopressure without volume correction), red circle (isopressure with volume correction), blue cross (average strategy without volume correction), and blue asterisk (average strategy with volume correction). The error bars show the standard deviation.

using the isopressure model combined with the volume fraction correction. For the bulk modulus, all effective medium models are almost equally good, but there are some variations in the quality of the shear modulus prediction. Hence, the result for the shear modulus constrains the number of models best suited for a combined modeling of both moduli. Then, all models except for Reuss and Voigt are good candidates, with HSBU being slightly better than the rest.

Examples of effective property predictions

For the wet samples, the HSUB with end members defined as a result of the isopressure strategy gives the best overall modeling predictions for bulk and shear moduli over the entire porosity range and for all lithologies. The modeled data (using HSUB) and measured data of the wet samples are shown in Figure 8. The results are improved when using the volume fraction correction (Figure 8c and d). Ignoring this correction (Figure 8a and b) leads to increasing deviations between modeled and observed data with increasing pressure (i.e., decreasing porosity). In particular, for 20% smectite and 80% kaolinite, HSUB gives a very good prediction when applying the volume correction for the whole porosity range. The prediction of the bulk modulus is improved when one of the clays has a dominant volume fraction; for the shear modulus, the result improves with increasing amount of kaolinite.

DISCUSSION

Poisson's ratio of the wet samples range from 0.40 to 0.49; for the dry samples, there is a large spread between -0.11 and 0.42. In fact, 18 of the 54 values for the dry samples are negative. Auxetic materials, which have negative Poisson's ratios, become thinner perpendicular to the applied force when being compressed. This is not the expected behavior of clay and can be the result of the samples being dried too much — losing some of their chemically bounded water in addition to the pore fluid and thus changing their mineral properties.

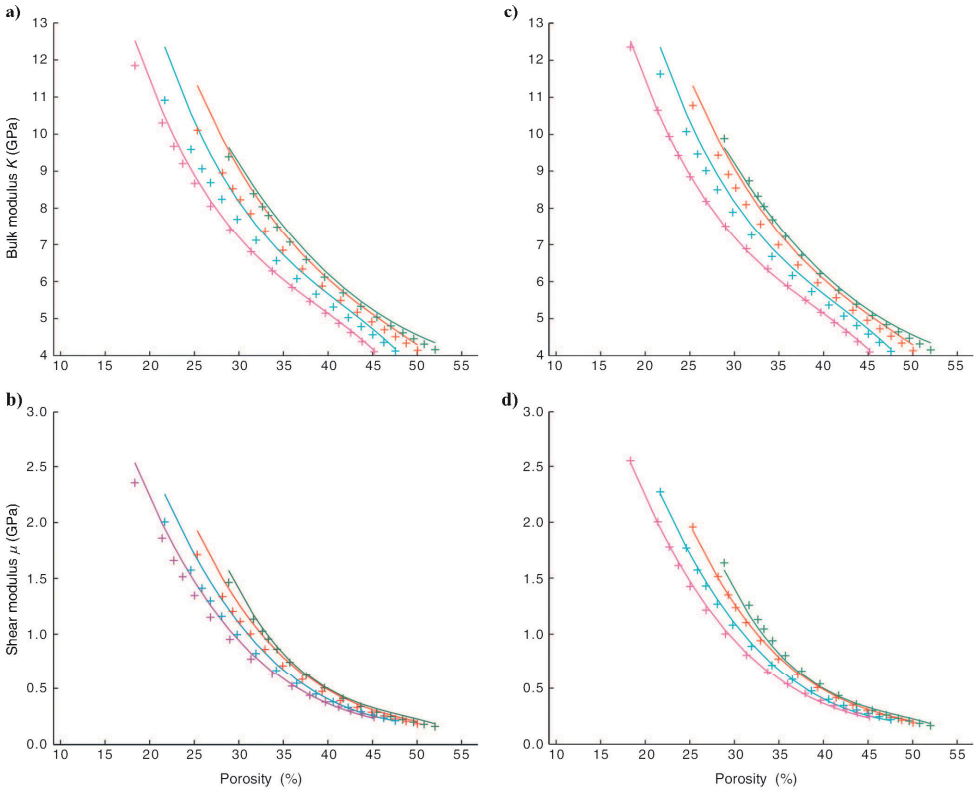

Figure 8. Estimated (a, c) bulk and (b, d) shear moduli for the wet samples using end members of equal pressure. The modeling is done using HSUBs without (a, b) and with (c, d) correction of the bulk volume fraction. Modeled data are plotted as crosses on top of the best-fit curves of the observed data for the various smectite-kaolinite mixtures using the color code: green (S80/K20), red (S60/K40), blue (S40/K60), and purple (S20/K80).

It is unlikely that overdried and wet clay minerals have the same properties. To confirm this, we performed a Gassmann fluid substitution using the observed data from the wet and dry samples of pure smectite and kaolinite to estimate the mineral properties of these two clays; negative bulk moduli values were found for both minerals. Another explanation for the large spread in Poisson's ratio of the dry samples is that there could be some erroneous measurements or specific problems with these samples. Either way, the measurements for the dry samples seem dubious and might be the reason why we have better predictions for the wet samples than the dry ones. This, combined with the fact that most natural clay rocks are water saturated, implies that most attention should be paid to our results for the wet samples.

The strategy for choosing the elastic end members seems to be the most significant factor for the quality of our predictions of the overall elastic moduli. Of the three tested strategies, isopressure and isoporosity are the least and most sensitive to the choice of rock physics models, respectively. This is because the differences in the elastic properties of the end members are smallest when following the isopressure approach and largest for the isoporosity approach. The difference in predicting the bulk modulus for the various models is shown in Figure 6. In the general case, however, the contrast in elastic properties of the mixing minerals might be larger than between smectite and kaolinite. Thus, in those cases, the choice of rock physics model becomes more important for the predicted elastic moduli than in the case of the isopressure approach. But smectite and kaolinite are end members with respect to grain size, surface area, and cation exchange rate (Mondol et al., 2008), and the difference in the elastic moduli of these minerals is expected to be significant — something the measured elastic properties of the two clays at equal porosity supports.

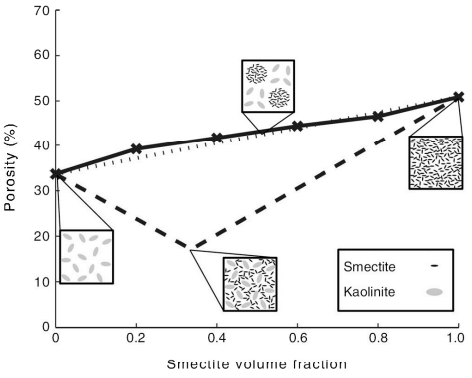

Figure 9. Porosity of mixed smectite-kaolinite sample as a function of volume fraction of porous smectite. A heterogeneous mixed composite (dotted line) will have a linear trend given by the weighted average of the constituents. In the dispersed model (dashed line), the pore space of the large grain-sized mineral (e.g., kaolinite) is filled initially by the small-grain-size mineral (e.g., smectite) (Marion, 1990; Yin, 1992; Dvorkin and Gutierrez, 2002). Plot of the porosity versus volume fraction for the wet sample at confining pressure of 5 MPa (solid line) does not follow the V-shaped trend of the dispersed model.

The isopressure model gives the best result, which is significantly improved when the volume fraction correction is applied. To study pore fluid substitution effects for various pressures, constituents, and rock structure, this correction can be linked to the porosity-distribution parameter of Gurevich and Carcione (2000).

An important assumption in our modeling is that we consider the mixed samples to be composed of clusters of the pure smectite and kaolinite minerals, as illustrated in Figure 1b. If the mixture were more homogeneous, as illustrated in Figure 1a, and because there is such a large difference in volume size of the two clay constituents, it should be possible to observe a V-shaped drop in porosity versus lithology because of the smaller grains filling the pore space of the larger grains (Marion, 1990; Yin, 1992; Dvorkin and Gutierrez, 2002). The trend of a heterogeneous composite mix and the V-shaped trend of a dispersed model are plotted in Figure 9 along with the porosity observations of the wet samples measured at 5 MPa. The observations follow the mixed model and show no V-shaped drop. This supports our assumption that the mixing is not taking place at the grain scale.

The axial (vertical) confining stress will usually cause mineral compaction and some mineral alignment in the horizontal direction, leading to elastic anisotropy. We do not consider this to affect our results seriously, however, because we have limited our analysis to vertical velocities.

CONCLUSIONS

We have demonstrated a procedure for estimating the elastic properties of mixtures of porous smectite and kaolinite from data observations of pure smectite and kaolinite for pressure values between 1 and 50 MPa. We have assumed the mixture constituents to be clusters of pure porous smectite and pure porous kaolinite. Hence, we do not rely the modeling on uncertain estimates of mineral values or pore geometries. Following this procedure, the various rock physics models we have tested show few variations and give almost equally good predictions of the elastic properties. Instead, the dominating factor is the choice of input values (end members) in the modeling.

We have tested three strategies for choosing the pure smectite and pure kaolinite end members: one where they have the same porosity, another where they have the same pressure, and a third that is an average between the other two. We find the best predictions when choosing end members having the same pressure. Furthermore, correcting the volume fractions of the constituents improves the results significantly, showing the importance of taking into account the effect of different compactions of the smectite and kaolinite domains.

The HSUB gives slightly better predictions of the shear modulus for the entire pressure range compared to the other rock physics models. It is therefore the best model to use for these samples of smectite and kaolinite mixtures because the bulk modulus is equally well predicted by all the tested rock physics models.

ACKNOWLEDGMENTS

We thank N. H. Mondol, K. Bjørlykke, J. Jahren, and K. Høeg for providing the data set used in this article. We also thank the Norwegian Research Council (Petromaks program) and Statoil for financial support of the doctoral programs of C. F. Andersen and E. H. Jensen.

APPENDIX A

END MEMBERS USED IN THE MODELING

Tables 1–3 list the porosity, bulk moduli, and shear moduli end members for the various modeling strategies.

APPENDIX B

DERIVATION OF CORRECTION TO THE BULK VOLUME FRACTION

We consider a heterogeneous mixture consisting of clusters of pure porous smectite and kaolinite minerals. One fraction of the pore space can therefore be associated with the smectite and the other with the kaolinite, as observed in Figure 1b. Furthermore, for this experiment, we assume the mineral volume to remain constant during compaction.

The initial smectite volume fraction V_S in the mixed samples only considers the solid phase and is given by

$$V_S = \frac{\text{smectite mineral volume}}{\text{total mineral volume}}. \quad \text{(B-1)}$$

The fraction of smectite mineral to the total volume in the mixed samples $V_{S,\text{mineral}}$ can be expressed as

$$V_{S,\text{mineral}} = V_S(1 - \phi), \quad \text{(B-2)}$$

where ϕ is the total porosity. The smectite volume fraction L_S used in our modeling must also consider the pore space:

$$L_S = \frac{(\text{smectite mineral volume}) + (\text{smectite pore volume})}{\text{total volume}}. \quad \text{(B-3)}$$

If we define $\phi_{S,\text{clusters}}$ as the porosity in the smectite mineral clusters,

$$\phi_{S,\text{clusters}} = \frac{\text{smectite pore volume}}{(\text{smectite mineral volume}) + (\text{smectite pore volume})}, \quad \text{(B-4)}$$

then we can also express $V_{S,\text{mineral}}$ as

$$V_{S,\text{mineral}} = L_S(1 - \phi_{S,\text{clusters}}). \quad \text{(B-5)}$$

Inserting equation B-2 into B-5 and solving for L_S gives

$$L_S = V_S \frac{1 - \phi}{1 - \phi_{S,\text{clusters}}}. \quad \text{(B-6)}$$

For the correction of the bulk volume fraction, we assume that the compaction of the pore space in the mixed samples is the same as for the pure samples. This implies that $\phi_S = \phi_{S,\text{clusters}}$, where ϕ_S is the porosity in the pure smectite sample and equation B-6 becomes equation 10. Observe that if $\phi = \phi_S$, which is always the case for the isoporosity strategy, then equation 10 can be simplified to become equation 9.

Table 1. Porosity, bulk and shear modulus end-member values for the dry and wet samples used in the modeling following the isoporosity approach.

	Smectite end member			Kaolinite end member		
Sample	Porosity (%)	Bulk modulus (GPa)	Shear modulus (GPa)	Porosity (%)	Bulk modulus (GPa)	Shear modulus (GPa)
Dry	45.00	2.268	2.108	45.00	0.3377	0.7005
	47.00	2.007	1.794	47.00	0.2890	0.5713
	49.00	1.761	1.506	49.00	0.2542	0.4600
	51.00	1.528	1.244	51.00	0.2291	0.3638
	53.00	1.310	1.007	53.00	0.2095	0.2800
	55.00	1.106	0.7941	55.00	0.1911	0.2055
	57.00	0.9147	0.6038	57.00	0.1696	0.1377
	59.00	0.7368	0.4356	59.00	0.1409	0.07366
Wet	35.00	8.726	1.238	35.00	5.114	0.4095
	37.00	8.025	1.005	37.00	4.713	0.3490
	39.00	7.387	0.8111	39.00	4.284	0.2978
	41.00	6.809	0.6508	41.00	3.817	0.2539

APPENDIX C

THEORETICAL MIXING MODELS

Voigt, Hill, and Reuss

Voigt (1928) and Reuss (1929) define the upper and lower bounds for the elastic moduli of any isotropic or anisotropic composite. The effective elastic modulus C for a mixture of two constituents with elastic parameters C_1 and C_2 and volume fractions V_1 and V_2 are given by Voigt,

$$C_V = V_1C_1 + V_2C_2, \tag{C-1}$$

and by Reuss,

$$\frac{1}{C_R} = \frac{V_1}{C_1} + \frac{V_2}{C_2}. \tag{C-2}$$

The Hill model (Hill, 1963) is the arithmetic average of the Reuss and Voigt methods, i.e., the elastic modulus is given by

$$C_H = \frac{C_V + C_R}{2}. \tag{C-3}$$

Table 2. Porosity, bulk, and shear modulus end-member values for the dry and wet samples used in the modeling following the isopressure approach.

	Smectite end member			Kaolinite end member		
Sample	Porosity (%)	Bulk modulus (GPa)	Shear modulus (GPa)	Porosity (%)	Bulk modulus (GPa)	Shear modulus (GPa)
Dry	45.46	2.207	2.034	29.21	1.703	2.681
	47.47	1.948	1.725	31.55	1.347	2.250
	49.05	1.754	1.499	32.99	1.161	2.013
	50.56	1.579	1.300	34.44	0.9963	1.795
	52.11	1.405	1.109	36.25	0.8205	1.548
	53.73	1.234	0.9268	38.46	0.6464	1.283
	55.35	1.071	0.7587	40.94	0.4969	1.030
	56.92	0.9218	0.6107	43.53	0.385	0.8088
	58.38	0.7907	0.4857	46.05	0.3102	0.6303
	59.68	0.6795	0.3836	48.38	0.2637	0.4925
	60.80	0.5875	0.3021	50.46	0.2352	0.3885
	61.76	0.5122	0.2379	52.26	0.2164	0.3097
	62.58	0.4505	0.1868	53.81	0.2021	0.2487
	63.29	0.3983	0.1448	55.18	0.1893	0.1991
	63.95	0.3513	0.1081	56.46	0.1759	0.1554
	64.62	0.3051	0.07298	57.77	0.1596	0.1127
Wet	34.92	8.755	1.248	10.23	12.93	2.778
	37.41	7.888	0.9622	13.58	11.12	2.208
	38.31	7.600	0.8742	15.25	10.35	1.960
	38.91	7.415	0.8195	16.62	9.774	1.774
	39.78	7.155	0.7448	18.29	9.141	1.567
	41.08	6.787	0.6451	20.39	8.435	1.335
	42.73	6.355	0.5362	22.82	7.725	1.104
	44.59	5.916	0.4358	25.40	7.073	0.8976
	46.48	5.517	0.3538	27.94	6.507	0.7296
	48.27	5.181	0.2920	30.29	6.027	0.6011
	49.89	4.911	0.2473	32.39	5.619	0.5062
	51.30	4.701	0.2150	34.20	5.270	0.4368
	52.52	4.538	0.1911	35.77	4.963	0.3851
	53.62	4.405	0.1721	37.15	4.681	0.3447
	54.67	4.291	0.1554	38.48	4.399	0.3104
	55.78	4.183	0.1388	39.87	4.086	0.2779

Hashin-Shtrikman bounds

The Hashin-Shtrikman bounds (Hashin and Shtrikman, 1963) are theoretical upper and lower limits of effective moduli of an isotropic mixture. An interpretation of these two bounds is that one of the constituents forms a shell around the other constituent. The upper limit yields a composition where a stiff shell surrounds a soft core, and the lower limit is where a soft shell surrounds a stiff core. For a mixture of two constituents, the upper bound (HSUB) is given by

$$K_{\mathrm{HSUB}} = K_1 + \frac{V_2}{(K_2 - K_1)^{-1} + V_1\left(K_1 + \frac{4}{3}\mu_1\right)^{-1}}, \tag{C-4}$$

$$\mu_{\mathrm{HSUB}} = \mu_1 + \frac{V_2}{(\mu_2 - \mu_1)^{-1} + 2V_1(K_1 + 2\mu_1)\left[5\mu_1\left(K_1 + \frac{4}{3}\mu_1\right)\right]^{-1}}, \tag{C-5}$$

where V, K, and μ are the volume fraction, bulk modulus, and shear modulus, respectively, and where indices 1 and 2 refer to the stiffer and softer materials, respectively. The lower bound (HSLB) is found using the same equations but with index 1 referring to the softer material and index 2 to the stiffer material.

Differential effective medium

In differential effective medium model (Sheng, 1990), one of the constituents acts as the host medium forming the initial background material the other constituents are treated as inclusions. The inclusions of known shape are gradually added into the background material, forming a new background material with new effective elastic properties. This can be realized mathematically using a recursive equation with L iterations; the effective elastic properties of one iteration become input to the next iteration. The total number of iterations must be large enough so that an additional iteration does not change the calculated effective bulk and shear moduli significantly.

We model spherical inclusions and mix only two constituents, so we can use the simplified version of the recursive coupled equations:

$$\frac{K_{n-1} - K_n}{3K_n + 4\mu_{n-1}} = V_n V_2 \frac{K_2 - K_{n-1}}{3K_{n-1} + 4\mu_2}, \tag{C-6}$$

$$\frac{\mu_n - \mu_{n-1}}{\mu_n + F_{n-1}} = V_n V_2 \frac{\mu_{n-1} - \mu_2}{\mu_{n-1} + F_2}, \tag{C-7}$$

Table 3. Porosity, bulk, and shear modulus end-member values for the dry and wet samples used in the modeling following the average approach.

	Smectite end member			Kaolinite end member		
Sample	Porosity (%)	Bulk modulus (GPa)	Shear modulus (GPa)	Porosity (%)	Bulk modulus (GPa)	Shear modulus (GPa)
Dry	44.56	2.328	2.182	36.25	0.8205	1.548
	46.36	2.088	1.891	38.46	0.6464	1.283
	48.18	1.860	1.621	40.94	0.4969	1.030
	49.96	1.647	1.377	43.53	0.3850	0.8088
	51.69	1.452	1.160	46.05	0.3102	0.6303
	53.34	1.275	0.9696	48.38	0.2637	0.4925
	54.90	1.116	0.804	50.46	0.2352	0.3885
	56.38	0.9724	0.6603	52.26	0.2164	0.3097
	57.79	0.8430	0.5350	53.81	0.2021	0.2487
	59.14	0.7244	0.4243	55.18	0.1893	0.1991
	60.47	0.6139	0.3252	56.46	0.1759	0.1554
	61.81	0.5086	0.2348	57.77	0.1596	0.1127
Wet	35.77	8.449	1.144	26.68	6.779	0.8085
	37.70	7.796	0.9337	29.14	6.257	0.6607
	39.55	7.222	0.7637	31.38	5.815	0.5499
	41.31	6.725	0.6289	33.33	5.438	0.4688
	42.97	6.298	0.5225	35.01	5.112	0.4092
	44.54	5.927	0.4381	36.48	4.820	0.3639
	46.07	5.599	0.3698	37.82	4.542	0.3271
	47.6	5.301	0.3133	39.16	4.249	0.2941
	49.20	5.022	0.2652	40.64	3.904	0.2613

$$F_2 = \left(\frac{\mu_2}{6}\right)\frac{9K_2 + 8\mu_2}{K_2 + 2\mu_2}, \tag{C-8}$$

where K_{n-1} is the bulk modulus of the background material, K_n is the effective bulk modulus after adding a volume fraction of V_n of the inclusion material, and μ_{n-1} and μ_n are the background material and effective shear moduli, respectively. The value V_2 is the volume fraction of the inclusion material. The iteration parameter n is given by $n = (2,3,\ldots,L+1)$ and results in index values $(1,2,\ldots,L)$. The host medium acts as the initial background material, identified with index 1 for the first iteration, i.e., $n = 2$. The second constituent acts as the inclusion material and is identified with index 2. The value V_n can be computed from

$$V_n = \frac{V_2}{L - (n-1)V_2}. \tag{C-9}$$

Differential effective medium is an asymmetric model because interchanging the constituents for the host and inclusions will lead to different results.

Self-consistent approximation

In self-consistent approximation (Berryman, 1980a, 1980b), none of the constituents defines a background medium. Instead, inclusions of both constituents are added into a host medium of unknown properties. These unknown properties are perturbed until the effects of the inclusions vanish, at which point these properties represent a unique solution for the effective elastic properties of the mixed material. In practice, this can be done by perturbing the effective elastic properties K^{SCA} and μ^{SCA} until equations C-10 and C-11 are satisfied:

$$\sum_{j=1}^{2}(K_j - K^{SCA})V_j P_j = 0, \tag{C-10}$$

$$\sum_{j=1}^{2}(\mu_j - \mu^{SCA})S_j Q_j = 0, \tag{C-11}$$

where V_j, K_j, and μ_j are the volume fraction, bulk modulus, and shear modulus of inclusion material j, respectively. The values P and Q are geometric factors, which for spherical inclusions are given by

$$P_j = \frac{K^{SCA} + \frac{4}{3}\mu^{SCA}}{K_j + \frac{4}{3}\mu^{SCA}}, \tag{C-12}$$

$$Q_j = \frac{\mu^{SCA} + F^{SCA}}{\mu_j + F^{SCA}}, \tag{C-13}$$

where parameter F is given by equation C-8 (when replacing K_2 and μ_2 with K^{SCA} and μ^{SCA}).

REFERENCES

Berryman, J. G., 1980a, Confirmation of Biot's theory: Applied Physics Letters, **37**, no. 4, 382–384, doi: 10.1063/1.91951.

———, 1980b, Long-wavelength propagation in composite elastic media: Journal of the Acoustical Society of America, **68**, 1809–1831, doi: 10.1121/1.385171.

Best, M. E., and T. J. Katsube, 1995, Shale permeability and its significance on hydrocarbon exploration: The Leading Edge, **14**, no. 3, 165–170, doi: 10.1190/1.1437104.

Birch, F., 1960, The velocity of compressional waves in rocks to 10 kilobars; Part 1: Journal of Geophysical Research, **65**, 1083–1102, doi: 10.1029/JZ065i004p01083.

Castagna, J. P., M. L. Batzle, and T. K. Kan, 1985, Relationships between compressional-wave and shear-wave velocities in clastic silicate rocks: Geophysics, **50**, 571–581, doi: 10.1190/1.1441933.

Dvorkin, J., and M. A. Gutierrez, 2002, Grain sorting, porosity, and elasticity: Petrophysics, **43**, no. 3, 185–196.

Gassmann, F., 1951, Über die Elastizität poröser Medien: Vierteljahrsschrift der Naturforschenden Gesellschaft in Zürich, **96**, 1–23.

Gurevich, B., and J. M. Carcione, 2000, Gassmann modeling of acoustic properties of sand-clay mixtures: Pure and Applied Geophysics, **157**, no. 5, 811–827, doi: 10.1007/PL00001119.

Hashin, Z., and S. Shtrikman, 1963, A variational approach to the theory of the elastic behaviour of multiphase materials: Journal of the Mechanics and Physics of Solids, **11**, no. 2, 127–140, doi: 10.1016/0022-5096(63)90060-7.

Hill, R., 1963, Elastic properties of reinforced solids: Some theoretical principles: Journal of the Mechanics and Physics of Solids, **11**, no. 5, 357–372, doi: 10.1016/0022-5096(63)90036-X.

Marion, D., 1990, Acoustical, mechanical, and transport properties of sediments and granular materials: Ph.D. dissertation, Stanford University.

Mavko, G., T. Mukerji, and J. Dvorkin, 1998, The rock physics handbook: Cambridge University Press.

Meade, R. H., 1966, Factors influencing the early stages of the compaction of clays and sands; review: Journal of Sedimentary Petrology, **36**, 1085–1101.

Mondol, N. H., K. Bjørlykke, J. Jahren, and K. Høeg, 2007, Experimental mechanical compaction of clay mineral aggregates — Changes in physical properties of mudstones during burial: Marine and Petroleum Geology, **24**, no. 5, 289–311, doi: 10.1016/j.marpetgeo.2007.03.006.

Mondol, N. H., J. Jahren, K. Bjørlykke, and I. Brevik, 2008, Elastic properties of clay minerals: The Leading Edge, **27**, 758–770, doi: 10.1190/1.2944163.

Reuss, A., 1929, Berechnung der Fliessgrenze von Mishkristallen auf Grund der Plastizitätbedingung für Einkristalle: Zeitschrift für Angewandte Mathematik und Mechanik, **9**, 49–58, doi: 10.1002/zamm.19290090104.

Sheng, P., 1990, Effective-medium theory of sedimentary rocks: Physical Review B: Condensed Matter and Materials Physics, **41**, 4507–4512, doi: 10.1103/PhysRevB.41.4507.

Voigt, W., 1928, Lehrbuch der Kristallphysik: Teubner.

Yin, H., 1992, Acoustic velocity and attenuation of rocks: Isotropy, intrinsic anisotropy, and stress induced anisotropy: Ph.D. dissertation, Stanford University.

”When one admits that nothing is certain one must, I think, also admit that some things are much more nearly certain than others.”

Bertrand Russell, *"Am I An Atheist Or An Agnostic?", 1947*

British author, mathematician, & philosopher (1872 - 1970)

II

APPENDIX II: PAPER 2

Consistent joint elastic-electrical differential effective medium modelling of compacting reservoir sandstones

Erling Hugo Jensen, Leiv-J Gelius, Tor Arne Johansen and Zhong Wang.

Submitted to *Geophysical Prospecting,* June 2011.

Consistent joint elastic-electrical differential effective medium modelling of compacting reservoir sandstones

Erling Hugo Jensen[1], Leiv-J. Gelius[2], Tor Arne Johansen[1,3] and Zhong Wang[4].

ABSTRACT

Improved reservoir characterization and monitoring can be achieved by combining seismic and controlled-source electromagnetic techniques. This requires developing coherent rock physics descriptions. In this paper we demonstrate consistent joint elastic-electrical modelling according to the differential effective medium theory. We test our modelling against data from a compaction experiment on a set of eleven reservoir sandstone core samples from the same well location. The mineralogy consists mainly of quartz, which we assume in our modelling to be spherical, and kaolinite. The aspect ratio of the clay grains and porosity reduction due to compaction we calibrate using the differential electrical effective medium modelling. These values are in turn used in the elastic differential effective medium modelling, resulting in a consistent joint elastic-electrical modelling scheme giving good fit with the laboratory measurements.

INTRODUCTION

Reservoir characterization and monitoring give vital information about a hydrocarbon reservoir that can be used to possibly improve its production history and life. Seismic is the primary tool for mapping the underground structure and identify potential hydrocarbon traps, but it does not perform equally well as the controlled-source electromagnetic (CSEM) method when it comes to fluid discrimination (Johansen *et al.* 2005). The information content obtained from using these two geophysical techniques often complement each other, therefore a large potential improvement exists if they can be combined in a clever way. To ensure an optimal data combination, there is a need to investigate how well the elastic and electric properties of a medium can be represented by the same type of rock-physics description. The overall goal should be to develop a consistent and coherent joint

[1] Department of Earth Science, University of Bergen, Bergen, Norway.
[2] Department of Geosciences, University of Oslo.
[3] NORSAR, Bergen, Norway.
[4] Bitswave Inc., Houston, TX77074, USA.

elastic-electrical modelling approach which can be used as an optimal constraint in the inversion of seismic and CSEM data.

If no structural information is assumed, both seismic and CSEM data can be modelled using the basic Reuss (1929) and Voigt (1928) bounds or eventually the more advanced Hashin-Shtrikman upper and lower bounds (Hashin and Shtrikman 1962). However, such a joint elastic-electrical modelling will give very imprecise results due to lack of detailed description of the actual medium. A better choice is to make use of the differential effective medium (DEM) theory (Bruggeman 1935) which makes it possible to include the various shapes of the different constituents in the actual modelling. Different DEM schemes exist for calculating the effective elastic properties (Norris 1985; Zimmerman 1991; Berryman 1992; Mukerji *et al.* 1995) as well as the electrical properties of rocks (Hanai 1960a,b; Bussian 1983; Gelius and Wang 2008).

To evaluate the accuracy of such joint rock-physics modelling, combined measurements of electric and elastic properties of core samples are needed. Wang, Gelius and Kong (2009) and Wang and Gelius (2010) were the first to acquire combined data at reservoir conditions employing a modified triaxial cell. Since the aim of these works was mainly to investigate and establish possible cross-property relationships between electric and elastic measurements, the number of core samples was quite limited. In a recent study, Han *et al*. (2011a) presented a rather comprehensive study of combined measurements at various differential stresses involving 63 brine saturated samples collected from various well locations around the world. In an accompanying paper, Han *et al*. (2011b) also presented results from a joint elastic-electrical effective-medium type of modelling. They used a combined self-consistent approximation and differential effective medium model to simulate both the elastic and electric properties. Based on these formulations joint elastic-electric properties were simulated and compared with measurements. For all cores considered, the differential effective stress was 8 MPa, and both the quartz and clay particles were modelled using an aspect ratio of 1.

This paper can be regarded as a continuation of their work but with more emphasis on the detailed structure in the samples. Therefore a subset of core samples from the original data set of Han *et al*. (2011a) is used, represented by a total number of eleven cores taken from the same well. They are all characterized by a fairly simple mineralogy mainly consisting of quartz and kaolinite. For each core, measurements at six different differential stresses, ranging from 8 MPa to 60 MPa, are available. A more detailed joint effective medium modelling can now be carried out since multiple measurements exist for each of the cores. To be able to handle variations in grain shapes and at the same time ensure a consistent and coherent approach, DEM theory is employed to model the conductivity (Gelius and Wang 2008) as well as the elastic moduli (Berryman 1992).

The paper is organized as follows. First a short review is given of the DEM formulations used to calculate the elastic and electrical properties. Then the core data set is briefly introduced and described before a sensitivity analysis is presented which purpose is to delimit the number of constituent properties important for the data calibrations. The actual joint elastic-electric modelling is then carried out in two steps. In the first step, estimation of the porosity reduction due to compaction as well as calibration of the clay aspect ratio is done based on the measured resistivities. In the second step, the corresponding elastic moduli are calculated for the same sets of cores. The feasibility of the proposed approach is then discussed followed by a set of conclusions.

DIFFERENTIAL EFFECTIVE MEDIUM THEORY

Differential effective medium or DEM theory (Bruggeman 1935) is an inclusion based technique, where one phase acts as a host medium and with the other phases being gradually introduced in an incremental manner. It models the effects of the constituent properties as well as the geometry of the inclusion materials. DEM represents an asymmetric formulation because interchanging the host and inclusion material will typically give a different result for the same volume fractions of the constituents.

The host material is here assumed to be connected, since in the electrical modelling the conducting brine must serve as the host. The pore space is then gradually closed by adding solid components. This choice poses a potential problem when doing joint elastic-electrical modelling because of the non-existence of shear for the fluid phase, which again results in unrealistic solutions for the elastic moduli of a solid rock. We mitigate this by using the modified differential effective medium theory (Mukerji *et al.* 1995) for the elastic DEM modelling where we redefine the porous end-member. The host now corresponds to the rock at a critical porosity, which again represents the transition between whether the fluid or the solid phase acts as the load-bearing component. Then, as in case of the electrical modelling, the pore space is closed using solid minerals as the inclusion material.

Elastic modelling

The effective elastic moduli is calculated by solving the coupled differential equations (Berryman 1992)

$$(1-y)\frac{d}{dy}\left[K^*(y)\right] = \left(K_{\mathrm{Q}} - K^*\left(y_{\mathrm{Q}}\right)\right)P_{\mathrm{Q}} + \left(K_{\mathrm{K}} - K^*\left(y_{\mathrm{K}}\right)\right)P_{\mathrm{K}}, \tag{1}$$

$$(1-y)\frac{d}{dy}\left[\mu^*(y)\right] = \left(\mu_{\mathrm{Q}} - \mu^*\left(y_{\mathrm{Q}}\right)\right)Q_{\mathrm{Q}} + \left(\mu_{\mathrm{K}} - \mu^*\left(y_{\mathrm{K}}\right)\right)Q_{\mathrm{K}}. \tag{2}$$

where the quartz and kaolinite inclusions have respectively bulk moduli K_Q and K_K and shear moduli μ_Q and μ_K. The rock at critical porosity acts as the host material with bulk moduli $K_{crit} = K^*(y=0)$ and shear moduli $\mu_{crit} = \mu^*(y=0)$. The total volume fraction of the inclusion materials is $y = y_Q + y_K$ (quartz respective kaolinite). The actual shape of the inclusions is incorporated in the geometrical factors P and Q (Berryman, 1992). For further details the reader is referred to Mukerji *et al*. (1995).

Electrical modelling

The effective conductivity σ is calculated by solving (Gelius and Wang 2008)

$$\sigma(T,\phi,s,S_w) = \sigma_w S_w^m \phi^m \left(\frac{B(s,T) + lB(s,T)\sigma_K(s,T)/\sigma(s,T,S_w)}{B(s,T) + lB(s,T)\sigma_K(s,T)/\sigma_w} \right)^n, \quad (3)$$

where T, ϕ, s, S_w, σ_w, σ_K are the temperature, porosity, brine salinity, water saturation, water and kaolinite conductivities, respectively. The ease of which cations move along the clay surface is given by the equivalent electrical conductance parameter B. The geometrical parameters l, m and n are functions of the porosity, water saturation and volume fraction of kaolinite, as well as the quartz and clay grain alignment factors m_Q and m_K, respectively. In our modelling, m_Q is set to 1.5 because we assume spherical quartz grains. As in the work of Han *et al.* (2011b), the clay grains are assumed to be dispersed in the pore space. However, unlike Han *et al*. (2011b), we allow for an oblate or disc shape which is more realistic. It is also assumed a polarization effect where the clay particles are aligned with their major axis parallel with the electric field. If the depolarization factor of the major axis is A_a, this implies that the clay alignment factor m_K is set to $1/A_a$. More details can be found in Gelius and Wang (2008).

DATA SET

We use data from a mechanical compaction experiment published recently by Han *et al.* (2011a). They measured resistivity, P- and S-wave velocities at various differential pressures on sixty three samples from various well locations spread around the world. In this joint elastic-electric modelling study, a series of eleven core samples have been selected. The cores are labelled SX1 through SX11 and originate from the same well location. They are all characterized by a rather homogeneous mineralogy consisting of mainly quartz and some kaolinite. In addition, a very small amount of other minerals (mainly calcite) is present in some of the core samples (Han *et al.* 2011a). The mineralogy is listed in Table 1 as well as the initial porosity, bulk and grain densities. The measured

resistivities, P- and S-wave velocities for the various differential pressures can be found in Han *et al*. (2011a).

The samples were dried at 40 °C for three days before being saturated with 35 g/l brine. Ultrasonic velocity and electrical resistivity (at 2 Hz) were measured at differential pressures of 60, 40, 26, 20, 15 and 8 MPa, while the pore pressure was kept constant at 5 MPa. Between each unloading the pressure was kept constant for at least one hour for the samples to equilibrate before measurements were done. The temperature remained at 19 °C throughout the whole experiment (Han et al., 2011a).

Constituent properties

The initial constituent properties used in this study are listed in Table 2. For the elastic properties of quartz we use the typical values found in Mavko, Mukerji and Dvorkin (2009, p. 459). The elastic moduli of kaolinite are much more uncertain. A number of different values have been reported in the literature spanning from 1.5 to 55 GPa for the bulk modulus and 1.4 to 31.8 GPa for the shear modulus (Mondol, Jahren and Bjørlykke 2008). Since no precise information about the elastic moduli of kaolinite is available for this

Table 1 Mineralogy and initial porosity, bulk and grain density of the studied samples.

				Mineral solid volume fractions		
Sample	**Bulk density**	**Grain density**	**Porosity**	**Quartz**	**Kaolinite**	**Other**
	g/cm^3	**g/cm^3**	**%**	**%**	**%**	**%**
SX1	2.333	2.638	11.573	83.18	16.56	0.26
SX2	2.367	2.648	10.605	81.88	16.22	1.90
SX3	2.329	2.637	11.682	79.46	20.54	0.00
SX4	2.313	2.637	12.282	84.75	15.06	0.19
SX5	2.312	2.637	12.304	80.46	19.54	0.00
SX6	2.343	2.639	11.212	70.77	29.23	0.00
SX7	2.314	2.640	12.368	72.95	27.05	0.00
SX8	2.320	2.640	12.107	85.35	14.37	0.28
SX9	2.303	2.642	12.835	82.30	17.68	0.02
SX10	2.336	2.643	11.620	80.76	17.79	1.45
SX11	2.324	2.639	11.946	79.45	20.55	0.00

Table 2 Constituent properties. (* We use the effective grain density for the solid phase, see Table 1).

Constituent	**Bulk modulus**	**Shear modulus**	**Density**	**Conductivity**
	GPa	**GPa**	**g/cm^3**	**S/m**
Quartz	37	44	*	0
Kaolinite	20	8	*	0.02
Other minerals	37	44	*	0
Brine	2.38	0	1.0235	4.6948

data, the moduli are treated as unknown variables to be calibrated during the effective-medium modelling. The remaining minerals are mainly calcite which is stiffer than quartz. But for simplicity and because the volume fraction of them is so small, we will use the elastic properties of quartz to characterize them.

The bulk modulus and density of brine depends on the salinity, fluid pressure and temperature. We use the relations of Batzle and Wang (1992) to calculate their values. For the density for the solid phase we use the effective grain densities measured by Han *et al.* (from email correspondence with Angus I. Best) found in Table 1.

Considering the electric properties, the fluid represents the main conductive phase of a brine saturated rock, while in case of a clean sandstone the solid phase has an insulating effect. Quartz is regarded as non-conducting and its conductivity is set to zero in the DEM-model used here (Gelius and Wang, 2008). The clay minerals are conductive but their actual values are rather uncertain. In this study we adapted the same clay and brine conductivities as used by Han *et al.* (2011b) in their modelling of the same samples.

SENSITIVITY ANALYSIS OF CLAY MINERALOGY

The differential effective medium based modelling which is the core of this study considers many different parameters: composition, inclusion geometries, constituent properties and volume fractions, as well as the rock properties at the critical porosity. It follows from the discussion in the previous section that both the elastic and electric properties of clay minerals are not very well known. It is therefore very useful to carry out a sensitivity analysis of the clay mineralogy, so that feasible constraints can be put on the relevant property parameters.

Electric properties of clay

In all simulations, a brine saturated rock sample is assumed with equivalent characteristics as those in the studied cores. The property values shown in Table 2 are used as the reference. In the first sensitivity study, the effect of varying the volume fraction and conductivity of kaolinite is investigated as shown in Figure 1. Note that the most relevant porosity interval is defined by the two vertical bars and follows from the expected range of values of the cores being studied (e.g. porosities between 7% and 13%). The aspect ratios of respectively clay and quartz were set to 0.1 and 1.0. The volume fraction of clay was allowed to vary between 15% and 30% which represents the minimum and maximum values found in the core samples of investigation. Since the clay is modelled as a dispersed phase, the higher clay fraction the lower conductivity. This is due to the fact that the clay minerals will fill the pore space and lower the effective conductivity compared to the

saturated brine case. This trend can also be easily observed in Figure 1. Because the clay fraction is fairly well known in this study (Han *et al*. 2011b), the apparently significant sensitivity to this parameter is not so critical. The conductivity of kaolinite is a much more important parameter due to the high uncertainty in its value. In the joint elastic-electric modelling results to follow later, we have used the value of 0.02 S/m adapted from Han *et al*. (2011b). However, in order to verify this choice the sensitivity to this parameter has been also investigated (cf. Figure 1). The initial value of the clay conductivity was perturbed by ±100 % and it follows from Figure 1 that only a modest change in effective conductivity can be observed (especially when only considering the most relevant porosity interval). This makes the choice of 0.02 S/m a confident value.

The shape of the clay particles also contribute to the final effective conductivity. Figure 2 shows the results obtained when varying the aspect ratio of the clay grains assuming an oblate shape. Even in the low-porosity range relevant for this study, we see a clear dependency on grain shape. The conductivity decreases significantly with increasing aspect ratio. We observed no effect on the modelled elastic moduli for the same variation in clay aspect ratio. The quartz grains are expected to be close to spherical. Reducing the aspect ratio from 1 to 0.8 for oblate shaped non-aligned quartz grains have no measurable effect on the effective conductivity or elastic moduli in the porosity interval of interest.

The high sensitivity in effective conductivity with respect to the shape of clay particles is further elaborated on in the next section. A combined technique is then proposed to estimate both the shape parameter of kaolinite and the porosity changes with compaction.

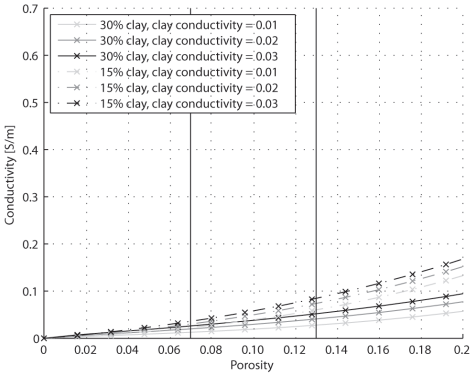

Figure 1 Modelled effective conductivities versus porosity for various clay conductivities. The porosity interval of interest in this study is within the two vertical black lines.

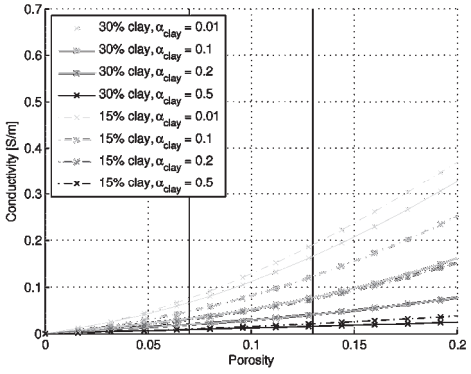

Figure 2 Modelled effective conductivities versus porosity with varying clay aspect ratios. The porosity interval of interest in this study is within the two vertical black lines.

Elastic properties of clay

The effective elastic moduli will increase with increasing values of the kaolinite moduli. The same will happen for the effective moduli, if the effective composite moduli at critical porosity are increased. Increasing the critical porosity will also have a stiffening effect on the rock. In the sensitivity simulations the bulk and shear moduli are both set to 5 GPa assuming a critical porosity of 45 %. Figure 3 shows how the effective elastic moduli will vary when the kaolinite elastic moduli are perturbed plus/minus 10 % around the reference values in Table 2. Two different volume fractions of clay are also considered: 15 % and 30 %, respectively. Inside the most relevant porosity interval only a small increase with increasing elastic moduli can be observed (for a fixed volume fraction of kaolinite).

ESTIMATION OF POROSITY AND CLAY GRAIN ASPECT RATIO

Han *et al*. (2011a) used a helium porosimeter to measure the porosity of each dry core sample at room conditions. During the experiment the porosity was reduced as the samples undergo mechanical compaction when the differential effective stresses were increased to 60 MPa, and then the porosity gradually increased again during the unloading cycle down to a pressure of 8 MPa. In the original work of Han *et al*. (2011a) and their subsequent modelling (Han *et al*. 2011b), this issue was not addressed. We propose here a technique to estimate these porosity changes by constraining them using differential effective medium (DEM) modelling of the conductivity. The quartz grains are expected to have a shape close to spherical and our sensitivity analysis showed no significant variation with a 20 % reduction in aspect ratio. Therefore the choice of an aspect ratio of one for the quartz minerals seems feasible. The sensitivity analysis also revealed that the effective conductivity is highly sensitive to the actual shape of the clay particles.

The procedure now goes as follows. First, the effective conductivity is calculated at the initial porosity and with clay aspect ratios in the range from 0.01 to 0.155 (an increment of 0.001). The modelled conductivity giving the best fit to the measured conductivity at a differential pressure of 8 MPa is used as a first approximation of the clay aspect ratio. Because the clay grains are not expected to change shapes during the given loading and unloading cycles the aspect ratio is therefore considered to remain constant during the compaction experiment. Next, the estimated aspect ratio for the clay grains are used to calculate a conductivity-porosity trend for each core sample so that the remaining porosity values are constrained in a way that the modelled and measured conductivity values are the same. Figure 4 shows an example of such a calibrated curve in case of core sample SX5. Based on these calculations corresponding porosity-pressure trend curves can be easily established. Figure 5 shows an example of such a curve, again in the case of core sample

SX5. Each porosity-pressure curve is then fitted by a third-order polynomial which makes an extrapolation back to a zero differential pressure possible. At this pressure value, the corresponding porosity can be estimated. The difference between this porosity estimate and the actual value measured by Han *et al.* (2011a) at room conditions is used to translate the original trend curve so that the new trend has a porosity value equal to the measured one at zero differential pressure.

We then recalibrate the clay aspect ratio using the updated porosity for the low-compaction measurement (8 MPa) and use the corresponding conductivity-porosity trend as a constraint to finally predict the porosity for the other compaction measurements.

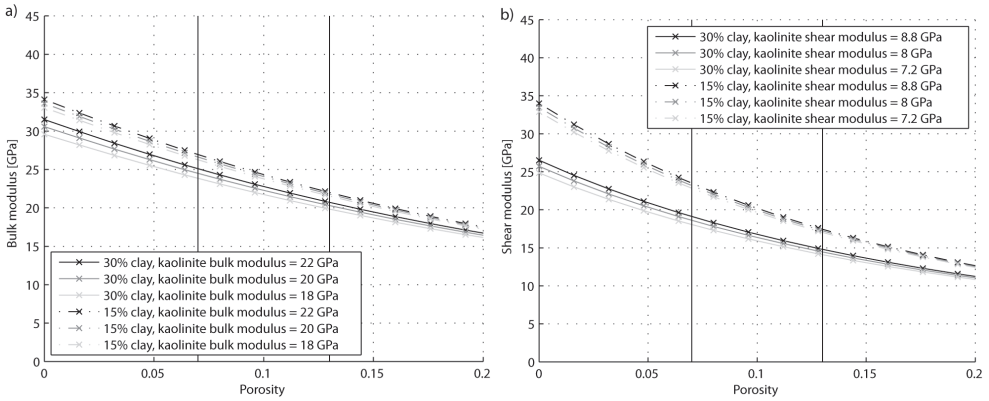

Figure 3 Modelled elastic moduli versus porosity when varying a) the kaolinite bulk modulus and b) the shear modulus. The porosity interval of interest in this study is within the two vertical black lines.

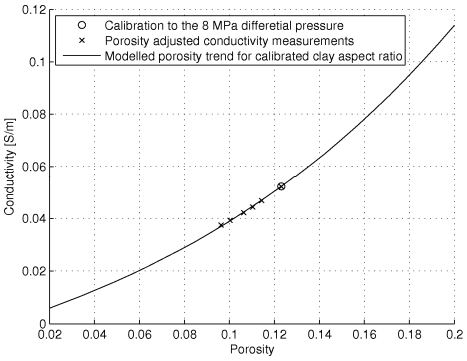

Figure 4 Fitting of the compaction measurements to the conductivity-porosity trend defined by the first approximation of the clay aspect ratio for the 8 MPa differential pressure measurement of sample SX5.

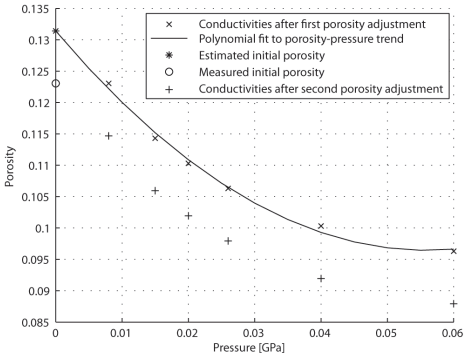

Figure 5 Porosity-pressure trend for sample SX5 for the compaction measurements after the first porosity adjustment and used for calculating the second porosity adjustment.

Table 3 Calibrated aspect ratios of oblate clay grains in each sample and estimated porosities for the various differential pressures.

Sample	Aspect ratio	Porosities at differential pressure					
		8 MPa	15 MPa	20 MPa	26 MPa	40 MPa	60 MPa
		%	%	%	%	%	%
SX1	0.087	10.77	9.92	9.52	9.12	8.72	8.32
SX2	0.034	9.80	9.11	8.71	8.31	7.71	7.31
SX3	0.105	10.64	9.72	9.12	8.72	7.92	7.52
SX4	0.081	11.27	10.32	9.72	9.32	8.92	8.32
SX5	0.108	11.47	10.52	10.32	9.92	9.32	9.12
SX6	0.153	10.30	9.51	9.11	8.71	8.11	7.71
SX7	0.145	11.45	10.52	10.12	9.72	9.12	8.72
SX8	0.052	11.25	10.72	10.12	9.92	9.52	9.32
SX9	0.072	12.21	11.73	11.33	11.13	10.53	10.13
SX10	0.032	10.81	9.72	9.52	9.12	8.72	8.32
SX11	0.095	10.88	9.92	9.52	9.12	8.32	7.72

Repeating the procedure for all core samples shows that the lowest aspect ratio is found to be 0.034 (sample SX2) and the highest 0.153 (sample SX6). The calibrated clay aspect ratios for the various core samples together with the estimated porosities for the various differential pressures are all listed in Table 3. These values are employed in the subsequent DEM modelling of the elastic moduli.

Based on the estimated porosities for the compaction experiment we calculate the effective density, bulk and shear moduli corresponding to the various differential pressures. Cross plotting of these parameters versus porosity is shown in Figure 6. In the same figure, cross plots of conductivity and velocities are shown as well. The two core samples SX2 and SX10 are characterized by a lower conductivity than the other samples. These samples also have the highest volume fraction of the unknown minerals. The bulk modulus of core sample SX1 is significantly lower than in case of the other samples. Apparently, there is nothing in the mineralogy or initial porosity which can explain this discrepancy. The bulk modulus trends for samples SX1, SX4, SX6 and SX7, and the shear modulus trend for sample SX7 show a less smooth behaviour then the others.

MODELLING OF EFFECTIVE ELASTIC MODULI

Initially, the effective elastic moduli of the dry rock are calculated using the differential effective medium (DEM) model as described by Mukerji *et al.* (1995). The dry rock at critical porosity is assigned as the host medium and with the quartz and clay grains acting as inclusions. Next, the effective properties of the brine saturated rock are computed

from Gassmann type of fluid substitution (Gassmann, 1951). To make sure that the elastic and electrical DEM modelling is consistent we use the calibrated aspect ratio of the oblate clay grains and assume spherical non-clay grains.

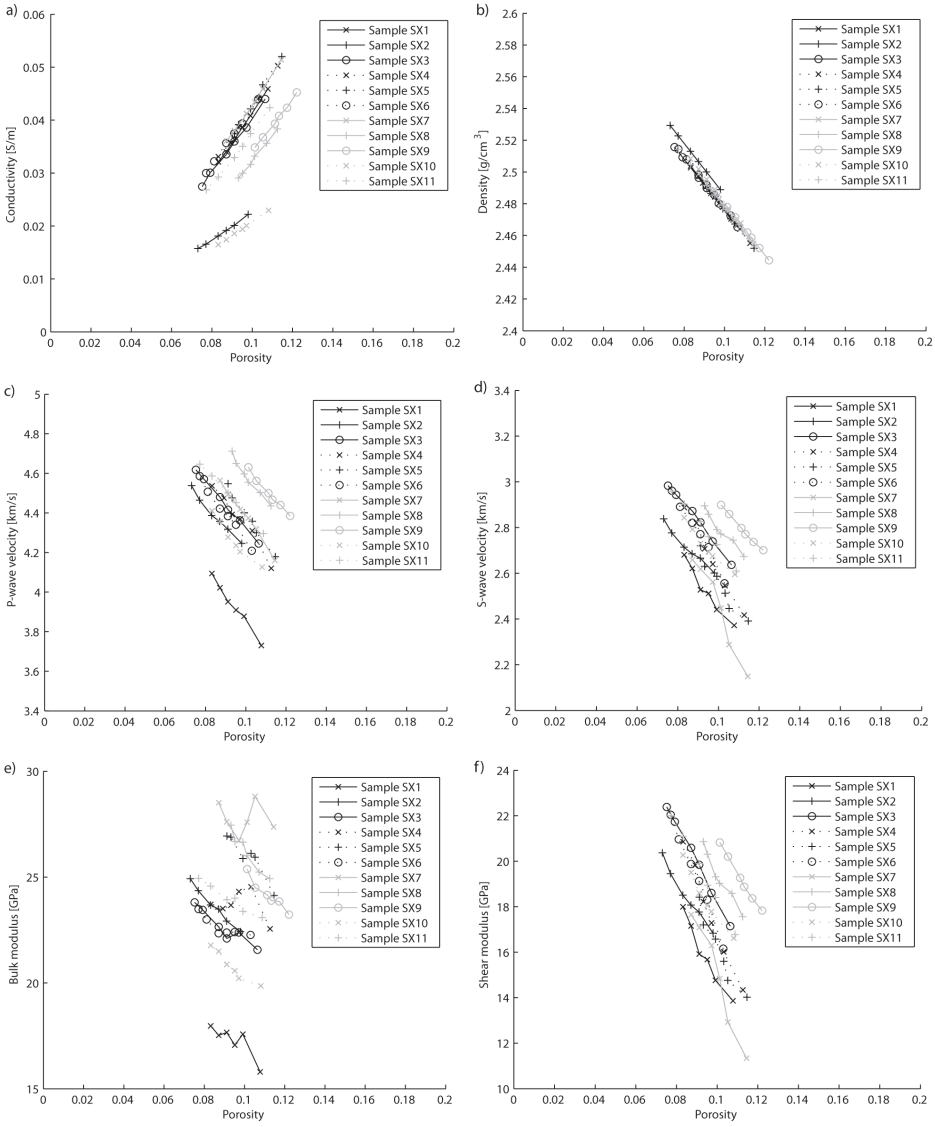

Figure 6 Derived porosity trends for a) conductivity, b) density, c) P-wave velocity, d) S-wave velocity, e) bulk modulus and f) shear modulus.

We have no certain knowledge about the elastic properties of kaolinite and the dry rock at the critical porosity. The critical porosity itself is also an uncertain parameter. In the following, we therefore treat these parameters as unknown during the DEM modelling.

Constrained multivariable nonlinear regression approach

The elastic moduli of kaolinite, the critical porosity and its corresponding elastic moduli are calculated following the strategy of Dræge (2009). A constrained multivariable nonlinear regression analysis is used to seek and find a best fit in a least square sense between the modelled data and the measurements from the different compaction experiments. This is equivalent to finding the minimum of the cost-function

$$F(K_{\mathrm{K}}, \mu_{\mathrm{K}}, \phi_{\mathrm{crit}}, K_{\mathrm{crit}}, \mu_{\mathrm{crit}}) = \sum_{n=1}^{N} w_n R_n \,, \tag{4}$$

where N, K_{K}, μ_{K}, ϕ_{crit}, K_{crit} and μ_{crit} are respectively the total number of core samples, the bulk and shear moduli of kaolinite, the critical porosity and the bulk and shear moduli at the critical porosity. The factor w_n is a weight for the summed root mean square deviation R_n between the calculated effective elastic moduli and those derived from the actual compaction measurements.

The following constraints are applied to the unknown parameters during the nonlinear regression analysis:

1. Elastic moduli of kaolinite

Because all core samples are taken from the same well location it is reasonable to assume that the elastic moduli of kaolinite are almost the same for all samples. Hence, a constant value should be acceptable. Furthermore, we limit the shear modulus to be equal or less than the bulk modulus, in accordance with the trend reported in the literature study by Mondol *et al*. (2008). In the actual regression analysis we constrained the bulk and shear moduli of kaolinite to be respectively in the range of 1 to 40 GPa and 1 to 15 GPa.

2. Properties at critical porosity

Even though the source material is probably the same for all samples, the conditions at deposition might not be identical. This can lead to variations in critical porosity and corresponding elastic moduli of the rock. Hence, we allow these properties to be independent for the various samples. We constrain the critical porosity ϕ_{crit} to be between 0.36 and 0.5, and the bulk modulus K_{crit} and shear moduli μ_{crit} to be in the range of 1 to 8 GPa. Also here, we constrained the shear modulus to be equal or less than the bulk modulus.

3. Deviation weight factors

From inspection of the various cross plots in Figure 6, it can easily be seen that for some of the core samples the porosity trends look anomalous. To put less confidence on these cores we use different weight factors for the various core samples. In this analysis the following set of weights are applied:

$$w_n = \begin{cases} 1.0, & n \in (2,\ 3,\ 5,\ 8,\ 10,\ 11) \\ 0.8, & n \in (1,6) \\ 0.7, & n = 4 \\ 0.6, & n = 7 \end{cases} . \qquad (5)$$

RESULTS

According to the regression analysis, the best fits for the bulk and shear moduli of kaolinite were found to be 20.6 and 8.46 GPa, respectively. The calibrated properties of the host medium at the critical porosity are listed in Table 4 for all core samples. It follows from this table that the elastic moduli at the critical porosity varied significantly between the various samples. In fact, in some cases the values obtained were close to those given as boundary values.

Figure 7 shows modelled elastic moduli and conductivity versus porosity for all 11 core samples considered, superimposed the actual measurements. In case of conductivity, the fitting between the modelled and experimental data are almost perfect due to the constraints imposed earlier (cf. Section 'Estimation of porosity and clay grain aspect ratio').

For the elastic properties, error bars are given for each modelled value corresponding to a given porosity or compaction measurement. These errors were calculated by assuming a ±5 % error in the estimated values for the elastic end members and the critical porosity. Generally, a good fit can be observed between the actual data and the modelling for most of the core samples. The best results are achieved for most of the core samples which we had the highest confidence in, i.e. samples SX2, SX3, SX5 and SX8-SX11. The results for the other cores are slightly

Table 4 Calibrated properties for the host medium at critical porosity.

Sample	Critical porosity %	Bulk modulus GPa	Shear modulus GPa
SX1	36.0	3.086	3.086
SX2	36.0	4.450	4.450
SX3	36.0	4.810	4.809
SX4	42.6	4.990	3.483
SX5	49.3	7.888	2.561
SX6	36.2	5.698	5.689
SX7	50.0	8.000	2.957
SX8	50.0	8.000	3.446
SX9	45.2	7.061	5.517
SX10	36.0	4.552	4.552
SX11	36.0	6.548	6.548

more incoherent. The reasons for that can be multiple, including both the possibilities of measurement errors as well as the lack of the current differential effective medium formulations to properly describe the data well enough.

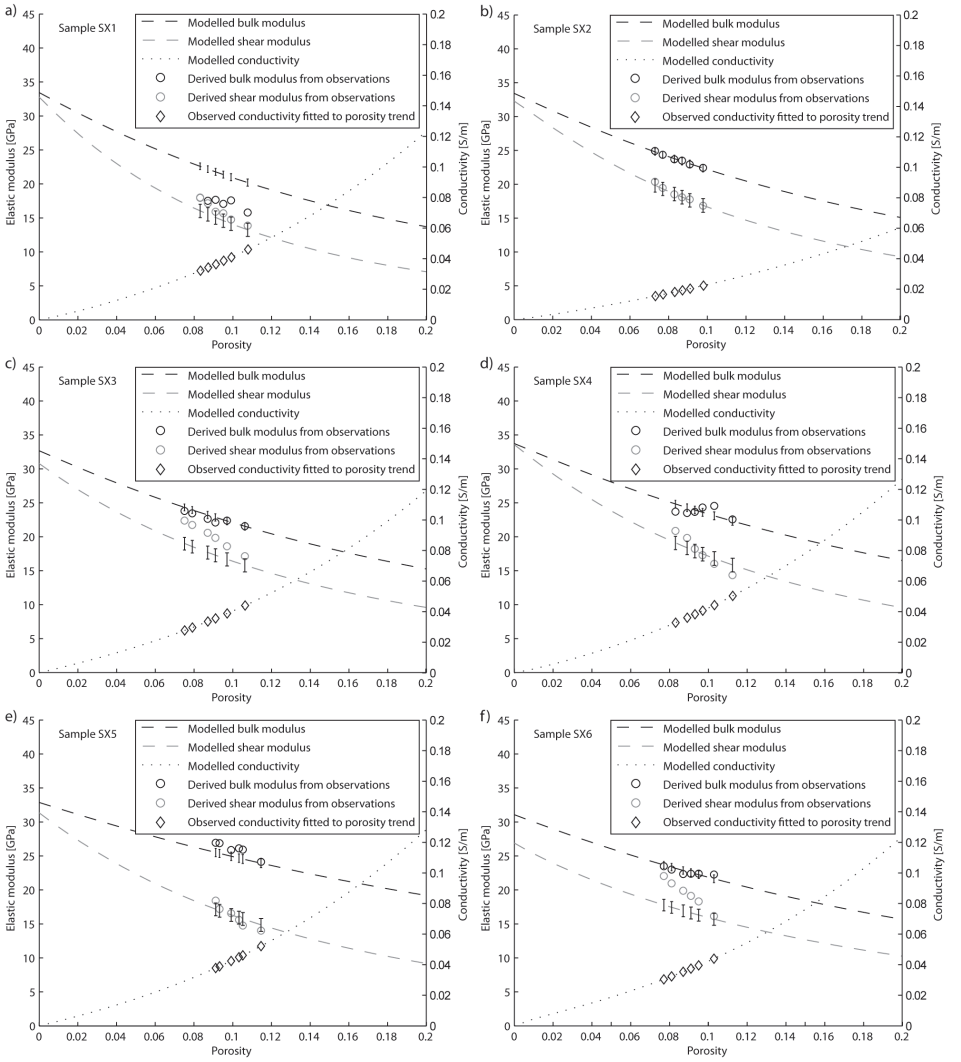

Figure 7 … continues on the next page.

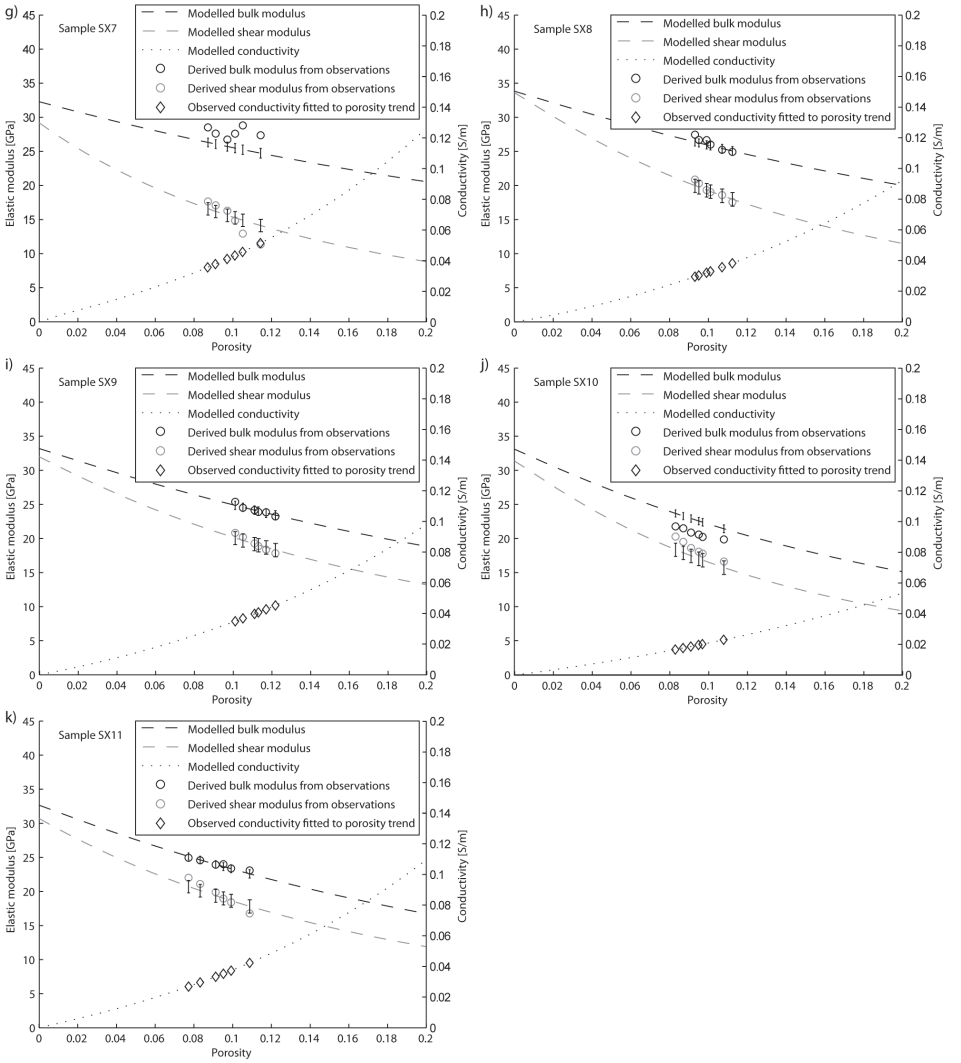

Figure 7 Modelled porosity trends for the bulk and shear moduli together with the derived moduli from the compaction measurements for the various samples. The error bars are for modelled values with ±5 % to the kaolinite bulk and shear moduli, critical porosity and bulk and shear moduli at the critical porosity.

DISCUSSIONS

The main objective of this paper is to present a unified joint elastic-electrical effective-medium modelling approach to analyse laboratory measurements carried out on a series of core samples under compaction (Han *et al*. 2011a). The joint modelling is based on consistent differential effective medium theories for both elastic and electric properties. In general, we achieved an overall good fit as shown in Figure 7. This is a very encouraging result since this supports the basic idea that both electric and elastic properties can be jointly modelled within the same type of rock-physics description. As far as the authors are aware of, this is the first systematic evidence published in the open literature.

As always in rock physics modelling, several parameters need to be assigned proper values. In many cases, this can be a challenging task. To minimize this issue, we carried out a sensitivity analysis to identify those parameters having less impact on the final result. Such parameters were given a fixed reasonable value with good confidence. The remaining variables were calibrated using the actual measurements. In order to arrive at the final results the following issues needed to be addressed and given a solution:

- **Porosity**: no porosity measurements exist for the various differential stress regimes (only at room conditions). A possible approach was introduced in this paper based on a combined update of aspect ratio of clay (through conductivity) and porosity. We found the lowest differential stress of 8 MPa to result in a reduction of approximately 5 to 9 % from the initial porosity. This must be considered as a first order approximation. Even though it represents a significant reduction in porosity it is probably slightly underestimated. The reason for this is that our calculations are based on an extrapolation of a pressure-porosity trend curve. Such curves are characterized by an initial gradient being normally the largest one in a compaction experiment (closing of the compliant porosity part).

- **Grain aspect ratios**: in the simulations, spherical quartz grains have been assumed. This must be considered as an average, and is not exactly true for rocks in general. However, our sensitivity analysis revealed that reducing the aspect ratio with 20 % gave an insignificant contribution to the final modelling result. Regarding the clay grains, their shape was calibrated to the measurements for each specific core sample. The aspect ratio was found to vary between 0.03 and 0.15. These values must also be considered as average values and as discussed before they all depend on our porosity estimates. In case of underestimation of the actual porosity reductions the aspect ratios of the clay minerals have been overestimated.

- **Accuracy of mineralogy:** according to Han *et al*. (2011a) the accuracy is ±5 %. Our sensitivity analysis showed that the volume fraction of clay has an impact on several of the properties we model in this study. However, the error is relatively small within the band of porosities of most interest, and we do not expect it to cause a large variance in the results. Density estimation of the quartz grains based on the given mineralogy results in an under prediction compared to an expected value of 2.65 g/cm^3.

- **Properties of kaolinite:** we modelled the bulk and shear moduli of kaolinite to be 20.6 and 8.46 GPa, respectively. Property values of clay minerals are dubious and it is often difficult to evaluate the realism in them. In most cases the best way to quality control them is by making sure that they give a good fit between data and model and equally important that they fall within the range of values reported in the literature (Mondol *et al.* 2008). The values obtained in this study are also quite close to the values used by Han *et al*. (2011b) in their joint modelling study. Following Han *et al.* (2011b) we also assumed that the clay particles were dispersed. However, in the original work of Han and co-workers the clay grains were assumed spherical due to limitations in their effective-medium formulation. Here, we used a more feasible shape of oblate/disc type and also allowed for polarization effects. This latter implies that we assumed that the clay minerals aligned with their major axis parallel with the electric field. For completeness, we also tried to see the effect of the more non-physical situation where the clay grains aligned with their minor axis. In this case the computations lead to solutions with non-spherical quartz grains with unrealistic low aspect ratios.

Concerning the few core samples in Figure 7 where the modelled results did not fit so well with the measurements: If one considers the estimated porosity compaction trends for these core samples they indicate possible errors in the actual laboratory measurements. The calibrated properties for a subset of them were also at the extreme limits of the bounds set in the constrained multivariable nonlinear regression analysis. Extending the bounds will probably result in a better fit, but maybe less realistic results. Though, the upper boundary for the critical porosity could possibly be extended to some extent in some of the cases. Also, our rigorous constraint on the shear modulus to be less or equal to the bulk modulus for the critical porosity end member, could possible be loosened if one considers the elastic properties of the quartz mineral. However, based on the available data it is impossible to say what the actual critical porosity really is, and our predictions of them and corresponding elastic moduli must not be taken literally.

CONCLUSION

The combined use of seismic and controlled-source electromagnetic (CSEM) techniques in connection with life-of-field managing is foreseen to develop in the near future. By combining electric and elastic measurements a more reliable monitoring of a reservoir under production can be obtained. Combined geophysical techniques may also play an important role in connection with quality control of secondary and tertiary recovery techniques. By placing permanent multi-component/multi-wave sensor arrays on the seafloor both passive and active data can be recorded.

In order to utilize the large potential inherent in such joint elastic/electric data acquisitions, a coherent rock-physics description is in demand. The latter serves as a link or bridge between the measurements and key reservoir parameters such as saturations, pressure and temperature. Effective medium theories can also aid the understanding of cross property relations between electrical and elastic data. Such relations can be used to constrain joint inversion of seismic and CSEM data.

This paper proposes a DEM type of platform which can coherently and jointly model both elastic and electric data. This formulation has been tested using a set of joint electric-elastic laboratory measurements carried out on eleven core samples taken from the same well. The results obtained show an overall good fit between the joint modelling and the corresponding measurements.

ACKNOWLEDGEMENT

We are grateful to Tongcheng Han and co-workers, for publishing their extensive joint elastic-electrical dataset and providing us with the density measurements of the core samples studied in this paper. We also thank the Norwegian Research Council (Petromaks program) and Statoil for financial support of the doctoral program of Erling Hugo Jensen.

REFERENCES

Batzle M. and Wang Z. 1992. Seismic properties of pore fluids. *Geophysics* **57**, 1396-1408.

Berryman J.G. 1992. Single-scattering approximations for coefficients in Biot's equations of poroelasticity. *J. Acoust. Soc. Am.* **91**, 551-571.

Bruggeman D.A.G. 1935. Berechnung verschiedener physikalischer Konstanten von heterogenen Substanzen. *Ann. Physik (Leipzig)* **24**, 636-679.

Bussian A.E.. 1983. Electrical conductance in a porous medium. *Geophysics* **48**, 1258-1268.

Dræge A. 2009. Constrained rock physics modeling. *The Leading Edge* **28(1)**, 76-80.

Gassmann F. 1951. Über die Elastizität poröser Medien. *Vierteljahrsschrift der Naturforschenden Gesellschaft in Zürich* **96**, 1-23.

Gelius L.-J. and Wang Z. 2008. Modelling production caused changes in conductivity for a siliciclastic reservoir: a differential effective medium approach. *Geophysical Prospecting* **56**, 677-691.

Han T., Best A.I., Sothcott J. and MacGregor L.M. 2011a. Joint elastic-electrical properties of reservoir sandstones and their relationships with petrophysical parameters. *Geophysical Prospecting* **59**, 518-535.

Han T., Best A.I., MacGregor L.M., Sothcott J. and Minshull T.A. 2011b. Joint elastic-electrical effective medium models of reservoir sandstones. *Geophysical Prospecting* **59**, 777-786.

Hanai T. 1960a. Theory of the dielectric dispersion due to the interfacial polarization and its applications to emulsions. *Kolloid-Zeitschrift* **171**, 23-31.

Hanai T. 1960b. A remark on "Theory of the dielectric dispersion due to the interfacial polarization and its applications to emulsions". *Kolloid-Zeitschrift* **175**, 61-62.

Hashin Z. and Shtrikman S. 1963. A variational approach to the elastic behavior of multiphase materials. *Journal of the Mechanics and Physics of Solids* **11**, 127-140.

Johansen S.E., Amundsen H.E.F, Røsten T., Ellingsrud S., Eidesmo T. and Bhuyian A.H. 2005. Subsurface hydrocarbons detected by electromagnetic sounding. *First Break* **23**, 31-36.

Mavko G., Mukerji T. and Dvorkin J. 2009. *The rock physics handbook*. Cambridge Univeristy Press. ISBN 978-0-521-86136-6.

Mondol N.H., Jahren J., Bjørlykke K., and Brevik I. 2008. Elastic properties of clay. *The Leading Edge* **27**, no. 6, 758-770.

Mukerji T., Berryman J.G., Mavko G. and Berge P.A. 1995. Differential effective medium modeling of rock elastic moduli with critical porosity constraints. *Geophys. Res. Lett.* **22**, 555-558.

Norris A.N. 1985. A differential scheme for the effective moduli of composites. *Mech. Mater.* **4**, 1-16.

Reuss A. 1929. Berechnung der Fliessgrenzen von Mischkristallen auf Grund der Plastizitätsbedingung für Einkristalle. *Z. Ang. Math. Mech*. **9**, 49-58.

Voigt W. 1928. *Lehrbuch der Kristallphysik.* Teubner.

Wang Z., Gelius L.-J. and Kong F.N. 2009. Simultaneous core sample measurements of elastic properties and resistivity at reservoir conditions employing a modified triaxial cell – a feasibility study. *Geophysical Prospecting*. **57**, 1009-1026.

Wang Z. and Gelius L.-J. 2010. Electric and elastic properties of rock samples: a unified measurement approach. *Petroleum Geoscience* **16**, 171-183.

Zimmerman R.W. 1991. Elastic moduli of a solid containing spherical inclusions. *Mech. Mater.* 12, 17-24.

"Prediction is very difficult, especially about the future."

Niels Bohr

Danish physicist (1885 - 1962)

APPENDIX III: PAPER 3

Inverse rock physics modelling

Tor Arne Johansen, Erling Hugo Jensen, Gary Mavko and Jack Dvorkin.

In preparation to be submitted to *Geophysics,* 2011.

III

Inverse rock physics modelling

Tor Arne Johansen[1, 2], Erling Hugo Jensen[1], Gary Mavko[3] and Jack Dvorkin[3].

ABSTRACT

Seismic reservoir characterization requires a transform of seismically derived properties such as P and S wave velocities, acoustic impedances, elastic impedances or other seismic attributes into parameters describing lithology and reservoir conditions. A myriad of different rock physics models have been developed to obtain this link. Their relevance is however regulated by the type of lithology, porosity range, textural complexity, saturation conditions and the dynamics of the pore fluid. Since the number of rock physics parameters is often higher than the number of seismic parameters, this is known to be an underdetermined problem with non-unique solutions. In this paper, we discuss the framework of inverse rock physics modeling which aims for direct quantitative prediction of lithology and reservoir quality from seismic parameters, but where also non-uniqueness and data error propagation are handled. The procedure is based on a numerical reformulation of rock physics models so that the seismic parameters are input and the reservoir quality data are output. The modeling procedure can be used to evaluate the validity of various rock physics models for a given data set. Furthermore, it provides the most robust data parameter combinations to use for either porosity, lithology and pore fluid prediction, whenever a specific rock physics model has been selected for this cause.

INTRODUCTION

Robust methods for the estimation of lithology and reservoir quality of subsurface rocks from acoustic or seismic data are important in both static and dynamic reservoir characterization. Essentially this process requires a transform of the seismically derived properties as P and S wave velocities, acoustic impedances, elastic impedances or other seismic attributes into parameters describing the lithology and reservoir conditions, i.e. porosity, fluid saturation, and fluid drainage potential. Furthermore, in reservoir monitoring the surveillance of the temporal variations of the fluid pressure and fluid saturation within a reservoir unit during production is key information for obtaining increased oil recovery.

[1] Department of Earth Science, University of Bergen, Bergen, Norway.
[2] NORSAR, Bergen, Norway.
[3] Department of Geophysics, Stanford University, California, USA.

Due to the large variations in physical properties and geometrical distributions of the constituents, the physical behavior of rocks accordingly covers a large span, e.g. from behaving mechanically like a fluid to being nearly incompressible. Correspondingly a myriad of different rock physics models have been developed, but usually their applications are regulated by the type of rock, porosity range, textural complexity, saturation conditions and/or dynamics of the pore fluid (frequency effects) et cetera. For instance, contact theories (CT) (Walton, 1987; Digby, 1981; and Mindlin, 1949) and contact cement theory (CCT) (Dvorkin and Nur, 1996) are combined with the Gassmann model (Gassmann, 1951) to derive the elastic properties of fluid-filled high-porous unconsolidated or weakly consolidated sediments. These theories have been demonstrated to predict quite confidently the elastic properties of pure quartz sandstones to shaley sandstones (Avseth et al., 2005). Another set of models referred to as inclusion models relate to more consolidated rocks as the textural descriptions to a larger degree pinpoint the shapes of pores and their geometrical orientations (Jakobsen et al., 2003; Berryman, 1992; Sheng, 1990; Kuster Toksöz, 1974). Such models have also been shown applicable for predicting elastic properties of shales (Hornby, 1994) and carbonates (Agersborg et al., 2007), but also for compacted sandstones (Dræge et al., 2006). Yet several hybrid approaches are used to model transitions of the elastic properties from one model domain to others using bounding methods (Avseth et al., 2010; Dræge et al., 2006). Finally, a range of empirical models have been suggested for the same cause (Mavko et al., 2008).

An ideal rock physics model should to a maximum degree capture the underlying physics in the derivation of the overall physical properties as well as providing good predictions of these when reservoir properties are perturbed. However, for model verification and applications these demands are less ideal. The need for extracting geometrical details of the small-scale rock texture in describing the dynamic stress distribution (e.g. related to pore fluid flow) increases the number of required model parameters, and, thus, complicates the ability to perform controlled laboratory experiments.

The imbalance in the number of model parameters (often high) to the number of available data parameters (usually low) counteracts a proper formulation of an inverse rock physics model. Accordingly, the estimation of reservoir quality from seismic data suffers from being a highly underdetermined problem; thus contributing to give non-unique solutions. Furthermore, since we know that e.g. the P-wave velocity and bulk modulus vary nonlinearly with e.g. gas-to-oil saturation, this also states that this is a nonlinear problem.

In spite of these problems, several approaches are however used to make predictions of lithology and reservoir quality data from geophysical measurements. The simplest way is by cross plotting the observational data along with modeled data using a suite of rock physics theories, and by studying correlations within these plots one can make

interpretations of the rock properties. This is basically the foundation of the Rock Physics Templates (RPT) described by Ødegaard and Avseth (2004). Statistical methods can also be used where the concept is to obtain statistical correlations based on data fitting of a significant set of training data where both data and rock parameters are well described, and which subsequently are used for lithology and reservoir characterization.

In this paper we propose another strategy referred to as inverse rock physics modeling for estimation of lithology and other rock properties from seismic parameters. The basic idea is to numerically restructure the rock physics model so that the typical observational data are the input parameters and the corresponding rock physics parameters are output. The approach is flexible with respect to both which data parameters to use for the estimation and how they are combined. It also provides the possibility to model error estimates of the reservoir properties whenever uncertainties are attached to the input data. The paper is organized as follows. We first review the basic concepts of the method and then discuss some possible areas of application. The focus is to review the methodology itself, and less attention is paid on the numerical techniques used for solving the various tasks. However, along with the examples we briefly discuss strategies for its implementation.

MODELING ROCK PHYSICS CONSTRAINTS

In the following we use the term data parameter to refer to the kind of measurement we consider. In rock physics analysis of isotropic rocks these are usually P-velocity (V_P,), S-velocity (V_S), P and S acoustic impedances (ρV_P and ρV_S), V_P/V_S, bulk modulus (K), shear modulus (μ), the Poisson ratio (σ) or combinations of these. When V_P, V_S, and ρ are known, the two elastic moduli are given from

$$K = \rho\left(V_P^2 - \frac{4}{3}V_S^2\right), \tag{1}$$

and

$$\mu = \rho V_S^2. \tag{2}$$

We use the term model parameter to represent quantities that describe lithology or reservoir quality. For siliciclastic rocks usual parameters to consider are porosity (ϕ), pore fluid saturation (S) (pore volume fractions of the pore fluids), and the clay-to-sand fraction (C). Additional model parameters will be the elastic and density parameters of all the minerals and fluids composing the rock, as well as parameters describing the pore space properties. If higher frequency effects are to be studied, parameters describing pore fluid dynamics (viscosity and permeability) are needed.

Along with examining the concepts of the method, we will illustrate the basic principles through simple numerical examples. In this we are elaborating on how to estimate 3 model parameters with the use of 1, 2 or 3 data parameters. The data parameters considered in this example are usually K, μ and ρ, but sometimes we will compare results using V_P, V_S and ρ. The model parameters to be evaluated in the examples are porosity, clay-to-sand fraction and gas-to-water saturation. The rock physics models applied for the numerical examples are based on differential effective medium theories (Berryman, 1992), contact theory (Walton, 1987), contact cement theory (Dvorkin and Nur, 1996) and bounding methods (Walpole, 1966a,b; Hashin and Shtrikman, 1963), and they are briefly explained in Appendix A.

The model transform

A rock physics model provides a transform of the model parameters to the data parameters. Thus, since essentially many rock physics models can be applied we can use an index (k) to separate them. Using vector formalism, a forward rock physics modeling for M model and N data parameters, may be given by

$$\vec{R}_k(\vec{m}) = \vec{d}, \tag{3}$$

where $\vec{m} = (m_1, m_2, ..., m_M)$ and $\vec{d} = (d_1, d_2, ..., d_N)$ are the model and data parameters respectively, while $\vec{R}_k = [R_{k1}(\vec{m}), R_{k2}(\vec{m}), ..., R_{kN}(\vec{m})]$, i.e. the component $R_{ki}(\vec{m})$ is a rock physics formulae providing the data parameter d_i from $\vec{m}$. An estimation of rock properties from the data parameters thus formally requires an inverse rock physic model, so that

$$\vec{R}^{-1}{}_k(\vec{d}) = \vec{m}. \tag{4}$$

However, since often $M > N$ and that there are no linear dependence of the model parameters, and, furthermore, $\vec{R}_k$ may represent a nonlinear mapping of $\vec{m}$ onto $\vec{d}$, generally there exist no $\vec{R}_k^{-1}$. Thus, a parameter estimation procedure must be based on a set of constraints relating model parameters to data parameters. In our case we use the forward model to generate an M-dimensional space of data for each data parameter d_i, where each of the various model parameters m_j (j=1,...,M) takes L_{m_j} values, i.e. $m_{jl} = m_{j,\min} + (l-1)\Delta m_j$ with $\Delta m_j = (m_{j,\max} - m_{j,\min})/(L_{m_j} - 1)$ and where $m_{j,\min}$ and $m_{j,\max}$ are the predefined minimum and maximum values of this parameter. We denote this as a discrete forward rock physics model. Let $\hat{D}_i(\vec{m})$ denote such a discrete model, representing a sampled scalar field of the data parameter d_i, where the model parameters are

coordinates and varied as described above. We hereafter denote $\hat{D}_i(\vec{m})$, i=1,...,N, as a set of rock physics constraints. Figures 1a, b, and c show a 3D representation of modeled constraints for the bulk modulus (K), shear modulus (μ) and density (ρ) obtained from a Differential Effective Model (DEM) (Berryman, 1992) with constituent parameters as defined in Table 1 and pore geometry defined in Table 2, and using 26 equidistant values for the model parameters where $0 \le \phi \le 0.4$, $0 \le S \le 1.0$ and $0 \le C \le 1.0$.

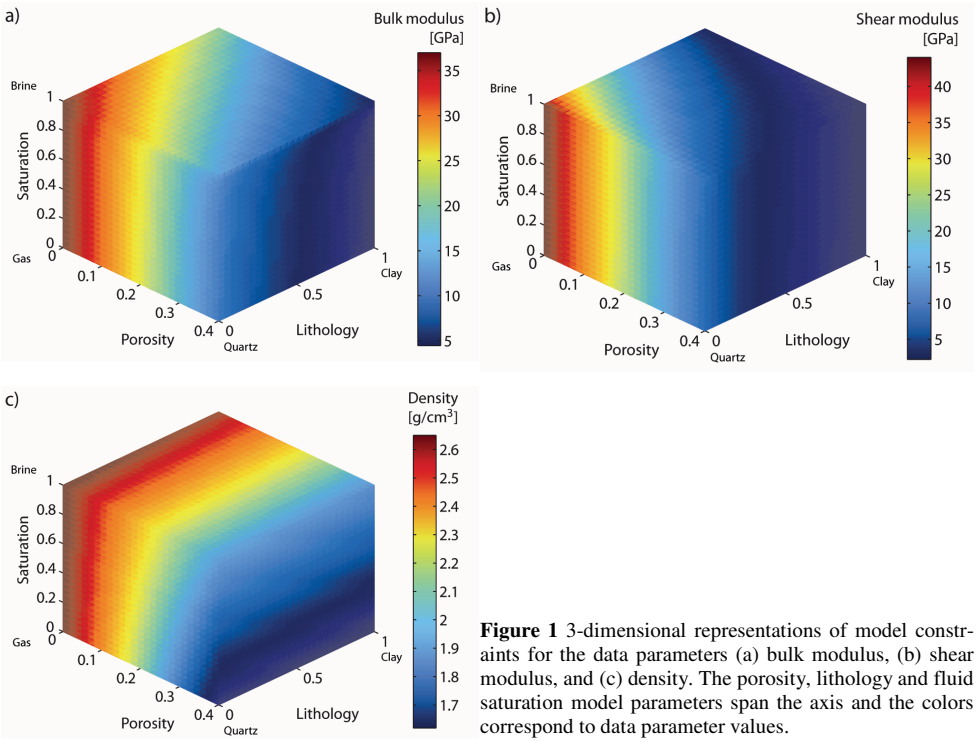

Figure 1 3-dimensional representations of model constraints for the data parameters (a) bulk modulus, (b) shear modulus, and (c) density. The porosity, lithology and fluid saturation model parameters span the axis and the colors correspond to data parameter values.

Table 1 Constituent properties for the various examples until and including the synthetic modeling.

Constituent	**Density [g/cm^3]**	**Bulk moduli [GPa]**	**Shear moduli [GPa]**
Quartz	2.65	37	44
Clay	2.6	21	7
Brine	1.017	2.62	-
Gas	0.146	0.0417	-

Table 2 Pore model geometry for the various examples until and including the synthetic data case.

Aspect ratio spectrum	1.0000	0.5000	0.1000	0.0100	0.0010	0.0001
Concentration	0.9254	0.0579	0.0149	0.0015	0.0002	0.0001

RESAMPLING ROCK PHYSICS CONSTRAINTS

We now perform a resampling of the discrete rock physics model $\hat{D}_i(\vec{m})$ with the aim to extract all the model parameter combinations corresponding to a set of fixed data parameter values. In a 2D-model this corresponds to extracting contours, in a 3D model the parameter combinations are often described by surfaces, and so forth. In Figures 2a and b examples of resampling two values of the bulk modulus constraint cube of Figure 1a at saturation S=0 and S=1 are illustrated, while the corresponding correlations of porosity ϕ and lithology C are shown in Figure 2c. In order to obtain relative simple topological properties of the resampled data from the data parameters, it is favorable to organize the forward rock physics model, so that, eventually, the data parameters are monotonically varying functions of the model parameters. Hence, in the 3D example of Figure 1 we can see, for instance, that bulk modulus K is monotonically changing with all the model parameters. We will further debate this issue in the discussion part.

Before resampling, the minimum ($d_{i,\min}$) and maximum ($d_{i,\max}$) values of $\hat{D}_i(\vec{m})$ are retrieved. Subsequently, resampling is performed at data parameter values $D_{ij} = d_{i,\min} + (j-1)\Delta d_i$ with $\Delta d_i = (d_{i,\max} - d_{i,\min})/(L_{d_i} - 1)$ and j=1, L_{d_i}, where L_{d_i} denotes a predefined number of values of the particular data parameter to be extracted. The scalar D_{ij} annotates the j-th value of the data parameter d_i.

Essentially, the extracted model parameter data for one specific data parameter value represent an M-dimensional tabulation defining a correlation of the model parameters. We therefore define the tabulated function obtained for data parameter D_{ij} as the model correlation function $\varphi_{D_{ij}}(\vec{m})$. Figure 3 shows the two model correlation functions (in this case 3D surfaces) obtained for two bulk moduli values K_1=17 GPa and K_2=25 GPa by resampling the bulk constraints of Figure 1a.

CONCEPT OF INVERSE ROCK PHYSICS MODELING

We can now use the model correlation functions $\varphi_{D_{ij}}(\vec{m})$ to obtain the rock physics solutions for any data parameter value $\hat{d}_i$, denoted $\varphi_{\hat{d}_i}(\vec{m})$, whenever $d_{i,\min} \le \hat{d}_i \le d_{i,\max}$ by performing a careful interpolation. The simplest way of locating a solution is by a linear interpolation using only $\varphi_{D_{ij}}(\vec{m})$ and $\varphi_{D_{ij+1}}(\vec{m})$ where $D_{i,j} \le \hat{d}_i \le D_{i,j+1}$, i.e.

$$\varphi_{\hat{d}_i}(\vec{m}) = \varphi_{D_{ij}}(\vec{m}) + \frac{(\hat{d}_i - d_{ij})}{(d_{ij+1} - d_{ij})}\left[\varphi_{D_{ij+1}}(\vec{m}) - \varphi_{D_{ij}}(\vec{m})\right]. \quad (5)$$

Say we believe in a specific rock physics model, and that it has been resampled as described in the previous section. Now we want to find the rock physics parameters

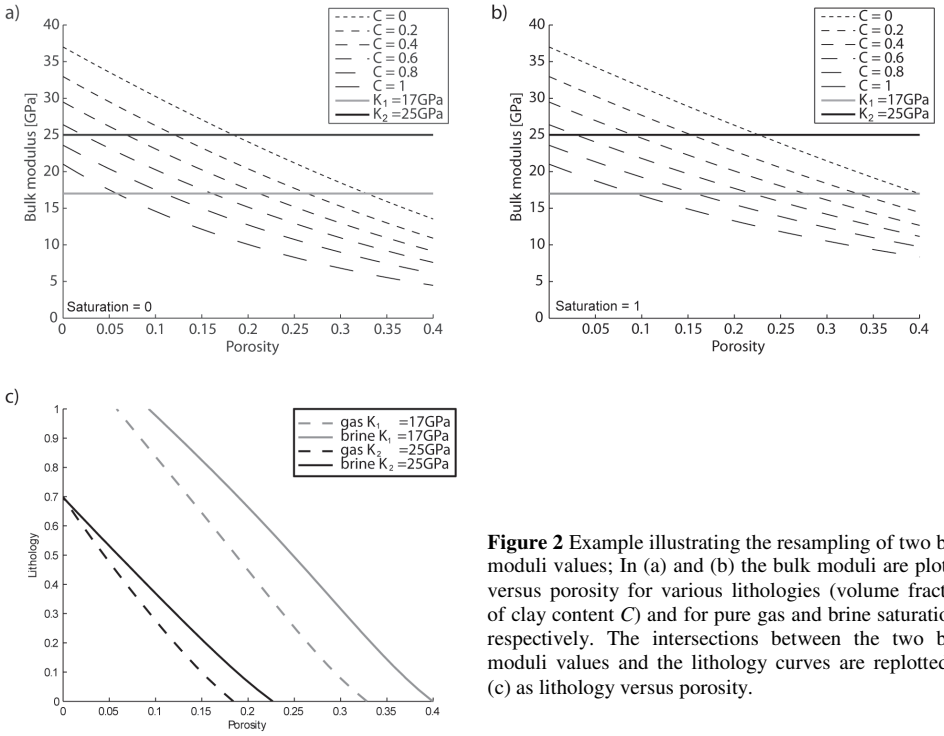

Figure 2 Example illustrating the resampling of two bulk moduli values; In (a) and (b) the bulk moduli are plotted versus porosity for various lithologies (volume fraction of clay content *C*) and for pure gas and brine saturations, respectively. The intersections between the two bulk moduli values and the lithology curves are replotted in (c) as lithology versus porosity.

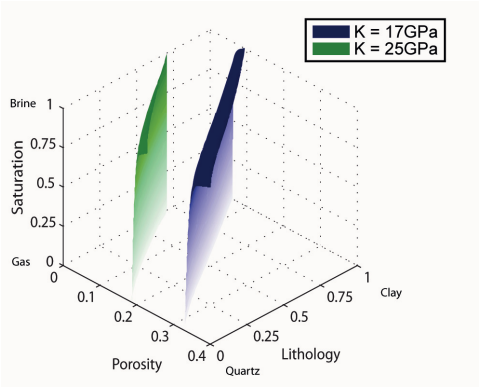

Figure 3 The bulk modulus correlation function plotted for two moduli values. They form surfaces in the porosity, lithology and fluid saturation coordinate system.

consistent with one pair of data parameters $\hat{d}_i$ and $\hat{d}_k$. The solution to this problem is accordingly

$$\varphi_{\hat{d}_i}(\vec{m}) - \varphi_{\hat{d}_k}(\vec{m}) = 0, \tag{6}$$

which is simply the intersection of the two model correlation functions. Let the solution obtained using one pair of data parameters be denoted $\varphi_{\hat{d}_i\hat{d}_k}(\vec{m})$, i.e. $i \neq k$. In Figure 4a the intersection considering one bulk modulus and one shear modulus is shown. We clearly see the nonlinearity of the problem as the intersection curve becomes strongly curved. A combination of the bulk modulus and a density value is seen in Figure 4b. Now the intersection curve becomes quite different, clearly pinpointing the consequence of facing an underdetermined problem. However, the inverse modeling provides us with all combinations of model parameters consistent to a given set of data parameters. Any additional information about any of the three model parameters would directly gain in defining a more constrained solution. Moreover, information about two or more of the model parameters may furthermore help in rejecting or verifying the use of the applied rock physics model itself.

When a third data parameter $\hat{d}_m$ is added, the solution is analogously found by locating the intersections of the various solutions of equation 6, i.e. though three intersections we may find $\varphi_{\hat{d}_i\hat{d}_k}(\vec{m})$, $\varphi_{\hat{d}_i\hat{d}_m}(\vec{m})$, and $\varphi_{\hat{d}_k\hat{d}_m}(\vec{m})$, but only two of these are needed for obtaining the solution. Hence, it is given by

$$\varphi_{\hat{d}_{n1}\hat{d}_{n2}}(\vec{m}) - \varphi_{\hat{d}_{n1}\hat{d}_{n3}}(\vec{m}) = 0, \tag{7}$$

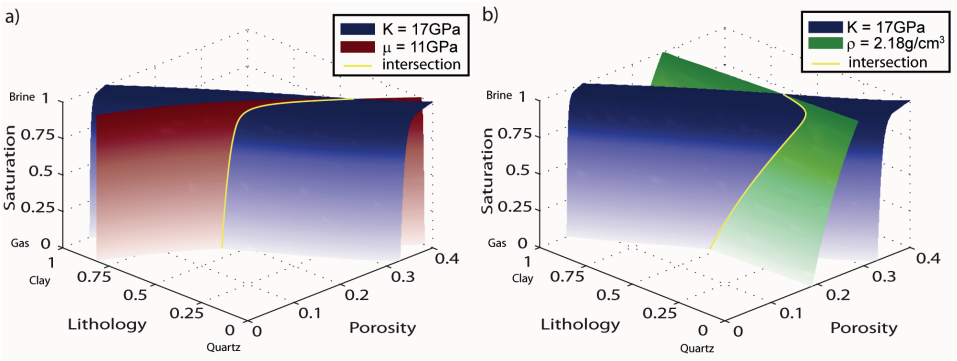

Figure 4 Plot of correlation functions and intersections between (a) bulk modulus K and shear modulus μ and (b) K and density ρ.

i.e. *i*, *k* and *m* can be associated with any (but only one) of the indices n_1, n_2 and n_3. The solution can furthermore be defined as $\varphi_{\hat{d}_{n_1}\hat{d}_{n_2}\hat{d}_{n_3}}(\vec{m})$. We can now build a hierarchic system for obtaining the solutions $\varphi_{\hat{d}_1\hat{d}_2\ldots\hat{d}_N}(\vec{m})$ in case *N* different data parameters are combined

$$\varphi_{\hat{d}_{n_1}\hat{d}_{n_2}\ldots\hat{d}_{n_{N-2}}\hat{d}_{n_{N-1}}}(\vec{m}) - \varphi_{\hat{d}_{n_1}\hat{d}_{n_2}\ldots\hat{d}_{n_{N-2}}\hat{d}_{n_N}}(\vec{m}) = 0. \tag{8}$$

Again, each of the indices i=1,...*N* can essentially be associated with n_1, n_2,...n_N. In Figure 5a, the solution of the three model-parameter exercise is defined at the intersection point of the two contour lines. This is furthermore also illustrated in Figure 5b by the intersection

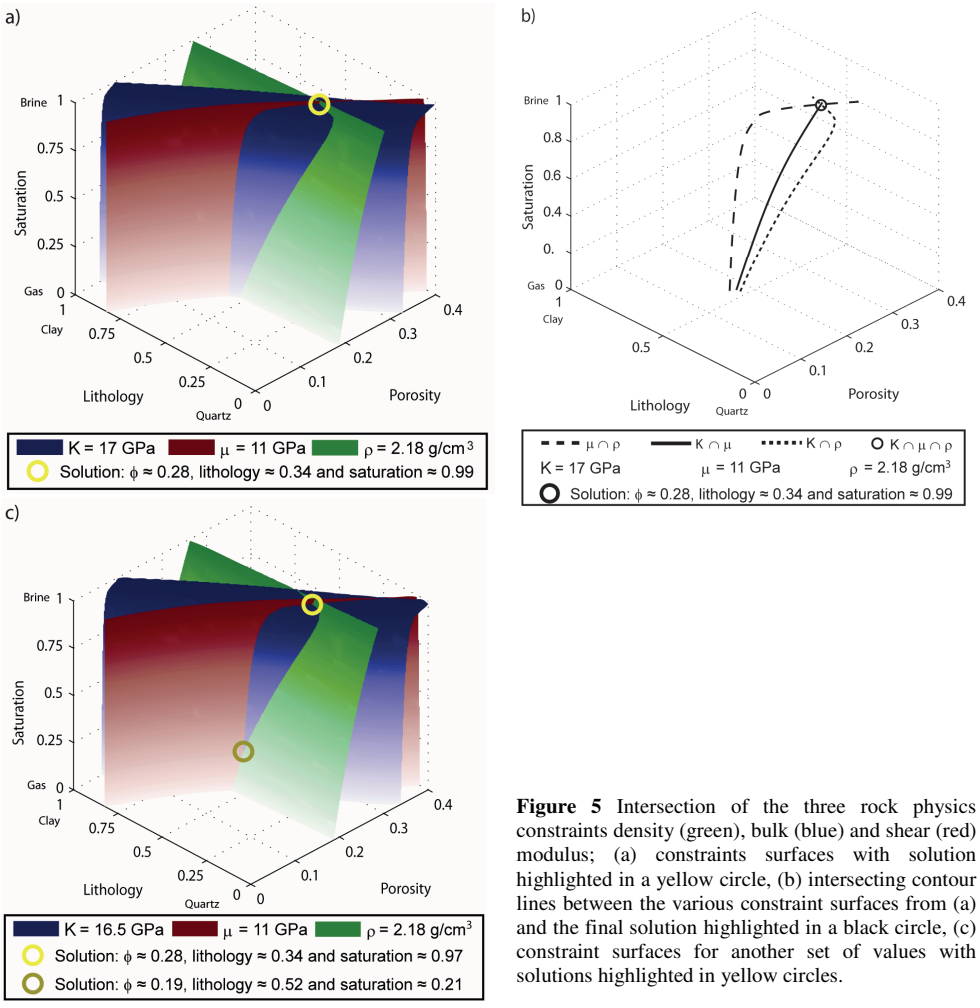

Figure 5 Intersection of the three rock physics constraints density (green), bulk (blue) and shear (red) modulus; (a) constraints surfaces with solution highlighted in a yellow circle, (b) intersecting contour lines between the various constraint surfaces from (a) and the final solution highlighted in a black circle, (c) constraint surfaces for another set of values with solutions highlighted in yellow circles.

point of all three model correlation functions. In this case the solution is unique, while in Figure 5c two intersection points occur. This clearly demonstrates that there is not always a unique solution also in the case when the number of model parameters is equal to the number of data parameters. In this case a rock model where porosity $\phi = 0.19$, saturation $S = 0.21$, and lithology $C = 0.52$ will have the same elastic moduli and density as when $\phi = 0.28$, $S = 0.97$, and $C = 0.34$. This will be further demonstrated in following examples.

Numerically, the choice of parameter combination to use for obtaining stable solutions depends on the local shape of the model correlation functions at the intersection points. This is evident from studying Figure 6a and b where the intersection of the model correlation functions using the density and P-velocity is more stable for small alterations of the P-velocity, compared to when, for instance, combining the P and S velocities. In this example, we can understand the stability – or a measure of the goodness of the solution - by comparing the normal vectors of the model correlation functions (here surfaces) at the intersection points. A well conditioned solution would occur whenever these are, or, close to, orthogonal. Hence, a measure of the conditioning can be obtained by considering the scalar product of the normal vectors. Let $\hat{\nabla}\varphi_{\hat{d}_i}$ and $\hat{\nabla}\varphi_{\hat{d}_j}$ denote the normalized gradient vectors (here also normal vectors) numerically derived from $\hat{D}_i(\vec{m})$ at $\varphi_{\hat{d}_i}(\vec{m})$ and from $\hat{D}_j(\vec{m})$ at $\varphi_{\hat{d}_j}(\vec{m})$ at an intersection point, respectively. Then an appropriate condition of local stability means that the scalar product of the normal vectors

$$\varepsilon_{\hat{d}_i\hat{d}_j} = \left| \hat{\nabla}\varphi_{\hat{d}_i} \cdot \hat{\nabla}\varphi_{\hat{d}_j} \right|, \tag{9}$$

is close to zero. We denote this quantity as the orthogonality factor.

Similarly, we can define a mean orthogonality factor $\bar{\varepsilon}_{\hat{d}_i\hat{d}_j}$ for a combination of the two data parameters by integrating the scalar product along the intersection contour $C = \varphi_{\hat{d}_i\hat{d}_j}(\vec{m})$ and dividing by the length of the contour, i.e.

$$\bar{\varepsilon}_{\hat{d}_i\hat{d}_j} = \frac{1}{|C|}\int_C \varepsilon_{\hat{d}_i\hat{d}_j}\, dC, \tag{10}$$

which accordingly again should be as small as possible.

Figure 7 shows modeled orthogonality factors using equations 9 and 10 for three dual data parameter combinations, e.g. K and μ, V_p/V_s and ρ and V_p/V_s and ρV_p for the example discussed in Figure 5a. Figure 7a reveals that, in this case, the combination of V_p/V_s and ρ in general gives the most stable solutions, while a combination of K and μ provide low stability solutions. However, combining V_p/V_s and ρV_p is only slightly poorer than using

V_p/V_s and ρ. This is further demonstrated in Figure 7b where the mean orthogonality factor is plotted for 6 different data parameter combinations.

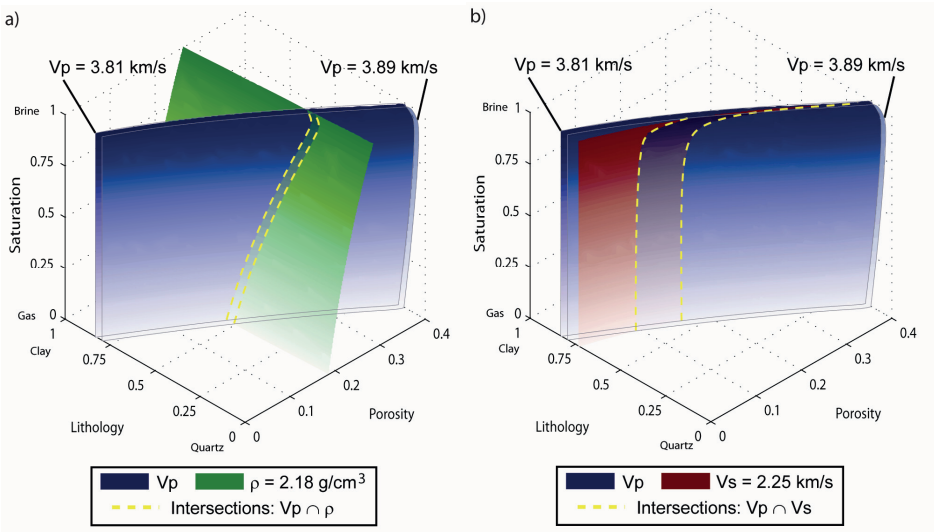

Figure 6 Good (a) and bad (b) conditioned intersections of the constraints density (green), P-wave velocity (blue) and S-wave velocity (red). The P-wave velocity constraint is plotted for two values, which are the same in both figures. The difference in solution sensitivity can be inferred from the displacement of the yellow stippled lines along the intersections of the surfaces.

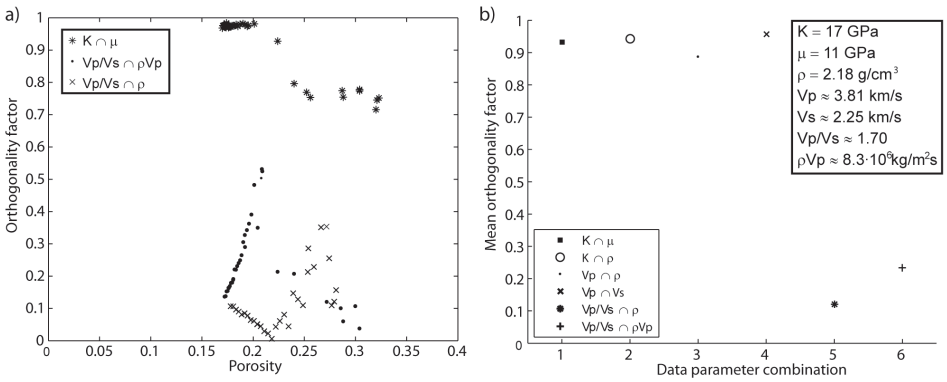

Figure 7 Orthogonality (a) and mean orthogonality factors (b) for various intersections between the bulk modulus (K), shear modulus (μ), density (ρ), P-wave velocity (V_p), S-wave velocity (V_s), P-wave acoustic impedance (ρV_p) and V_p/V_s ratio.

At a solution point $\vec{m}_s$ we may now also estimate the sensitivity of the various rock parameters, i.e. $\Delta\vec{m}_s$ to a perturbation in any of the applied data parameters. Again we use the estimated gradient vectors at the solution points, i.e. $\nabla\varphi_{\hat{d}_i}$, $i = 1,\ldots,N$. Now, say we alter the data parameter d_i with a value δd_i. The intersection point between $\varphi_{\hat{d}_i+\delta\hat{d}_i}$ and, for instance, $\varphi_{\hat{d}_j}$ (see Appendix B) will then displace $\Delta\vec{m}_{j|i}$ from $\vec{m}_s$ and along $\hat{\nabla}\varphi_{\hat{d}_i}$ as

$$\Delta\vec{m}_{j|i} = \left(\frac{\delta d_i \left|\nabla\varphi_{\hat{d}_i}\right|}{\sin\theta} \right) \frac{\hat{\nabla}\varphi_{\hat{d}_i} - \hat{\nabla}\varphi_{\hat{d}_j}\cos\theta}{\left|\hat{\nabla}\varphi_{\hat{d}_i} - \hat{\nabla}\varphi_{\hat{d}_j}\cos\theta\right|}, \tag{11}$$

with

$$\theta = \arccos(\hat{\nabla}\varphi_{\hat{d}_i} \cdot \hat{\nabla}\varphi_{\hat{d}_j}). \tag{12}$$

Thus, a weighted solution for the displaced solution $\vec{m}_s$ due to a perturbation δd_i can be written as

$$\vec{m}_s(\delta d_i) = \vec{m}_s + \frac{1}{M}\sum_{j=1}^{N} \left|\Delta\vec{m}_{j|i}\right| \Delta\vec{m}_{j|i}, \tag{13}$$

where $M = \sum_{j=1}^{N} \left|\Delta\vec{m}_{j|i}\right|$.

Figure 8 displays reservoir properties (i.e. ϕ, C and S) obtained by inverse modeling given the two sets of values for the bulk modulus, shear modulus, and density listed in Table 3. The set of values in Figure 8a, which is equivalent to the high saturation point in Figure 5c, represents a slightly softer material than in Figure 8b. Furthermore, the figures show the displacements of the solutions (according to equation 11) due to ±5% deviations in each of the input parameters. We readily see the nonlinear nature of the problem as the solutions for a perturbation in one data parameter do not become symmetric about the initial solution point.

Using equation 13 we can furthermore also evaluate the partial derivatives of any model parameter with respect to any data parameter, i.e. $\frac{\partial m_j}{\partial d_i}$ which provides a simple way of modeling data error propagation.

In case the inverse modeling is to be applied on a larger data set, the numerical performance can be improved using a proximity search. In this case the solver allows a

certain tolerance towards the intersection of the model correlation functions. Hence, in addition to the solutions where the model correlation functions intersect, solutions up to a certain distance (delta) in the model parameter domain are included. In the real data case study to follow in next section, we use this latter implementation.

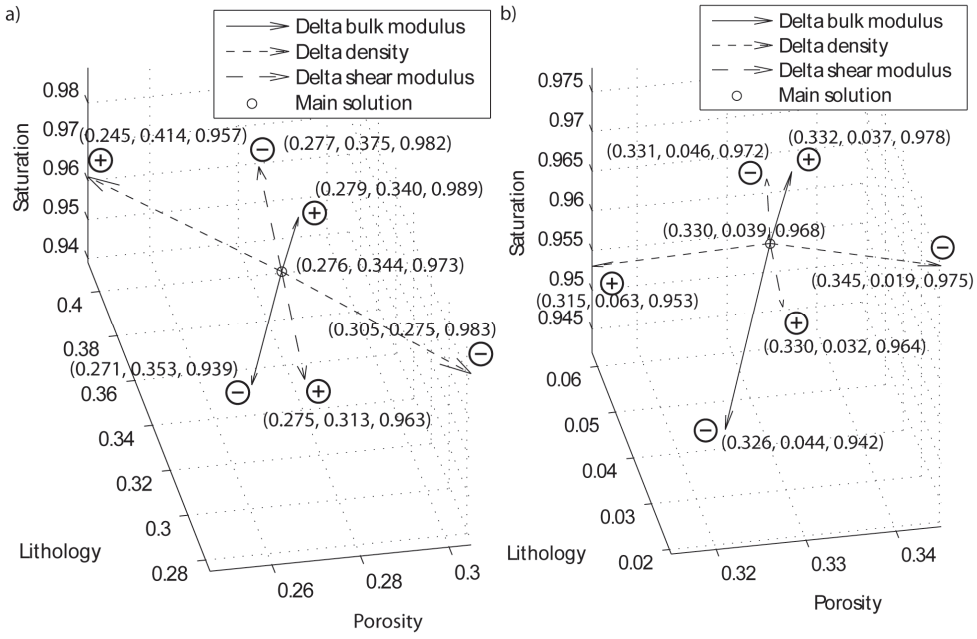

Figure 8 Sensitivity analysis when perturbing the density, bulk and shear moduli for two sets of data parameters values (see Table 2). The main value is plotted as a circle, and the perturbed solutions are plotted as arrows identified with a plus and minus symbol for the higher and lower perturbed values, respectively.

Table 3 Data parameter values used in the inverse modeling shown in Figure 8.

Figure	Data parameters	Initial value	– perturbed value	+ perturbed value
8a	Bulk modulus [GPa]	16.5	15.88	17.13
	Shear modulus [GPa]	11	10.53	11.46
	Density [g/cm^3]	2.18	2.14	2.22
8b	Bulk modulus [GPa]	18	17.62	18.38
	Shear modulus [GPa]	15	14.72	15.29
	Density [g/cm^3]	2.1	2.08	2.12

AREAS OF APPLICATION

The main idea of the inverse rock physics modeling is to provide a flexible and consistent framework for the evaluation of lithology and reservoir quality data from geophysical (seismic) parameters. Flexible in the sense that one may consider different rock physics models, use various combinations of input data parameters, and even obtain results when only one data parameter is available. Estimation of rock physics parameters from seismic parameters is in general a strongly underdetermined problem. Here, this problem is handled by displaying all possible solutions corresponding to the selected set of data parameters input. Furthermore, it provides a simple way to test for the sensitivity of the obtained reservoir quality properties due to errors in the various input data parameters. Hence, error bars may be modeled for the estimated reservoir quality data when error bars of the measured data parameters are available. Also, it may be used as a diagnostic tool in evaluation of which parameter combinations to use for a specific estimation problem by considering the stability criteria in equations 9 and 10.

An alternative way of studying effects of data parameter errors is by a Monte Carlo simulation. Now an ensemble of values following some probability distribution function (PDF) is first established for each data parameter, which, subsequently, through inverse rock physics modeling provides the distributions of the reservoir parameters. Figure 9 shows an example of modeled Gaussian PDFs of the data point (K, μ, and ρ) in Figure 5a, with standard deviations of each data parameter set to 1 unit. Again, we see the complexity of the estimation problem due to the non-symmetric signature of the solution distributions, and, also, that there for some values are two solutions.

Figure 10 shows synthetic logs of V_p, V_s, ρ, K, and μ for 27 different reservoir conditions, where ϕ, C and S have been varied systematically to cover a wide range of reservoir parameters. We now use the synthetic data to reproduce these reservoir conditions by inverse rock physics modeling using different data parameter combinations of the log data. Figures 11a, b, and c show the true reservoir parameters and results obtained, in case of considering an underdetermined problem, by applying various two data parameter combinations, i.e. K and μ, K and ρ, and μ and ρ. The solutions fluctuate differently about the solution points indicating that the various parameter combinations will result in different variances of the reservoir estimates, e.g. comparing Figures 11a and c, we see that most of the lithology estimates in Figure 11a are under-predicted, while in Figure 11c they are over-predicted, and correspondingly, the opposite trend is seen for the porosity.

In Figure 12 we use the three data parameters K, μ, and ρ to reproduce the reservoir conditions, but now also various uncertainties in the input data are included. Four situations are considered: a) Noise-free data, b) K (±5%), μ (0%), and ρ (0%), c) K (0%), μ

(±5%), and ρ (0%), and d) K (0%), μ (0%), and ρ (±5%). For noise-free data (Figure 12a) we see that often two reservoir models occur. Particularly, we can see at for sample Id 3 the two solutions indicate almost opposite fluid properties, with rather minor differences in lithology and porosity. For the use of seismic parameters in pore fluid discrimination, this example is worth noticing. It also pinpoints the necessity of doing this type of modeling studies in order to explore the uniqueness of interpreted reservoir property data whenever a rock physics model has been selected for this cause.

Another problem for obtaining a trustworthy prediction of reservoir properties from seismic parameters is to evaluate the validity of the rock physics model(s) considered for the analysis of the data. In the following example we again use the inverse modeling to screen a set of different rock physics models, to test their relevance. For simplicity we again use the differential effective medium (DEM) model to produce the rock physics constraint data, but aside from varying ϕ, S, and C, also the pore structure is systematically altered. As

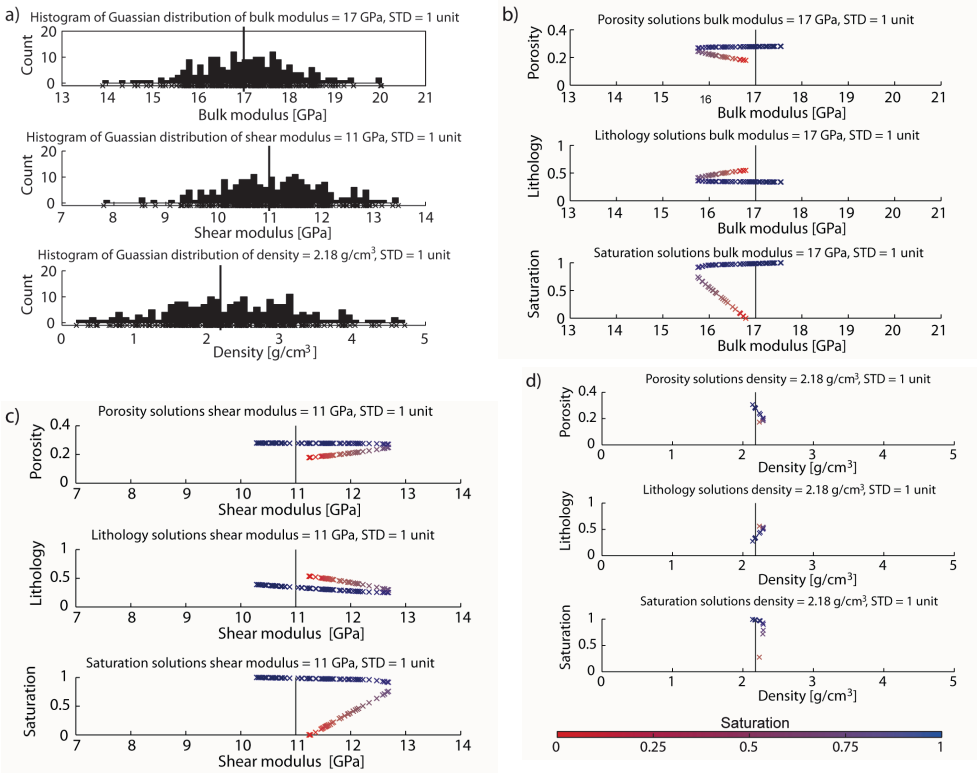

Figure 9 Monte Carlo simulation with (a) probability density distribution (PDF) for the density, bulk and shear moduli with inverse modeled porosity, lithology and fluid saturation solutions when perturbing (a) the bulk modulus, (b) the shear modulus, and (c) the density.

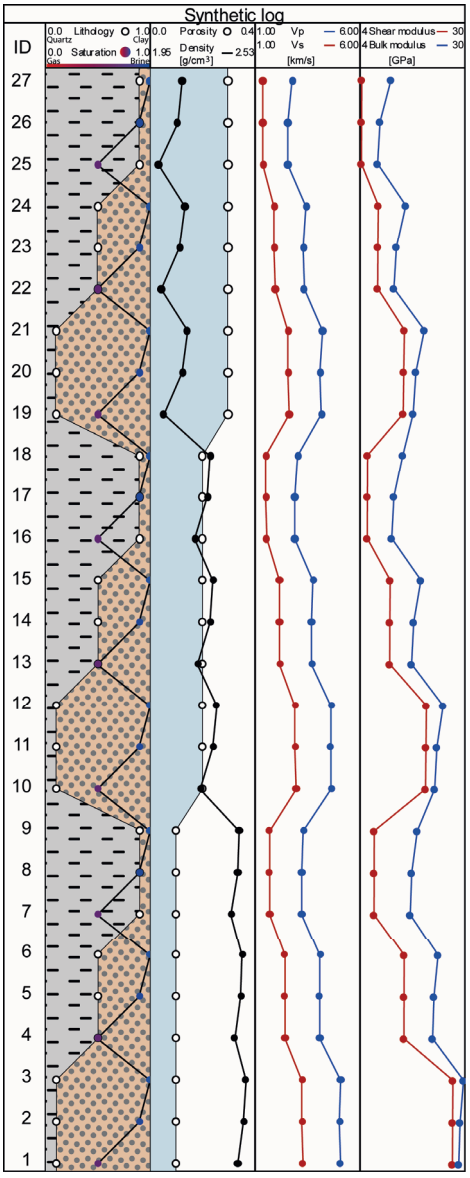

Figure 10 Synthetic log with model and corresponding data parameters.

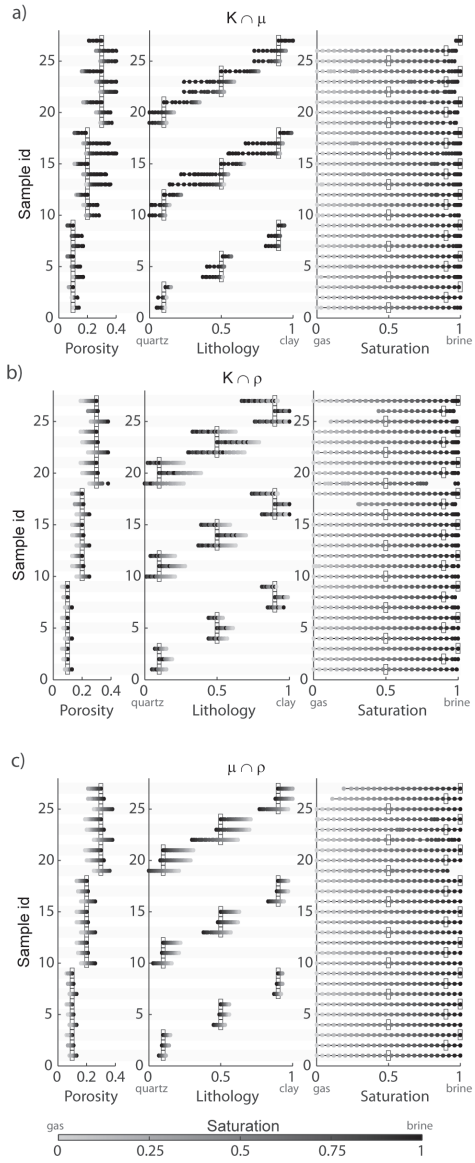

Figure 11 Model parameter solutions from inverse modeling using (a) bulk modulus K and shear modulus μ, (b) K and density ρ, and (c) μ and ρ. The correct model parameters are plotted as squares and the modeled solutions as dots where the gray gradient corresponds to fluid saturation. The dimmed zebra stripes on the background separate the various data samples.

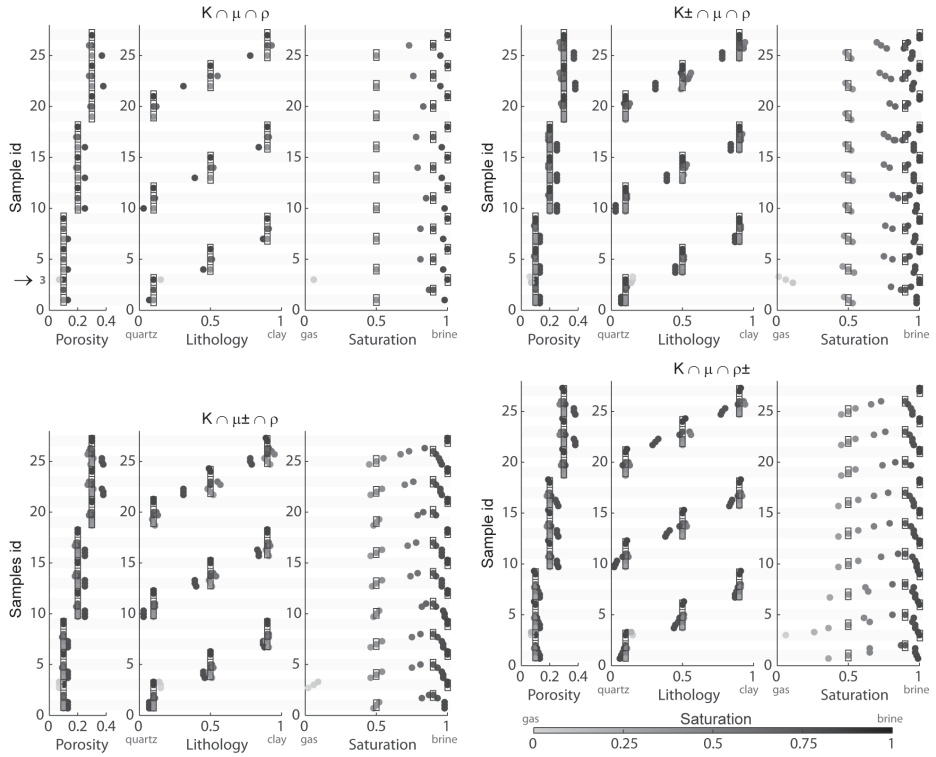

Figure 12 Model parameter solutions from inverse modeling using bulk modulus K, shear modulus μ, and density ρ, (a) for the noise-free data, (b) when perturbing K, (c) when perturbing μ, and (d) when perturbing ρ. The correct model parameters are plotted as squares and the modeled solutions as dots where the gray gradient corresponds to fluid saturation. The solutions from the perturbations are plotted above and below the noise-free solution for positive and negative perturbations, respectively. The dimmed zebra stripes on the background separate the various data samples.

such, we now consider the pore model as a fourth dimension in the inverse modeling scheme. Twenty pore models are made, where all (except from one) have the same pore geometries (spectrum of aspect ratios), while the individual volume concentrations of the pore geometries vary from one model to another. We use a pore model index l to define the volume concentration according to

$$c_l(\alpha_i) = \begin{cases} (N+1-l)c_l(\alpha_i)/N; i>1 \\ 1-\sum_{i=2}^{N\alpha} c_l(\alpha_i); i=1, \end{cases} \tag{10}$$

where N_α is the number of different pore geometries, i=1 denotes spherical pores (i.e. aspect ratio α_1=1), and the $c_{10}(\alpha_i)$'s are as defined for the rock physics model the synthetic

data is generated from (see Table 2). An increasing pore model index now means increasing pore model stiffness and *l=N* denotes spherical pores only. We now use $R_1,...R_N$ to separate the various rock physics models. Figure 13 shows the results of inverse modeling sequentially considering $R_1,...R_N$ using K, μ, and ρ from the synthetic log of Figure 10 as input. The reservoir properties obtained vary quite strongly with the selected pore model, which is seen particularly to influence on the estimation of fluid properties. The example pinpoints the importance of using a proper pore model when performing seismic pore fluid prediction.

In the final example, we consider a sequence of real well data from the Glitne field in the North Sea (Avseth et al., 2005). Again, our objective is to evaluate possible rock physics models to use for characterizing a reservoir unit. A rock physics study of the reservoir has previously been reported in Avseth et al., (2005). The log data are shown in Figure 14a, and cover an oil saturated zone with two facies identified IIb and IIc. Facies IIb is clean, massive sandstone with clay coatings, but with some presence of pore-filling clay. Facies IIc is plane-laminated sandstone with a higher content of pore-filling clay and with a dominant grain size generally smaller than in IIb. Table 4 shows recommended constituent properties to use for rock physics modeling of the reservoir units (Avseth, 2005). First, we adopt the procedure of Avseth et al. (2005) to define a first set of rock physics constraint data (for details, see Appendix A): The Hashin-Shtrikman (1963) lower bounds are used to calculate the effective moduli of the mixed solid mineral components. Wood's (1955) equation is used to obtain the bulk modulus of the mixed fluid phase. The elastic moduli of the dry rock are modeled using the Hashin-Shtrikman-Walpole (Walpole, 1966) upper bounds with the effective mineral elastic moduli as the zero porosity end-

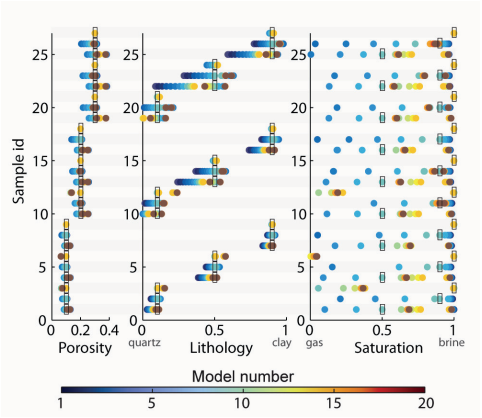

Figure 13 Inverse modeling for rock physics models with various pore geometries, using bulk modulus, shear modulus, and density as input data parameters. The correct model parameters correspond to rock physics (pore) model number ten and are plotted as squares. The modeled solutions as dots where the color code corresponds to the various rock physics models, i.e. pore geometries. The dimmed zebra stripes on the background separate the various data samples.

Table 4 Constituent properties recommended using in the Glitne data modeling.

Constituent	Density [g/cm^3]	Bulk moduli [GPa]	Shear moduli [GPa]
Quartz	2.65	36.8	44
Clay	2.6	17.5	7.5
Brine	1.09	2.8	-
Oil	0.78	1.005	-

member. The high porosity end-member at $\phi = 0.4$, we calculate using Hertz-Mindlin theory (Mindlin, 1949) using a coordination number of 8.3, which is in accordance with data compiled by Murphy (1982). Finally, we perform a Gassmann (1951) fluid substitution to calculate the effective moduli of the fluid saturated rock.

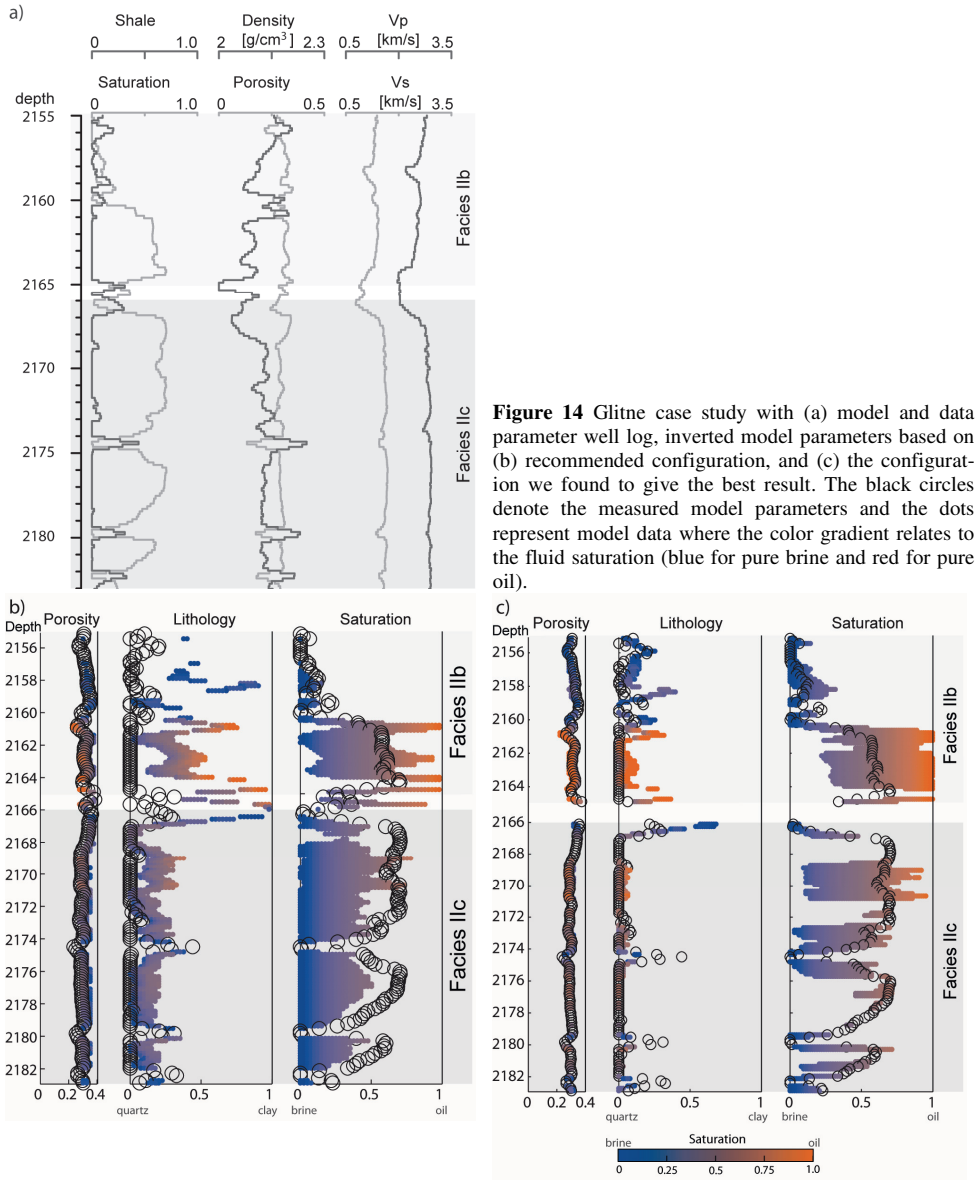

Figure 14 Glitne case study with (a) model and data parameter well log, inverted model parameters based on (b) recommended configuration, and (c) the configuration we found to give the best result. The black circles denote the measured model parameters and the dots represent model data where the color gradient relates to the fluid saturation (blue for pure brine and red for pure oil).

The estimated reservoir properties from an inverse modeling using V_p, V_s, and ρ are shown in Figure 14b where black circles identify the measured reservoir parameters and colored dots those modeled. The large number of identified solutions, even when using three data parameters, is due to the solver we have used which identifies solutions in regions where the isosurfaces are within certain proximity of each other. We see that porosity is generally well predicted, while clay volume is over-predicted and oil-saturation is under-predicted. Extending the library of rock physics constraint data by also perturbing the coordination number, improved the results when using an unrealistic low coordination number (~1) for the high porosity end-member. Also, improved results were obtained using the Hashin-Shtrikman-Walpole lower bound, instead of the upper bound, but then an unrealistic high coordination number (~14) for the high-porosity member was needed.

To possibly improve the results a wide range of rock physics models were used to generate constraint data. We also defined a small perturbation of the clay mineral properties to be allowed. Our final rock physics model differs from the initial one (Avseth et al., 2005) by the following: Instead of Hashin-Shtrikman-Walpole to interpolate between the porosity end-members, we use a DEM model with a pore model as defined in Table 5 and where the inclusions are defined by the physical properties of the high-porous end member. The elastic parameters of the high-porosity end-member were calculated using the model of Walton (1987) and applying a mixed slip factor model (Duffaut, 2010; Bachrach, 2008). A mixed slip-factor model implies a volume weighted averaging of the elastic moduli obtained at rough and zero friction. The best match was obtained using a slip factor of 0.4 for facies IIb and 0.6 for facies IIc, and the mineral properties given in Table 6. Our final results shown in Figure 14c fairly consistently reproduce all the parameters of the reservoir zone. Still, we see that some of the reservoir data (at depths around 2167 m and 2178 m) are not captured. Thus, we have obtained a proper rock physics model, where all the rock physics parameters are in the plausible range of such lithologies.

Table 5 Pore model geometry used in the improved inverse modeling on the Glitne data.

Aspect ratio spectrum	1.0000	0.5000	0.1000	0.0100	0.0010	0.0001
Concentration	0.6419	0.3205	0.0321	0.0050	0.0005	0.0001

Table 6 Constituent properties we found to give the most consistent results when modeling the Glitne data. The highlighted values are the ones we have changed from the recommended configuration in Table 4.

Constituent	Density [g/cm^3]	Bulk moduli [GPa]	Shear moduli [GPa]
Quartz	2.65	36.8	44
Clay	**2.56**	**13**	**4**
Brine	**1.0**	2.8	-
Oil	0.78	1.005	-

DISCUSSION

The basic idea of inverse rock physics modeling is by numerical means to reformulate a rock physics model so we can use various seismic parameters as input and obtain parameters describing lithology and reservoir quality as output. In early exploration only P-wave interval velocities may be known, while subsequent Amplitude Versus Offset analysis and seismic inversion may provide P-wave acoustic impedances and V_p/V_s ratios (alternatively Poisson's ratios and elastic impedances (Connolly, 1999)). In some cases S velocities may be available from pure S-wave reflections (land seismic), or from P-to-S converted waves (long offset marine seismic data). Thus, in wells often both P and S velocities and densities are extracted together with a suite of rock property data. Consequently, a system for inverse rock physics modeling needs to be flexible to the number of input parameters as well as the kind of seismic parameters considered, i.e. any combination of V_P, V_S, and ρ should be possible to apply as often less than three seismic parameters are known. Our examples have been limited to predict reservoir condition based data on elastic moduli, velocities and density, but similar analyses could as well have been based on acoustic and elastic impedances, as well as typical AVO derived attributes (intercept and gradient parameters).

Cross plots of seismic parameters in combination with various rock physics templates are frequently used to do both qualitative and quantitative predictions of lithology and reservoir properties. Even more precise quantitative estimates can subsequently be achieved applying statistical measures of the data points with reference to specific rock physics templates. For details see Avseth et al. (2005). In this approach, there is no particular consistency check of the applied rock physics model. The inverse rock physics modeling automatically checks for this consistency since if no model parameters are found for a specific set of data parameters, the considered rock physics model is rejected. In principle, this approach can be used to sort out the most appropriate (and consistent) rock physics models to be used for characterizing a specific set of data. Hence, if the various rock physics models scrutinized are related to a geological framework (e.g. we usually associate contact models with unconsolidated sediments), such a consistency check can be used to clearly pinpoint the type of lithology, along with the estimated parameters.

The complexity of the numerical routines to be used in deriving resampled constraint data, which is used in the inverse modeling, will depend on the topology of the functional relationships between the data parameters and the various model parameters. To keep this operation relative simple, the forward rock physics model should (if possible) be organized so that the data parameters appear as monotone functions of the various model parameters. In our case, where we mainly consider the data parameters bulk modulus, shear modulus and density, we know that all these are generally constant or monotonically increasing or decreasing with ϕ, S and C. This is also the case when the varying pore model

was inferred as a fourth variable because an increase in the pore model index implies increasing bulk and shear moduli, while the density remains fixed. Similarly, fluid patchiness can be introduced as a fifth variable, e.g. by using a fluid mixing index taking the values j=1,…,N_m. A homogenous mixing is associated with j=1. Index j≥2 annotates that a fraction $(j\text{-}1)/N_m$ of the pore volume (ϕ) contains the pore fluid defined at S=1, while the remaining porosity contains the pore fluid defined at S=1. Increasing fluid mixing index then causes the bulk modulus, shear modulus and density to increase, decrease or remain constant. Among other conditions that can be easily included within the constraint data are the effects of pore pressure, confining pressure and temperature.

For some parameters, as for instance the V_p/V_s it might be difficult to get control of the topology of the data parameters, and thus the numerical implementation of the resampling may be more cumbersome. One solution here is to find the model correlation function for various V_p/V_s–values via the resampled bulk and shear moduli constraints. Then, first by defining an appropriate set of values of K and μ corresponding to a fixed V_p/V_s–ratio, retrieving the two model correlation functions for each pair and locating the intersection between them, will finally provide a model correlation for this specific V_p/V_s–ratio.

The various scales of earth heterogeneities are viewed as a major obstacle for the use of rock physics models in quantitative seismic analysis, e.g. the earth usually occur layered, while rock physics models predict the response of a homogeneous effective medium. However, the rock physics constraint models can to some extent take this into account by establishing a set of upscaled models. Upscaled models, e.g. using Backus averaging, can for instance be made by composing various layering models, where the individual layers are characterized by some rock physics constraints for the relevant (homogeneous) lithology. Finally, the inverse modeling is performed on the basis of the upscaled rock physics models.

CONCLUSIONS

We have presented a framework for inverse rock physics modeling which can serve as a tool in prediction of lithology and reservoir parameters from seismic parameters. The basis of the method is numerical restructuring of rock physics models so that seismic parameters are input and reservoir parameters are output. In general, this is a highly underdetermined problem which has non-unique solutions.

The modeling provides a simple way to display this non-uniqueness, and also to estimate probability distributions of the estimated parameters when error distribution functions are attached to the input parameters. Furthermore, the inverse modeling can be used to obtain a validity check of various rock physics models considering a given set of

data, and to provide the most robust parameter combinations to use for specific reservoir parameter estimation problems.

Our approach was applied to predict reservoir properties from both synthetic and real data. The synthetic data example revealed the severe non-uniqueness of this problem as models with different reservoir properties provided the same set of seismic parameters. For the real data case, inverse modeling were applied to obtain a consistent rock physics model to be used as a transform from seismic parameters to reservoir data for a previously published North Sea case study.

ACKNOWLEDGEMENT

We thank Per Avseth for his input regarding the Glitne case study. We also thank the Norwegian Research Council (Petromaks program) and Statoil for financial support of the doctoral program of Erling Hugo Jensen.

APPENDIX A
ROCK PHYSICS MODELS

Differential effective medium

The differential effective medium (DEM) theory (Berryman 1992; Berryman 1995) is an inclusion based theory taking into account higher order interaction. Here, one of the constituents is considered the host medium while the remaining components are embedded as inclusions. This is an asymmetric model because given the same volume fractions of the constituents, interchanging the host with one of the embedding components result in different elastic moduli. For a two phase composition the elastic moduli can, according to the differential effective medium theory, be solved from the coupled differential equations

$$(1-y)\frac{d}{dy}\left[K^*(y)\right] = \left(K_2 - K^*(y)\right)P_2^*(y), \tag{A-1}$$

$$(1-y)\frac{d}{dy}\left[\mu^*(y)\right] = \left(\mu_2 - \mu^*(y)\right)Q_2^*(y). \tag{A-2}$$

Phase one acts as the host material with bulk moduli $K_1 = K^*(y=0)$ and shear moduli $\mu_1 = \mu^*(y=0)$, while the bulk and shear moduli of phase two is K_2 and μ_2, respectively, and y

is the volume fraction of phase two. The geometrical factors $P_2^*(y)$ and $Q_2^*(y)$ are calculated having phase two as the inclusion material in a host with effective moduli K^* and μ^*.

Hashin-Shtrikman bounds

The Hashin-Shtrikman bounds (Hashin and Shtrikman, 1963) are theoretical upper and lower limits of effective moduli of an isotropic mixture. An interpretation of these two bounds is that one of the constituents forms a shell around the other constituent. The upper limit yields a composition where a stiff shell surrounds a soft core, and the lower limit is where a soft shell surrounds a stiff core. For a mixture of two constituents, the upper bound (HSUB) is given by

$$K_{\mathrm{HSUB}} = K_1 + \frac{V_2}{(K_2 - K_1)^{-1} + V_1\left(K_1 + \frac{4}{3}\mu_1\right)^{-1}}, \tag{A-3}$$

$$\mu_{\mathrm{HSUB}} = \mu_1 + \frac{V_2}{(\mu_2 - \mu_1)^{-1} + 2V_1(K_1 + 2\mu_1)\left[5\mu_1\left(K_1 + \frac{4}{3}\mu_1\right)\right]^{-1}}, \tag{A-4}$$

where V, K, and μ are the volume fraction, bulk modulus, and shear modulus, respectively, and where indices 1 and 2 refer to the stiffer and softer materials, respectively. The lower bound is found using the same equations but with index 1 referring to the softer material and index 2 to the stiffer material.

Hashin-Shtrikman-Walpole bounds

The Hashin-Shtrikman-Walpole bounds (Walpole, 1966a,b) is a more general form of the Hashin-Shtrikman bounds, and the elastic moduli are given by

$$K = K_1 + \frac{V_2}{(K_2 - K_1)^{-1} + V_1\left(K_1 + \frac{4}{3}\mu_m\right)^{-1}}, \tag{A-5}$$

$$\mu = \mu_1 + \frac{V_2}{(\mu_2 - \mu_1)^{-1} + V_1\left[\mu_1 + \frac{\mu_{\mathrm{m}}}{6}\left(\frac{9K_{\mathrm{m}} + 8\mu_{\mathrm{m}}}{K_{\mathrm{m}} + 2\mu_{\mathrm{m}}}\right)\right]^{-1}}. \tag{A-6}$$

Index 1 and 2 refers to the two components, and now, the upper bound is found when K_m and μ_m are the maximum bulk and shear moduli of the two components. The lower bound is found when they are the minimum moduli of the two components.

Walton model and the no-slip factor

In the Walton model (Walton, 1987) the elastic moduli are calculated under the assumption that the normal and shear deformations due to compaction of two grains occur simultaneously. Typically, two variations of this model are considered; 1) rough grains: the grains have an extremely high friction, and 2) smooth grains: the friction coefficient of the grains is zero. The effective bulk modulus K_W is the same in both cases and given by

$$K_W = \frac{1}{6}\left[\frac{3(1-\phi)^2 C^2 P}{\pi^4 B^2}\right]^{1/3}, \tag{A-7}$$

where ϕ, C, P are the porosity, coordination number, and pressure, respectively, and B is a parameter given by

$$B = \frac{1}{4\pi}\left(\frac{1}{\mu} + \frac{1}{\mu+\lambda}\right), \tag{A-8}$$

where μ and λ are the shear modulus and Lamé's coefficient of the grain material, respectively. The effective shear modulus for smooth grains μ_{W-}, is simply given by

$$\mu_{W-} = \frac{3}{5}K_W, \tag{A-9}$$

while for rough grains it is given by

$$\mu_{W+} = \frac{3}{5}K_W\frac{5-4\nu}{2-\nu} = \mu_{W-}\frac{5-4\nu}{2-\nu}, \tag{A-10}$$

where ν is Poisson's ratio of the grain material. Here we are assuming that the compacting grains are two identical spheres, which is not the typical geometry of e.g. clay. But the coordination number takes to some degree into account the shape of the grains and the model have been found to work fairly well for shales as well as sandstones (Avseth et al., 2005, p. 95).

The rough and smooth cases are extremes, therefore we consider a weighted average between them to model intermediate scenarios, and we get

$$\mu_{W^*} = f\mu_{W+} + (1-f)\mu_{W-} = \mu_{W-}\left[\frac{5-4\nu}{2-\nu} f + (1-f)\right] = \mu_{W-}\left[1 + \frac{3(1-\nu)}{2-\nu} f\right], \tag{A-11}$$

where f is a no-slip factor associated with the amount of friction between the grains; $f = 1.0$ implies only rough grains and $f = 0$ implies only smooth grains. This no-slip factor is the same as the no-slip factor f_t in the equation given by Bachrach and Avseth (2008) for the effective shear moduli under hydrostatic loading, and the Mindlin friction term $f(\mu)$ (Duffaut, 2010; Mindlin, 1949).

Contact cement theory

The contact cement theory (CCT) of Dvorkin and Nur's (1996) is used for calculating the effective dry rock elastic moduli of cemented granular rocks according to

$$K_{CCT} = \frac{1}{6} C(1-\phi_0) M_c S_n, \tag{A-12}$$

$$\mu_{CCT} = \frac{3}{5} K_{DN} + \frac{3}{20} C(1-\phi_0) \mu_c S_\tau, \tag{A-13}$$

$$M_c = \rho_c V_{pc}^2, \tag{A-14}$$

$$\mu_c = \rho_c V_{sc}^2, \tag{A-15}$$

where ϕ_0 is porosity of the starting framework, ρ_c, V_{pc} V_{sc} are the density, P- and S-wave velocities of the cement material, respectively. The S_n and S_τ parameters are proportional to the normal and shear stiffnesses, respectively, and they depend on the cement and grain properties as well as the amount of contact cement.

APPENDIX B

DISPLACEMENT OF INTERSECTION

Figure B-1 shows the displacement $\Delta\vec{m}_{j|i}$ of the intersection between $\varphi_{\hat{d}_i}$ and $\varphi_{\hat{d}_j}$ when the data parameter d_i is altered with a value δd_i. From vector and trigonometric relations it can be expressed as

$$\Delta\vec{m}_{j|i} = \left|\Delta\vec{m}_{j|i}\right| \Delta\hat{m}_{j|i} = \left| \frac{\delta d_i \left|\nabla\varphi_{\hat{d}_i}\right|}{\sin\theta} \right| \frac{\hat{\nabla}\varphi_{\hat{d}_i} - \hat{\nabla}\varphi_{\hat{d}_j}\cos\theta}{\left|\hat{\nabla}\varphi_{\hat{d}_i} - \hat{\nabla}\varphi_{\hat{d}_j}\cos\theta\right|}, \tag{B-1}$$

where $\Delta\hat{m}_{j|i}$ is the unit vector of $\Delta\vec{m}_{j|i}$. The factor $\cos\theta$ comes from the projection of $\hat{\nabla}\varphi_{\hat{d}_i}$, i.e. the unit gradient vector of data parameter d_i, onto $\hat{\nabla}\varphi_{\hat{d}_j}$, i.e. the unit gradient vector for data parameter d_j.

Equation B-1 can be extended to the displacement of an intersection in three dimensions between $\varphi_{\hat{d}_i}$, $\varphi_{\hat{d}_j}$, and $\varphi_{\hat{d}_k}$ when the data parameter d_i is altered with a value δd_i according to

$$\Delta\vec{m}_{k|j|i} = \Delta\vec{m}_{j|i} + \left|\Delta\vec{m}_{j|i}\right| \frac{\hat{\nabla}\varphi_{\hat{d}_i} \times \hat{\nabla}\varphi_{\hat{d}_j}}{\left|\hat{\nabla}\varphi_{\hat{d}_i}\right|\left|\hat{\nabla}\varphi_{\hat{d}_j}\right|\sin\theta} \tan(\frac{\pi}{2} - \gamma), \tag{B-2}$$

where γ is the angle between $\Delta\hat{m}_{j|i}$ and $\hat{\nabla}\varphi_{\hat{d}_k}$, i.e. the unit gradient vector of data parameter d_k.

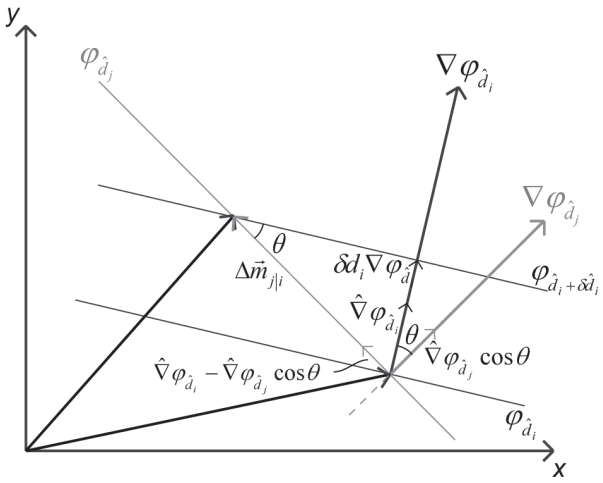

Figure B-1 Illustration of displacement $\Delta\vec{m}_{j|i}$ of intersection between the model correlation $\varphi_{\hat{d}_i}$ for data parameter value $\hat{d}_i$, and $\varphi_{\hat{d}_j}$ for data parameter value $\hat{d}_j$, when the data parameter d_i is altered with a small value δd_i. The corresponding gradients in the initial intersection is $\nabla\varphi_{\hat{d}_i}$ and $\nabla\varphi_{\hat{d}_j}$ with unit vectors $\hat{\nabla}\varphi_{\hat{d}_i}$ and $\hat{\nabla}\varphi_{\hat{d}_j}$, respectively.

REFERENCES

Agersborg, R., T. A. Johansen, M. Jakobsen, J. Sothcott, and A. Best, 2008, Effects of fluids and dual-pore systems on pressure-dependent velocities and attenuations in carbonates: Geophysics, **73**, N35-N47.

Avseth, P., 2000, Combining rock physics and sedimentology for seismic reservoir characterization of North Seat turbidite systems: Ph.D., Stanford University.

Avseth, P., T. Mukerji, and G. Mavko, 2005, Quantitative Seismic Interpretation. Applying Rock Physics Tools to Reduce Interpretation Risk: Cambridge University Press.

Avseth, P., T. Mukerji, G. Mavko, and J. Dvorkin, 2010, Rock-physics diagnostics of depositional texture, diagenetic alterations, and reservoir heterogeneity in high-porosity siliciclastic sediments and rocks -- A review of selected models and suggested work flows: Geophysics, **75**, 75A31-7547.

Bachrach, R., and P. Avseth, 2008, Rock physics modeling of unconsolidated sands: Accounting for nonuniform contacts and heterogeneous stress fields in the effective media approximation with applications to hydrocarbon exploration: Geophysics, **73**, E197-209.

Berryman, J. G., 1992, Single-scattering approximations for coefficients in Biot's equations of poroelasticity: The Journal of the Acoustical Society of America, **91**, 551-571.

Berryman, J.G. 1995. Mixture Theories for Rock Properties. In: *Physics and Phase Relations, A Handbook of Physical Constants* (ed. T.J. Ahrens), pp. 205-228. American Geophysical Union, ISBN 0-87590-853-5.

Connolly, P., 1999, Elastic impedance: The Leading Edge, **18**, 438-452.

Digby, P. J., 1981, The Effective Elastic Moduli of Porous Granular Rocks: Journal of Applied Mechanics, **48**, 803-808.

Dræge, A., T. A. Johansen, I. Brevik, and C. T. Dræge, 2006, A strategy for modelling the diagenetic evolution of seismic properties in sandstones: Petroleum Geoscience, **12**, 309-323.

Duffaut, K., M. Landro, and R. Sollie, 2010, Using Mindlin theory to model friction-dependent shear modulus in granular media: Geophysics, **75**, E143-152.

Dvorkin, J., and A. Nur, 1996, Elasticity of high-porosity sandstones: Theory for two North Sea data sets: Geophysics, **61**, 1363-1370.

Gassmann, F., 1951, Über die elastizität poröser medien: Vierteljahrsschrift der Naturforschenden Gesellschaft in Zürich, **96**, 1-23.

Hashin, Z., and S. Shtrikman, 1963, A variational approach to the theory of the elastic behaviour of multiphase materials: Journal of the Mechanics and Physics of Solids, **11**, 127-140.

Hornby, B. E., L. M. Schwartz, and J. A. Hudson, 1994, Anisotropic effective-medium modeling of the elastic properties of shales: Geophysics, **59**, 1570-1582.

Jakobsen, M., J. A. Hudson, and T. A. Johansen, 2003, T-matrix approach to shale acoustics: Geophysical Journal International, **154**, 533-558.

Kuster, G. T., and M. N. Toksoz, 1974, Velocity and attenuation of seismic waves in two-phase media: Part I. Theoretical formulations.: Geophysics, **39**, 587-606.

Mavko, G., T. Mukerji, and J. Dvorkin, 2008, The rock physics handbook, tools for seismic analysis in porous media: Cambridge University Press.

Mindlin, G. W., 1949, Compliance of elastic bodies in contact: J. Appl. Mech., **16**, 259-268.

Murphy, W. F., III, 1982, Effects of Microstructure and Pore Fluids on the Acoustic Properties of Granular Sedimentary Materials: Ph.D., Stanford University.

Sheng, P., 1990, Effective-medium theory of sedimentary rocks: Physical Review B, **41**, 4507.

Walpole, L. J., 1966a, On bounds for the overall elastic moduli of inhomogeneous systems--I: Journal of the Mechanics and Physics of Solids, **14**, 151-162.

Walpole, L. J., 1966b, On bounds for the overall elastic moduli of inhomogeneous systems--II: Journal of the Mechanics and Physics of Solids, **14**, 289-301.

Walton, K., 1987, The effective elastic moduli of a random packing of spheres: Journal of the Mechanics and Physics of Solids, **35**, 213-226.

Wood, A. B., 1955, A textbook of sound: being an account of the physics of vibrations with special reference to recent theoretical and technical developments: G. Bell.

Ødegaard, E., and P. Avseth, 2004, Well log and seismic data analysis using rock physics templates: First Break, **23**, 37-43.

"We cannot direct the wind, but we can adjust the sails."

Bertha Calloway

African-American, community activist and historian (1925-)

Founder of the Great Plains Black History Museum

APPENDIX IV: PAPER 4

Improved quantitative calibration of rock physics models

Bernardo Moyano, Erling Hugo Jensen and Tor Arne Johansen.

Accepted for publication in *Petroleum Geosciences,* July 2011.

IV

Improved quantitative calibration of rock physics models

Bernardo Moyano[1], Erling Hugo Jensen[1], Tor Arne Johansen[1,2].

ABSTRACT

In reservoir characterization, rock-physics models provide the link between seismic observables (density, compressional and shear wavespeeds) and reservoir parameters such as porosity, lithology and fluid saturation. However, the accuracy of these predictions is rarely explored. In fact, the validation of a model representing a dataset is often limited to the analysis of a cross-plot of two arbitrary magnitudes. The objective of this paper is to improve the calibration procedure through a quantitative assessment of the reservoir property predictions using various rock-physics models. The analysis is based on an inverse rock-physics modelling that organizes the rock-physics transforms into constraint data so that the seismic variables are direct functions of the reservoir parameters. It is revealed that the predictions of reservoir quality can assist in the diagnosis of the rock microstructure itself, such as the location of clay particles in clay-rich sediments. In addition, we found that a quantitative analysis is the only way to evaluate accurately the performance of various models when studying heterogeneous datasets.

INTRODUCTION

Selecting and calibrating the most suitable rock-physics model for a given dataset is an exercise with a non-unique solution. Rock-physics models capture one or a select few factors that influence the elastic properties of the rocks. In addition, these models typically are calibrated to a limited set of physical data (e.g. compressional (P) velocity data). One group of models based on contact theory (Mindlin 1949) treats rocks as a collection of grains and estimates their stiffnesses from the contact stress between two spheres of equal size. On the other hand, inclusion models (Berryman 1980) treat the rock as an elastic solid with cavities and accounts for the effects of shapes of multiple pores on elasticity. In practice, general guidelines and additional observations help to constrain the model space to a relatively small number of plausible options. For example, contact models have been used successfully to study the pressure dependence of velocity of unconsolidated sediments (Dvorkin & Nur 1996). Inclusion models are often preferable when analyzing well-

[1] Department of Earth Science, University of Bergen, Bergen, Norway.
[2] NORSAR, Bergen, Norway.

consolidated rocks (Sheng 1990; Berge *et al.* 1993). However, after selecting a modelling strategy, we are frequently left with several possible models that seem to represent experimental data equally well.

In reservoir characterization, the ultimate goal of a rock-physics model is to assist in the inversion of seismic data for porosity, lithology and pore fluid (PLF). These models define the transforms between seismic observables and reservoir parameters. Selecting a specific model implicitly defines the dominant parameters that control these relationships and determines the accuracy of the predictions. Therefore, a crucial step is to calibrate and to compare the predictions quantitatively when more than one model appears equivalently valid for a given area.

Various models are used to account for the dependence of elastic properties on different physical conditions. Pressure dependence has been captured by models based on contact theory (Mindlin 1949; Digby 1981; Walton 1987). The stiffness effect due to cement located at the grain contacts is often calculated using contact cement theory (Dvorkin & Nur 1996), whereas pore microstructure effects can be modelled by inclusion models (Kuster & Toksoz 1974; Berryman 1980). Self-consistent approximations (O'Connell & Budiansky 1974; Hornby *et al.* 1994; Berryman 1995) and differential effective medium (DEM) models (Berryman 1992) have been developed specifically to extend inclusion models to handle higher concentrations of inclusions. Shales, due to their complex lithology and reduced pore sizes have been idealized through inclusion models, (Hornby *et al.* 1994; Jakobsen *et al.* 2003; Johansen *et al.* 2004a; Draege *et al.* 2006). The equations of Gassmann (1951) simulate the low-frequency effects of different pore fluids on seismic velocities. Avseth *et al.* (2010) provide an overview of theoretical, empirical, heuristic and hybrid strategies to model diagenetic and depositional trends in unconsolidated high-porosity sediments. Thus, ambiguities can arise when we apply various models to estimate simultaneously reservoir properties such as lithology, porosity and saturation. Little work has been done to evaluate systematically PLF parameters obtained using different models. For a given dataset, the selection of a rock-physics model is uncertain, in terms of providing the most suitable relationship between the seismic and PLF parameters. The goal of this paper is to present a way to select and calibrate the most suitable rock-physics model for a given dataset and reduce the non-uniqueness of the reservoir characterization problem. We do this by quantifying the accuracy of different rock-physics models in the prediction of reservoir parameters when calibrated to experimental data. We use an approach (Johansen *et al.* 2004b) that organizes the rock-physics transforms into constraint data where the seismic variables (e.g., velocity and density) are direct functions of the selected PLF parameters. We start with a review of this strategy, and then we demonstrate the calibration procedure in two cases using real data. In case 1 we use the procedure to illustrate the shortcoming of the traditional cross-plot type of calibration. We do this by comparing the reservoir property predictions made with a model for dispersed clay (Dvorkin & Gutierrez 2001)

versus a model for structural clay (Avseth *et al.* 2005) on a set of laboratory measurements of clay-sand composites (Yin 1992). In case 2 we explore the accuracy of various rock-physics predictions of reservoir properties considering a more extensive dataset (Han *et al.* 1986). Subsequently, we select the most suitable models and then perturb individual parameters to optimize the final predictions.

INVERSE ROCK PHYSICS MODELLING

A common practice in rock-physics analysis is to use cross plots to study trends and property dependencies. For example, Figure 1a shows the predicted bulk modulus versus porosity trends for a particular fluid saturation and different lithologies using a rock physics model. In the strategy of Johansen *et al.* (2004b) such modelled dependencies are resampled into a scalar field of the reservoir properties. Figure 1b illustrates the resampling of two bulk moduli values into a lithology versus porosity cross plot. Repeating this for the other moduli values and various fluid saturations gives us the 3D cube in Figure 2. The resampled bulk modulus can be thought as a scalar field *K.* In this case, $K = K(\phi, C, S)$, where ϕ, C and S denote the porosity, clay and fluid volume fractions, respectively for a particular rock physics model. From $K(\phi, C, S)$, we calculate a numerical relationship between ϕ, C and S which corresponds to a specific bulk modulus value. For the 3D cube this typically produces a surface that we denote an iso-surface because all points on this surface correspond to the same modulus.

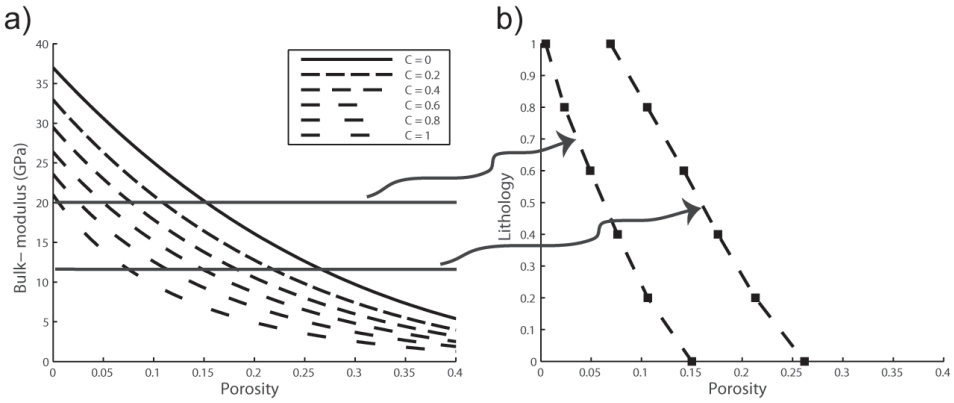

Figure 1 Resampling of a rock-physics model from velocity-porosity to lithology-porosity space. C_i are model results for various clay contents.

Estimating reservoir properties

An iso-surface can be used to study predicted reservoir property dependencies for a particular seismic parameter value and a given rock physics model. Any combination of ϕ, C and S corresponding to a point on such a surface is a possible solution for the particular seismic parameter value. Typically, we have data of more than one seismic parameter (compressional and shear wavespeeds, V_p and V_s, and bulk density ρ), and by combining their individual iso-surfaces we constrain the possible PLF solutions. A combination of two seismic observables (e.g. V_p and ρ) will normally lead to one or more curving lines in the PLF domain. Furthermore, a combination of three observables leads to one or more point solutions because we are dealing with a non-linear problem (see Figure 3). Another possible outcome of the inversion is that no intersection is found, i.e., no combination of reservoir properties is consistent with the set of observables. This means that the selected rock physics model fails to reproduce the data and other possible model candidates should be tested.

When working with real data, it is difficult to find a rock physics model that is able to predict the correct reservoir properties for every data point unless uncertainty is included. In case one, we include a few perturbed values of the input data in addition to the observed data and perform the inverse modelling. In the second case, we handle the uncertainty by using a so-called proximity based implementation of the inversion strategy. Here, the iso-surfaces are made up of densely sampled points. Intersections are identified when the points on one surface are within a maximum distance δ from points on another surface.

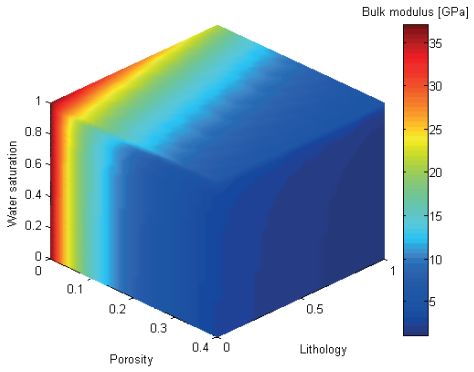

Figure 2 Bulk modulus constraint cube in the porosity, lithology, fluid space (PLF). The vertical axis is water saturation. The lithology axis varies from pure quartz (zero) to pure clay (one).

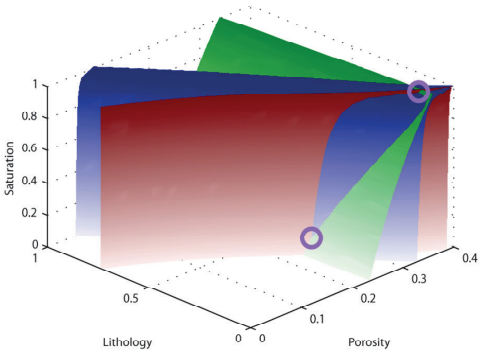

Figure 3 Three observations (Vp, Vs and density iso-surfaces) intersecting in the PLF space. Solutions exist at the two indicated points.

This maximum distance represents an absolute tolerance interval for the modelled ϕ, C and S. A sensitivity analysis of the applied models to the uncertainties in the measured rock properties can be made to derive a suitable tolerance interval for a given dataset. These point solutions are expanded to spherical point clouds with a radius $\delta/2$. An example of the inversion in Figure 3 using the proximity based implementation and a $\delta = 0.02$, is shown in Figure 4.

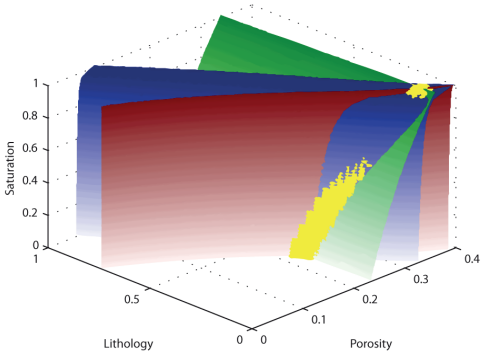

Figure 4 Three observations (Vp, Vs and density) intersecting in the PLF space. Uncertainty is implicitly handled by the proximity based implementation of the inverse modelling, providing a cloud of solutions as opposed to points as in Figure 3.

The calibration procedure

In the quantitative calibration of rock-physics models we compare predicted reservoir properties, i.e. axis readings at the intersecting points, to measurements of these properties from laboratory or well-log data. Through this analysis in the PLF space, we evaluate how accurate a model predicts reservoir properties from seismic data. In addition, we compare the predictions of reservoir properties from different models and discard those models that provide less accurate predictions. During the calibration process we can also maximize the tolerance in the intersections and quickly test the performance of several models, discard the less effective ones, and continue with the most promising ones. As the number of models is reduced to three or four, the uncertainty in the observations can be constrained to perform a more rigorous analysis. Finally, when the most suitable model has been identified, the same methodology can be repeated for various values of model parameters (aspect ratio, pressure, etc.) to optimize the calibration and improve prediction results. We applied this methodology to quantify the calibration of various rock-physics models to two datasets of clay-rich sandstones.

CASE 1: EVALUATING CLAY DISTRIBUTION IN CLAY-SAND COMPOSITES

We applied the methodology to a laboratory dataset of clay-sand composites prepared by Yin (1992). The samples consist of mixtures of pure kaolinite and Ottawa sand with a grain size ratio of 1/20, providing an ideal binary mixture. For low quantities of clay, the small clay particles likely occupy part of the pore space of the larger sand particles (a pore-

filling clay). This spatial distribution has a minimal effect on the structure of the composite. The dataset for 50 MPa of effective pressure is shown in Figure 5 where a reduction in porosity and increase in velocity are observed for increasing clay content. An overturned V-shape trend produced by the transition between sand and shale has been noted in the literature as an indicator of dispersed clay topology (Marion *et al.* 1992). In the context of rock-physics modelling, we denote shale as a fine-grained rock (clay-sized and silt-sized) in which clay minerals are the load-bearing phase. We calibrated a model for dispersed clay, and a model that is suitable for both structural and laminated clay to the dataset.

The model for dispersed clay (Dvorkin & Gutierrez 2001) is a velocity-porosity relationship that uses the Hashin-Shtrikman (HS) lower bound (Hashin & Shtrikman 1963) as a mixing law between two end members. The high-porosity end member is clean sand whose velocity is computed by contact theory (Mindlin 1949). The low-porosity end member represents the same sand with its pore space completely filled by clay. The porosity at this point is not zero because clay particles have intrinsic porosity. This is sometimes referred to as sand at critical clay content (Yin 1992). Dvorkin & Gutierrez (2001) computed this intermediate member by adding silt particles (quartz) to a pure shale also using the HS lower bound. The model consists of two domains. In the first domain, clay is the load-bearing phase (sandy-shale), whereas in the second domain, the sand pack is load bearing (shaley-sand), as in Figure 6.

In our modelling we focused on the shaley-sand section in which clay particles fill the pore space of the clean sand without significantly affecting its stiffness. Therefore, the

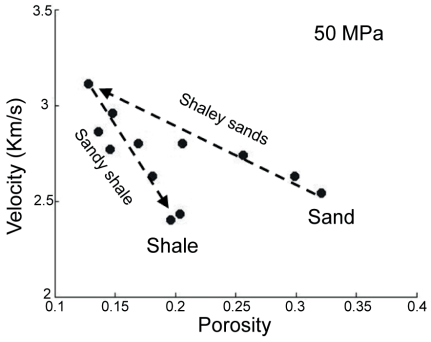

Figure 5 P-wave velocity versus porosity trend of clay-sand composites at constant pressure prepared by Yin (1992). Dashed arrows indicate increasing clay content. The V-shaped trend of increasing clay content, producing an increase of velocity (and a decrease in porosity) until clay content equals sand porosity, has been attributed to a pore filling clay topology.

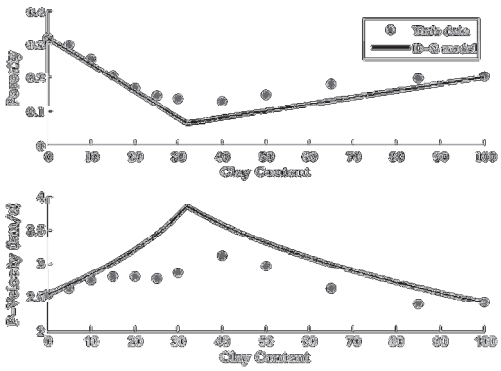

Figure 6 Dispersed clay model (Dvorkin-Gutierrez) calibrated to Yin's data. Note porosity is modelled well, but velocity is in general over-estimated. The model predicts that clay mineral becomes load-bearing (porosity minimum and velocity maximum) at about 30 % clay content.

properties of the mixture can be computed from the lower HS bounds of the clean sand and the sand at critical clay content. The elastic moduli of a shaley-sand with increasing clay content (C) are expressed as:

$$K_{MIX} = \left[\frac{1 - C/\phi_{ss}}{K_{ss} + (4/3)\mu_{ss}} + \frac{C/\phi_{ss}}{K_{cc} + (4/3)\mu_{ss}} \right]^{-1} - \frac{4}{3}\mu_{ss}\,, \tag{1}$$

$$\mu_{MIX} = \left[\frac{1 - C/\phi_{ss}}{\mu_{ss} + Z_{ss}} + \frac{C/\phi_{ss}}{\mu_{cc} + Z_{ss}} \right]^{-1} - Z_{ss}\,, \tag{2}$$

$$Z_{ss} = \frac{\mu_{ss}}{6}\left(\frac{9K_{ss} + 8\mu_{ss}}{K_{ss} + 2\mu_{ss}} \right), \tag{3}$$

where, K_{cc} and μ_{cc} are computed from the sandy-shale model at critical clay content. K_{ss}, μ_{ss} and ϕ_{ss} are the effective moduli and porosity of the clean sandstone.

In contrast, the constant clay model assumes the clay particles are located in the frame of the rock, reducing its overall stiffness. The model uses contact theory and the HS lower bound to model sands with a constant clay-quartz ratio in the velocity-porosity space (Avseth *et al.* 2005). This is suitable for sands with both structural and laminated clay. As Yin's dataset is composed of synthetic clay-sand aggregates we do not expect any laminations to be present and we refer to this as the model for structural clay. It is analogous to the unconsolidated sand model (Dvorkin & Nur 1996) but with a reduced critical porosity because a clay rich sand has lower critical porosity than a clean sand. The mineral point is computed by Hill's (1952) average of quartz and clay mineral moduli.

Conventional calibration

A conventional calibration consists of a qualitative fit of modelled curves for a given cross-plot domain. We calibrated both models to the dataset in the velocity-porosity space (Figure 7). The dispersed clay model matches well the clean sand and pure clay end members, but it misses the intermediate values of clay content. The structural clay model reproduces the variability of the P-wave velocity data, but its accuracy is difficult to evaluate. Note that the shear velocity data show no sensitivity to clay content.

In Figure 6, the dispersed clay model reproduces the decrease of porosity for increasing clay content shown by the data, and predicts a change in the load-bearing phase, from grain to matrix supported, for a clay volume of approximately 32%. Both models can be used to explain the data and to infer the internal organization of the clay particles in the

samples. However, we cannot determine which model explains the data better, nor, from these results, can we quantify how successfully either model represents the data.

Quantitative analysis in the PLF space

For the quantitative analysis, we used seven samples each with clay content <30%. When considering the intersections between three iso-surfaces for density, P- and S-wave velocities, we obtained a solution for only the pure sand sample, which constitutes a calibration point. This is due to the anomalous behaviour of shear velocities that none of the models could satisfactorily describe (Figure 7). Therefore, we continued using only P-wave velocity and density, ignoring S-wave velocity measurements. A comparison of the results can be seen in Figure 8, where the structural clay model produced solutions for the seven samples, good estimates of the porosity and less accurate estimates for lithology. On the contrary, the dispersed model found solutions for only four samples; three accurate in porosity and two in lithology.

If we include +/- 5 percent uncertainty in the P-wave velocity, the inverse modelling provides more solutions (see Figure 9). In this case the dispersed-clay model improves its performance and produces solutions for all seven samples with varying accuracy. The structural clay model also provides an increased number of solutions and shows a robust set of porosity and lithology predictions. A quantitative comparison of the modelling is

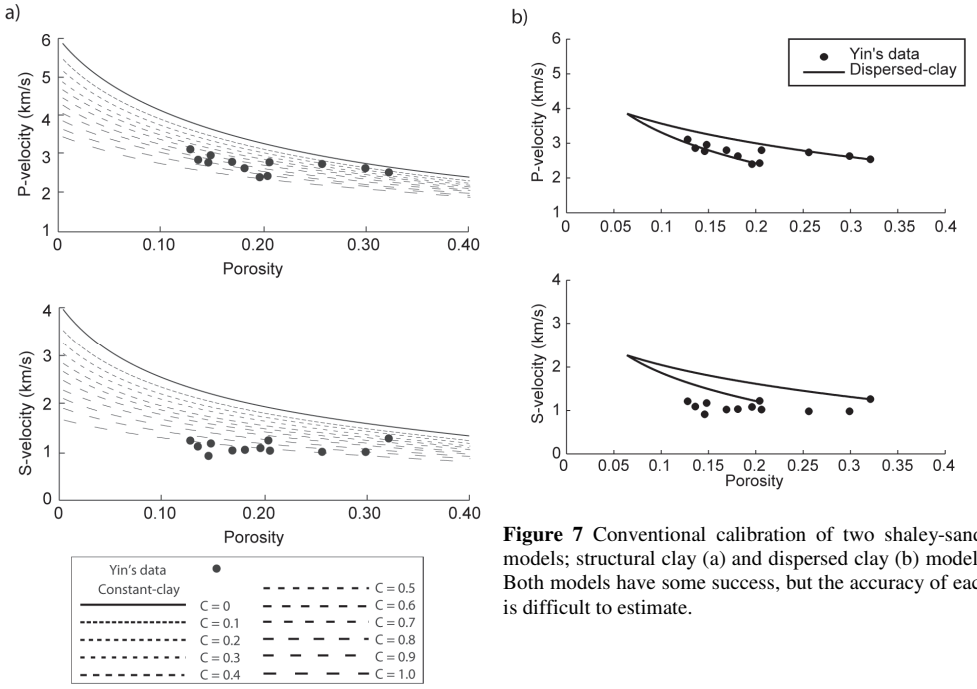

Figure 7 Conventional calibration of two shaley-sands models; structural clay (a) and dispersed clay (b) models. Both models have some success, but the accuracy of each is difficult to estimate.

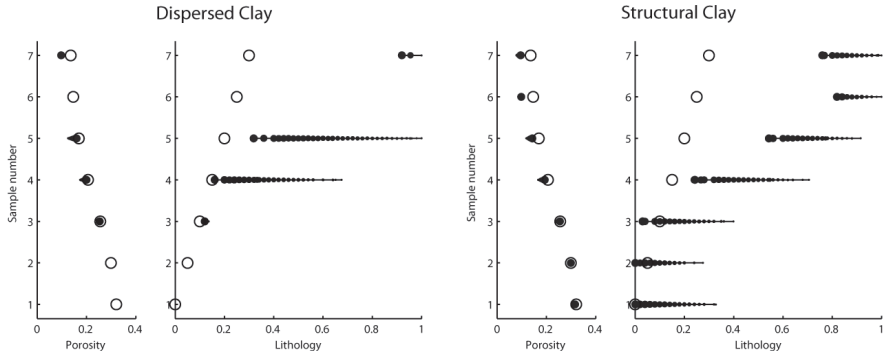

Figure 8 Quantitative calibration of dispersed clay (left) and structural clay (right) models. Vertical axis is sample number, empty circles are lab measurements and filled circles model predictions. Only 7 samples with clay content below 0.3 were used. Of the two models, the structural clay model produced more solutions.

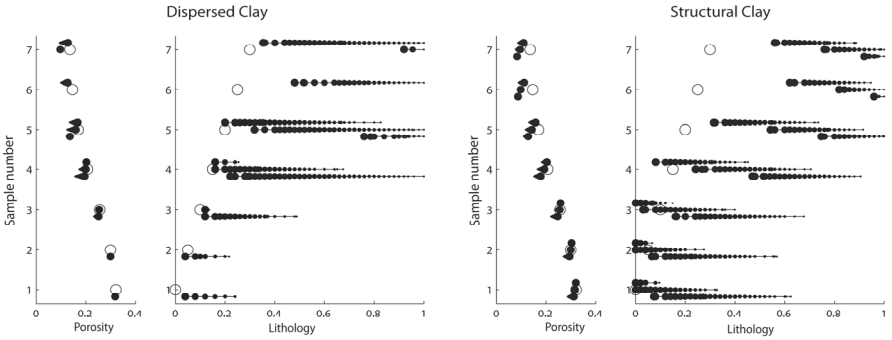

Figure 9 Quantitative calibration of the dispersed clay model (left) and structural clay model (right), using 5% uncertainty in *V*p. Vertical axis is sample number, empty circles are lab measurements and filled circles model predictions. More solutions were found relative to the results (Fig. 8) in which uncertainty was not included.

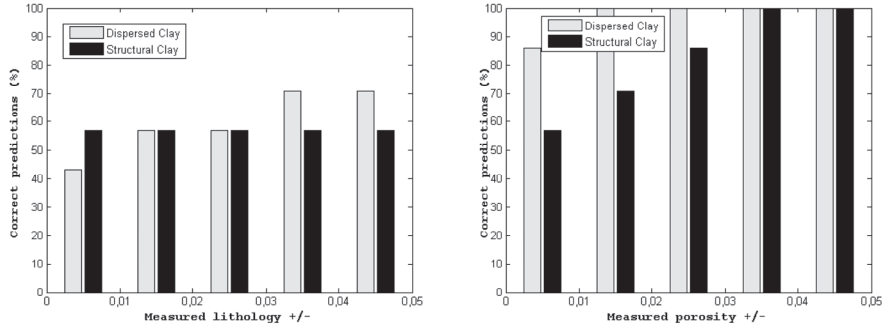

Figure 10 Quantitative calibration of dispersed clay (grey) and structural clay (black) models, using a 5 % of uncertainty in Vp. Vertical axis is percentage of predictions matching the data, versus various tolerance ranges in porosity and lithology predictions (+/– 0.01, 0.02, 0.03, 0.04, 0.05) in the horizontal axis.

shown in Figure 10, with the percentage of correct predictions along the vertical axis, and various tolerance ranges between observed and modelled porosities and lithologies (+/− 0.01, 0.02, 0.03, 0.04, 0.05) along the horizontal axis. Figure 10 shows that the two models predict similarly well the lithology, whereas the porosity is more precisely estimated by the dispersed clay model. However, Figures 8 and 9 show that the dispersed clay model is more sensitive to the uncertainty of the P-wave velocity.

CASE 2: VALIDATING ROCK-PHYSICS MODELS FOR CLAY-RICH SANDSTONES

In this case we assessed the calibration of various models to a larger dataset based on 80 sandstone samples with wide ranges of porosity, age and clay content (Han et al. 1986). We started by exploring three models. One is a granular model based on contact theory combined with HS bounds and the other two are inclusion models.

The first model is referred to as the modified Hashin-Shtrikman upper bound (MHS) and uses Hertz-Mindlin (Mindlin 1949) theory to compute a clean, high-porosity sand and an HS upper bound to estimate lower porosities towards the mineral point. This model has been used to describe a mixture of sediment deposited at critical porosity with some additional mineral. It mimics the steep diagenetic trend of clean sands in the velocity-porosity space (Avseth *et al.* 2005). For clay-rich data, it connects a lower critical porosity member with softer effective mineral moduli. We used quartz mineral properties, K_q = 37 GPa, μ_q = 44 GPa for bulk and shear moduli, and clay properties computed for this dataset K_c = 25 GPa and μ_c = 9 GPa (Han *et al.* 1986). Effective pressure was 40 MPa, nine contact points per grain on average (coordination number), and we assumed critical porosity to decrease linearly between 0.4 for clean sand and 0.2 when clay content is 1.

Then, we applied the model of Xu & White (1995) for clay-sand mixtures, which divides the pore space into sand related pores (stiff) and clay related pores (compliant), assigning different aspect ratios to them. For implementation we used a non-interaction approximation (Hudson & Knopoff 1989; Hornby *et al.* 1994) to compute the effective compliance tensor $\mathbf{S}^*$ from those of the host rock $\mathbf{S}^0$ and the pore space as:

$$\mathbf{S}^* = \mathbf{S}^0 - \sum_{n=1}^{N} v_n \left(\mathbf{S}^0 \mathbf{C}^n - \mathbf{I}\right) \mathbf{K}^n , \tag{4}$$

$$\mathbf{K}^n = \left[\mathbf{C}^0 \left(\mathbf{I} + \mathbf{G}^n \left(\mathbf{C}^n - \mathbf{C}^0\right)\right)\right]^{-1}. \tag{5}$$

In equations 4 and 5, $\mathbf{S}^*$ is the effective compliance tensor; $\mathbf{S}^0$ the compliance tensor of the isotropic host rock; v_n is the volume concentration of the nth phase; and $\mathbf{I}$ is the identity

tensor. The factor $\mathbf{G}^n$ is a fourth-rank tensor that depends on the stiffness tensor of the host rock ($\mathbf{C}^0$) and the shape/orientation of the n^{th} inclusion type that characterizes the elastic effect of individual inclusions. The excess compliance due to the pore space includes contributions of sand related pores (α_{stiff}) and clay related pores (α_{soft}). Aspect ratios of α_{stiff} = 0.1 for sand and α_{soft} = 0.05 for clay related pores were initially applied. The effective stiffness tensor is then obtained by inverting the effective compliance tensor. The effect of the fluid is computed using Gassmann's (1951) equations. Increasing clay content means increasing number of compliant pores and results in a softening of the effective properties of the rock.

The third model used differential effective medium (DEM) theory (Berryman 1992) to introduce empty isolated pores with a constant aspect ratio (α = 0.25) into a mineral host medium. This requires solving a coupled system of ordinary differential equations:

$$(1-y)\frac{d}{dy}\left[K^*(y)\right]=\left(K_2-K^*\right)P^{(*2)}(y)\ , \tag{6}$$

$$(1-y)\frac{d}{dy}\left[\mu^*(y)\right]=\left(\mu_2-\mu^*\right)Q^{(*2)}(y)\ , \tag{7}$$

where K^* and μ^* are the effective bulk and shear moduli, $K^*(0) = K_1$ and $\mu^*(0) = \mu_1$ are the effective elastic moduli at initial conditions (initial host material), K_2, μ_2 and y denote the moduli and concentration of the added inclusions. The terms P^* and Q^* are geometrical factors associated with the inclusion material. The fluid effect was again introduced using Gassmann's equations (Gassmann 1951).

All three models provided a satisfactory calibration in the velocity-porosity space for P- and S-velocities (Figure 11), but a quantitative analysis is required to evaluate and compare their successes further.

QUANTITATIVE ANALYSIS IN PLF SPACE

The quantitative analysis in the PLF space for the three models is summarized in Figure 12. All three models show similar porosity predictions, but lithology estimations by the DEM consistently under-performs. Hence, we discarded the DEM model and focused the quantitative analysis on the other two models (MHS and XW). A comparison between their results from the intersections of Vp, Vs and density iso-surfaces is shown in Figure 13. The empty circles represent (laboratory) measurements, and the filled circles are our modelling results. There is more than one prediction for each sample (vertical axis). Furthermore, for every porosity prediction, a corresponding lithology prediction exists, indicated in the figure by the size of the filled circles. The radius of the filled circles increases with

decreasing clay content. An inspection of Figures 12 and 13 shows that both model predictions are similar in number and accuracy, with a slight advantage for the MHS model. Therefore, we performed a sensitivity analysis on one key parameter for each of the models. We tested coordination numbers between 8 and 10 for the MHS model and various combinations of aspect ratios in the XW model. The MHS model shows stable results in terms of coordination number (C), but slightly favouring C = 8 over the other (Figure 14). To analyze the XW model we used five different models (1 to 5) with aspect ratios of sand and clay pores (α_{sand} , α_{clay}) as follows: M1 = (0.1, 0.035); M2 = (0.1, 0.06); M3 = (0.12, 0.035); M4 = (0.12, 0.05); M5 = (0.12, 0.06): see Figure 15. Porosity predictions of the XW model were highly dependent on the aspect ratios of sand and clay pores, whereas lithology estimations were less sensitive. This analysis demonstrated that the lithology results were improved when using aspect ratios of α_{sand} = 0.12 and α_{clay} = 0.035 (model 3). However, better porosity estimations were achieved with slightly stiffer clay pores (models 4 (α_{clay} = 0.05) and 5 (α_{clay} = 0.06) in Figure 15).

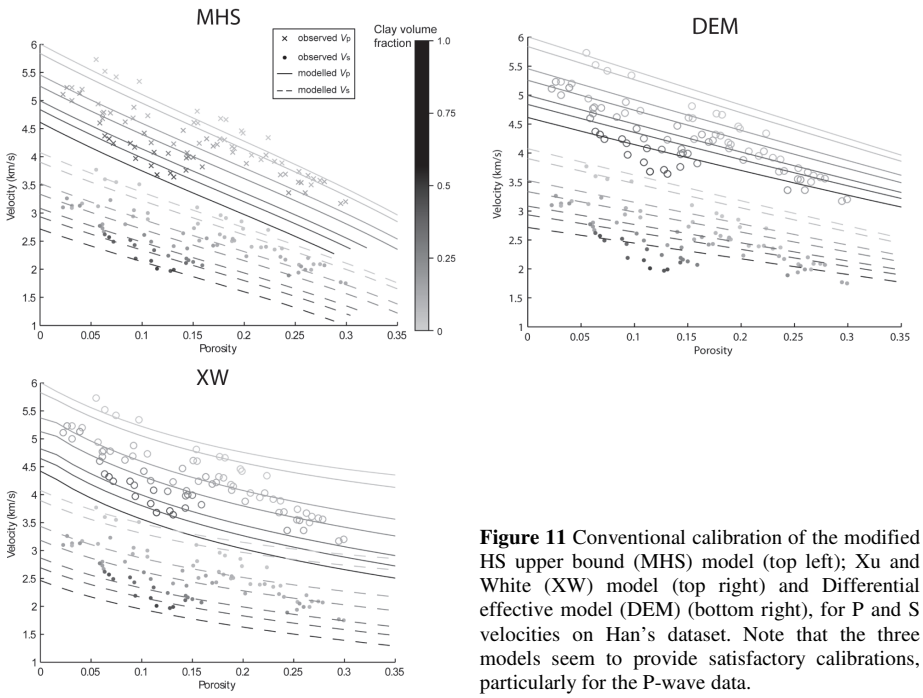

Figure 11 Conventional calibration of the modified HS upper bound (MHS) model (top left); Xu and White (XW) model (top right) and Differential effective model (DEM) (bottom right), for P and S velocities on Han's dataset. Note that the three models seem to provide satisfactory calibrations, particularly for the P-wave data.

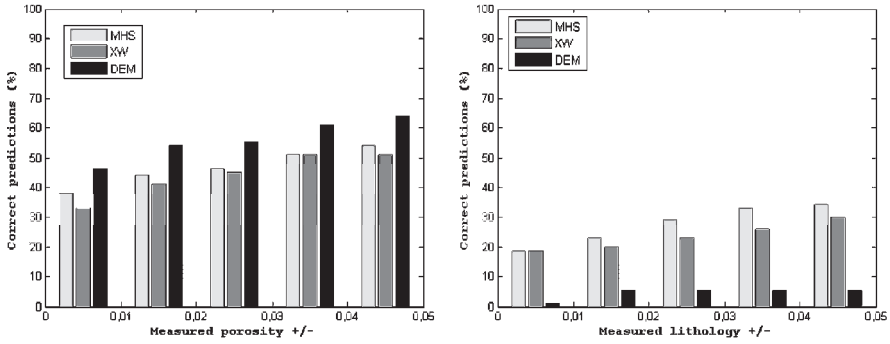

Figure 12 Results of the quantitative calibration of the modified Hashin-Shtrikman (MHS), Xu and White (XW) and differential effective modelling (DEM) models on Han's data set. Vertical axis is percentage of predictions matching the data, versus various tolerance ranges in porosity and lithology predictions (+/- 0.01, 0.02, 0.03, 0.04, 0.05) in the horizontal axis. Note the poor performance of the DEM model in terms of lithology.

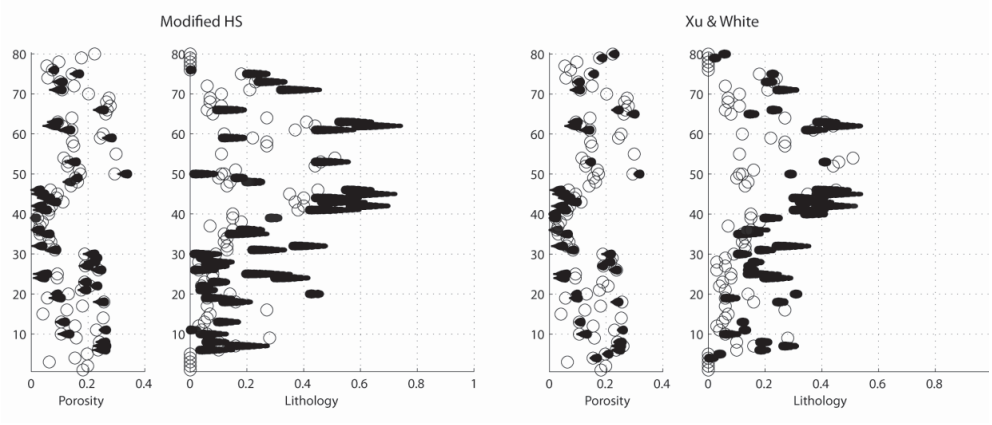

Figure 13. Quantitative calibration of the modified HS upper bound (MHS) on the left; Xu and White model (XW) on the right panel. Vertical axis is sample number, empty circles are lab measurements and filled circles model predictions. Note that both models provide a large number of accurate predictions.

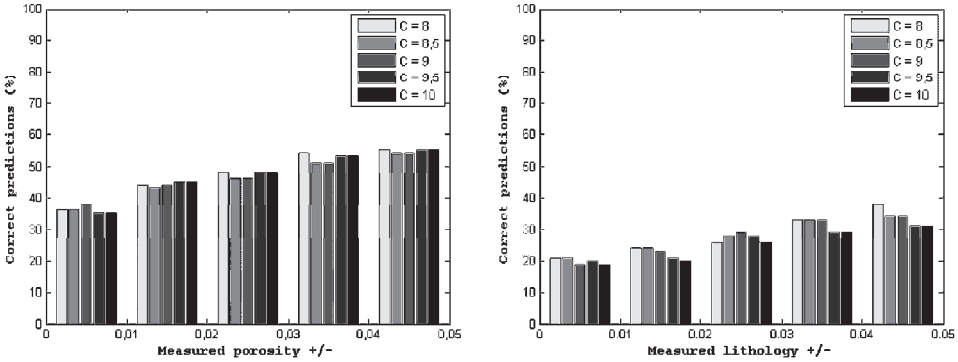

Figure 14 Improved calibration of the modified Hashin-Shtrikman model (MHS), on Han's data set for various coordination numbers (C). Vertical axis is percentage of predictions matching the data, versus various tolerance ranges in porosity and lithology (+/- 0.01, 0.02, 0.03, 0.04, 0.05) in the horizontal axis. Results are stable, and the calibration is not significantly dependent on coordination number.

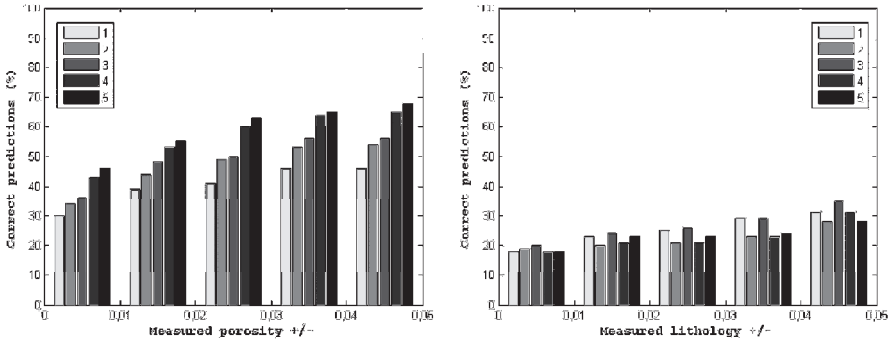

Figure 15 Improved calibration of the Xu and White model (XW), on Han's data set for various combinations of aspect ratios. Models 1 to 5 have aspect ratios (sand-pores, clay-pores) as follow: M1 = (0.1, 0.035); M2 = (0.1, 0.06); M3 = (0.12, 0.035); M4 = (0.12, 0.05); M5 = (0.12, 0.06). Vertical axis is percentage of predictions matching the data, versus various tolerance ranges in porosity and lithology (+/- 0.01, 0.02, 0.03, 0.04, 0.05) in the horizontal axis. Note that porosity predictions were optimized by using different aspect ratios whereas lithology maintains relatively stable.

DISCUSSION

The comparison between two models in the PLF space requires a conventional calibration of the models in a cross-plot domain, such as velocity-porosity space. This initial calibration step, however, can influence the first quantitative results in the PLF space. This ambiguity can be assessed by performing a (quantitative) sensitivity analysis (in the PLF space) for key parameters of each model (e.g., aspect ratios, pressure, and effective mineral properties), and selecting the combination of parameters that provides the higher number of solutions for the dataset under examination. After the optimal parameters have been found, further comparison with other models can be made.

The dataset used in the first case has been referenced in the literature to illustrate the effect of pore-filling clay on porosity and velocities of clay-sand mixtures. Its bimodal grain-size distribution and grain size ratio (1/20) suggest an ideal condition for a dispersed-clay microstructure. However, the predictions for the dispersed clay model were very sensitive to the uncertainty of the data. Overall, the structural-clay model produced a more robust set of predictions for both lithology and porosity. This can be explained from Figure 6. Where clay exceeds 10 % by volume, the dispersed model over-predicts P-velocity because structural clay becomes important in reducing the stiffness of the samples. This suggests that the effect of clay on the elasticity is predominantly inter-granular or structural, except for those with clay volumes below 10 % at which both dispersed and structural clay have similar impacts. This is likely related to the sample preparation procedures, and it is not a general condition of clay-rich sandstones. The quantitative analysis revealed this condition even though it was not evident from the conventional calibration process.

In the second case we used the quantitative calibration approach to select or discard the most suitable rock-physics models to reproduce a dataset. We compared the overall results of three models (MHS, XW and DEM) and were quickly able to discard the least accurate model (DEM). Through a sensitivity analysis of the remaining models, we explored the potential for optimizing the calibration in order to identify the model that provides the most stable and robust predictions. However, in cases with high uncertainty, where wide ranges of porosities and lithologies are expected, the model producing a wider range of results would be preferred. The dataset used in case 2 (Han's data) contains samples from various origins (quarries, well cores) with a wide range of porosities and clay contents, from clean tight sands to high porosity clay-rich sandstones. Therefore, dividing the dataset into more homogeneous subsets, for example in terms of origin, degree of consolidation, porosity or clay content, can improve the calibration and would allow inference of rock microstructure details from the model's success.

In both examples porosity predictions were more accurate than lithology predictions. Most observations of natural rocks indicate that elastic properties are more sensitive to

porosity than to lithology variations. Hence, higher correlations exist between velocity and porosity than between velocity and clay content. Variations of elastic moduli are more pronounced along porosity than lithology axes, which in turn produce less accurate predictions of lithology than porosity.

Our investigation in the PLF space included solutions with high water saturation (>90%) to simplify the analysis. In real cases, however, uncertainty in fluid saturation could lead to less accurate porosity and lithology predictions.

In order to compare the predictions of the different rock-physics models, in our examples we used only ultrasonic laboratory data, a procedure which provides maximum control of the lithology, porosity and saturation. But in a reservoir characterization context where predictions are evaluated in the scale of the field, a similar methodology could be used, calibrating the rock-physics models to log data up-scaled to seismic frequencies.

CONCLUSIONS

We applied an inverse modelling strategy that assesses the ability of a rock-physics model to predict porosity, lithology and saturation (PLF parameters) from seismic parameters. By analyzing the performance of the models in the PLF domain, we were able to select the model that provided the most robust estimations of reservoir properties. Additionally, in the first case we also diagnosed the dominant factor that affected elasticity of the samples.

We also illustrated how this quantitative approach can be used in a workflow to find a model for a large and heterogeneous dataset, considering a wide range of options, quickly discarding the less effective models and focusing on the most promising ones. Then, by testing several model parameters, we assessed the sensitivity of the selected models in terms of predictions of reservoir properties. This suggests that calibrating a rock-physics model only by best fitting in a cross plot domain, to relate inverted seismic data and reservoir parameters, can lead to inaccurate predictions of porosity and lithology. Analyzing the models in the PLF domain has the advantage of evaluating up to three seismic observables simultaneously and can point to inconsistencies in the model predictions between bulk and shear moduli. In conclusion, this is an integrated and robust approach to the inversion problem of finding the most appropriate rock physics model to explain measured data.

ACKNOWLEDGEMENTS

The authors acknowledge the Norwegian research council (NFR) for financial support through the Petromaks program and external sponsors (Statoil, Total, Rocksource). Moyano also would like to thank Statoil for granting a leave to pursue doctoral studies.

REFERENCES

Avseth, P., Mukerji, T., Mavko, G. & Dvorkin, J. 2010. Rock-physics diagnostics of depositional texture, diagenetic alterations, and reservoir heterogeneity in high-porosity siliciclastic sediments and rocks - A review of selected models and suggested work flows. *Geophysics* **75**, A31-A47.

Avseth, P., Mukerji, T. & Mavko, G. 2005. *Quantitative seismic interpretation: Applying rock physics tools to reduce interpretation risk*. Cambridge University Press.

Berge, P.A., Berryman, J.G., & Bonner, B.P. 1993. Influence of microstructure on rock elastic properties. *Geophysical Research Letters* **20**, 2619-2622.

Berryman, J.G. 1980. Long-wavelength propagation in composite elastic media I. Spherical inclusions. *Journal of the Acoustical Society of America* **68**, 1809-1819.

Berryman, J.G. 1992. Single-scattering approximations for coefficients in Biot equations of poroelasticity. *Journal of the Acoustical Society of America* **91**, 551-571.

Berryman, J.G. 1995. Mixture theories for rock properties. In: *Rock Physics and Phase Relations, AGU Reference Shelf 3, AGU, Washington, DC, 205-228* (ed. Ed. T.J.Ahrens), American Geophysical Union.

Digby, P.J. 1981. The effective elastic-moduli of porous granular rocks. *Journal of Applied Mechanics-Transactions of the Asme* **48**, 803-808.

Draege, A., Jakobsen, M. & Johansen, T.A. 2006. Rock physics modelling of shale diagenesis. *Petroleum Geoscience* **12**, 49-57.

Dvorkin, J. & Nur, A. 1996. Elasticity of high-porosity sandstones: Theory for two North Sea data sets. *Geophysics* **61**, 1363-1370.

Dvorkin, J. & Gutierrez, M.A. 2001. Textural sorting effect on elastic velocities, part II: Elasticity of a bimodal grain mixture. *SEG Technical Program Expanded Abstracts* **20**, 1764-1767.

Gassmann, F. 1951. Elastic waves through a packing of spheres. *Geophysics* **16**, 673-685.

Han, D., Nur, A. & Morgan, D. 1986. Effects of porosity and clay content on wave velocities in sandstones. *Geophysics* **51**, 2093-2107.

Hashin, Z. & Shtrikman, S. 1963. A variational approach to the theory of the elastic behaviour of multiphase materials. *Journal of the Mechanics and Physics of Solids* **11**, 127-140.

Hill, R. 1952. The elastic behaviour of a crystalline aggregate. *Proceedings of the Physical Society of London Section A* **65**, 349-355.

Hornby, B.E., Schwartz, L.M. & Hudson, J.A. 1994. Anisotropic effective-medium modeling of the elastic properties of shales. *Geophysics* **59**, 1570-1583.

Hudson, J.A. & Knopoff, L. 1989. Predicting the overall properties of composite-materials with small-scale inclusions or cracks. *Pure and Applied Geophysics* **131**, 551-576.

Jakobsen, M., Hudson, J.A. & Johansen, T.A. 2003. T-matrix approach to shale acoustics. *Geophysical Journal International* **154**, 533-558.

Johansen, T.A., Ruud, B.O. & Jakobsen, M. 2004a. Effect of grain scale alignment on seismic anisotropy and reflectivity of shales. *Geophysical Prospecting* **52**, 133-149.

Johansen, T.A., Spikes, K. & Dvorkin, J. 2004b. Strategy for estimation of lithology and reservoir properties from seismic velocities and density. *SEG Technical Program Expanded Abstracts* **23**, 1726-1729.

Kuster, G.T. & Toksoz, M.N. 1974. Velocity and attenuation of seismic-waves in 2-phase media I. Theoretical Formulations. *Geophysics* **39**, 587-606.

Marion, D., Nur, A., Yin, H. & Han, D. 1992. Compressional velocity and porosity in sand-clay mixtures. *Geophysics* **57**, 554-563.

Mindlin, R.D. 1949. Compliance of elastic bodies in contact. *Journal of Applied Mechanics-Transactions of the Asme* **16**, 259-268.

O'Connell, R.J. & Budiansky, B. 1974. Seismic velocities in dry and saturated cracked solids. *Journal of Geophysical Research* **79**, 5412-5426.

Sheng, P. 1990. Effective-medium theory of sedimentary-rocks. *Physical Review B* **41**, 4507-4512.

Walton, K. 1987. The effective elastic-moduli of a random packing of spheres. *Journal of the Mechanics and Physics of Solids* **35**, 213-226.

Xu, S.Y. & White, R.E. 1995. A new velocity model for clay-sand mixtures. *Geophysical Prospecting* **43**, 91-118.

Yin, H. 1992. *Acoustic velocitiy and attenuation of rocks, isotropy, intrinsic anisotropy, and stress induced anisotropy*. Ph.D. dissertation, Stanford University.

"The nicest thing about standards is that there are so many of them to choose from."

Ken Olsen

US computer engineer & industrialist (1926 -)

Founder of Digital Equipment Corp., 1977

APPENDIX V: PAPER 5

Conditioning of elastic and electrical parameters for use in reservoir characterization

Erling Hugo Jensen and Tor Arne Johansen

In preparation to be submitted to *Geophysical Prospecting,* 2011.

V

Conditioning of elastic and electrical parameters for use in reservoir characterization

Erling Hugo Jensen[1] and Tor Arne Johansen[1, 2].

ABSTRACT

There exist many elastic and electrical parameters with various degree of sensitivity to typical reservoir properties, e.g. porosity, lithology and fluid saturation. Some parameter combinations give better descriptions of the reservoir compared with others. The parameter sensitivities depend on lithological composition, texture and degree of consolidation which are reflected in the various models chosen when doing rock physics modelling. We present a method for obtaining a conditioned set of elastic and electrical parameters to be used for prediction of reservoir parameters. The best parameter combinations selected will on average give the most precise and robust predictions of porosity, lithology and fluid saturation. The method can be used to evaluate any number of parameters and rock physics models, and the results depend on the specific rock physics models considered.

INTRODUCTION

Geophysical reservoir characterization implies estimation of the amount and distribution of certain pore fluids within subsurface reservoirs. Furthermore, in reservoir monitoring of gas and oil production or CO_2 sequestration, it is vital to make an image of fluid flow due to injection and drainage of the various fluids. From a geophysical point of view this task essentially means to obtain properties like porosity, pore fluid saturation and lithology from seismic or electromagnetic data, or data obtained from other geophysical measurements.

A severe problem in seismic reservoir characterization is the imbalance in number of parameters retrieved from the seismic data and the number of reservoir parameters to be estimated. This means that the problem is initially often underdetermined, typically resulting in non-unique solutions. The functional relationships between reservoir data,

[1] Department of Earth Science, University of Bergen, Bergen, Norway.
[2] NORSAR, Bergen, Norway.

other rock properties as composition and texture, and the seismic parameters, e.g. the rock physics models, are neither unique. Models for unconsolidated, weakly consolidated and consolidated rocks are not unified, and they are partly formulated on different physical concepts.

The variation of the seismic properties due to variation in reservoir properties (sensitivity) may also be different for various rocks, and, thus, also from one rock physics model to another. For instance, it is well known that the sensitivity of seismic parameters to fluid saturation is more exposed in high porous (unconsolidated) sediments than in low porous consolidated rocks. However, in case the porosity contains a large fraction of compliant pores (cracks) the sensitivity of fluid saturation may also be significant even in low porosity rocks. The resistivity is also known to increase with increasing saturation of hydrocarbons and to decrease with reducing porosity as the conductive brine is replaced with insulating materials.

Studying the conditioning of elastic and electrical properties to use in reservoir characterization can aid in making more precise predictions which are less sensitive to data errors. Goodway, Chen and Downton (1997) suggested the potential use of $\rho\mu$ and $\rho\lambda$ inverted from amplitude versus offset data. The shear modulus μ can be used in lithology prediction as it is often insensitive to the fluid. Lamé's modulus λ is closely related to the bulk modulus and can be used to distinguish gas and brine saturated sandstones (Gray and Andersen 2000). The ambiguity introduced by the density ρ can be avoided following the improved method proposed by Gray (2002) for extracting μ and λ based on the re-expression of Lamé's parameters (Gray, Goodway and Chen 1999) from Aki and Richards (2002) approximation of the Zoeppritz equation. An even better parameter to characterize the fluid is supposedly the resistivity (or its reciprocal, the conductivity) which Johansen *et al.* (2005) showed can be a direct hydrocarbon indicator. Finally, λ/μ and $\lambda\rho$-$\mu\rho$, have also been proposed as good candidates for reservoir characterization (Liliana, Negchún and Vázquez 2004; Goodway *et al.* 1997).

Ødegaard and Avseth (2004) proposed a cross-plotting technique referred to as rock physics templates (RPT) to do quantitative predictions of porosity, lithology and fluid saturation. The typical parameter combination they use is the P- and S-wave velocity ratio versus the P-wave acoustic impedance. However, combinations of other parameters can also be considered. In the following, we study the conditioning of various elastic and electrical parameters to use in reservoir characterization with the aim to provide the parameter combination giving more precise solutions. Such information is important to have when attempting to do more precise quantitative prediction of the reservoir quality, e.g. using the inverse rock physics modelling of Johansen *et al.* (2011). They identify solutions by searching through a library of rock physics models relating the elastic and electrical properties to the reservoir parameters.

In this study we are not elaborating on the particular uncertainties of the studied parameters. Our focus is on examining the sensitivity of various combinations of elastic and electric parameters and how these influence on the stability of the solution, i.e. how susceptible our predictions are to errors in the input parameters. We present a general method for evaluating the conditioning of elastic and electrical properties to use in reservoir characterization. It is not limited to a particular rock physics model or specific parameters. The method provides a kind of sensitivity analysis which is useful when presenting estimations of the reservoir quality.

The paper is organized as follows. We start with quantifying the reservoir parameters and reviewing some geophysical relations. Then we explain the inverse rock physics modelling which the conditioning method is based on, before explaining the method itself. Finally, we apply the approach on two data examples; one based on a synthetic data and another based on data from laboratory measurements.

RESERVOIR AND GEOPHYSICAL PROPERTIES

There are several reservoir properties which are used as input in rock physics models to calculate the effective elastic and electrical properties. In the following, we will focus on porosity ϕ, lithology C and fluid saturation S, also referred to as the PLF parameters. However, permeability, pore and confining pressure, temperature, mineral and pore fluid composition, coordination number and cementation are examples of other properties which are also important for reservoir characterization.

The porosity is the volume fraction of the rock which does not contain minerals. The lithology can be attached as the volume fraction of certain minerals of the solid phase. In siliciclastic rocks, the clay content is used to discriminate between e.g. clean sands, shaley sands, sandy shales and shale. These various lithologies can have significant impact on the reservoir quality, and, thus, lithology is simplified to the clay volume fraction of the solid phase. In case of a rock composed of quartz and clay, we get

$$C = \frac{V_{\text{clay}}}{V_{\text{clay}} + V_{\text{quartz}}}, \tag{1}$$

where V_{clay} and V_{quartz} are the volumes of the clay and quartz minerals, respectively. Similarly, the fluid saturation is the volume fraction of the various fluids in the pore space. For a mixture of gas and brine, the brine saturation is given by

$$S = \frac{V_{\text{brine}}}{V_{\text{brine}} + V_{\text{gas}}}, \tag{2}$$

where V_{brine} and V_{gas} are the volumes of brine and gas, respectively.

Using these parameters, the density ρ of a siliciclastic rock is accordingly

$$\rho(\phi, C, S) = \phi\left[S\rho_{\text{brine}} + (1-S)\rho_{\text{gas}}\right] + (1-\phi)\left[C\rho_{\text{clay}} + (1-C)\rho_{\text{quartz}}\right], \quad (3)$$

where ρ_{brine}, ρ_{gas}, ρ_{clay} and ρ_{quartz} are the brine, gas, clay and quartz densities, respectively. Applying a rock physics model, we can use the PLF parameters as input to calculate the effective bulk modulus $K(\phi, C, S)$ and shear modulus $\mu(\phi, C, S)$. Various models exist for describing the physical properties of different types of rocks. The minimum and maximum elastic moduli of any isotropic or anisotropic material are given by the Reuss (1929) and Voigt (1928) bounds, respectively. Hashin-Shtrikman (Hashin and Shtrikman 1963) is another bounding model which can for example be used for modelling coated minerals. We have contact theories (Walton 1987; Digby 1981; Mindlin 1949) suitable for computing the elastic parameters of loose unconsolidated material, and shown to be reliable for pure quartz sandstones and shaley sandstones (Avseth *et al.* 2005). For more consolidated rocks inclusion based models (Berryman 1992; Sheng 1990; Kuster Toksöz 1974) are more appropriate. Those referred are only some of many rock physics models presented in the literature.

From the density, bulk and shear moduli we can derive other elastic properties. The P and S velocities (V_{p} and V_{s}) of homogeneous and isotropic materials are

$$V_{\text{p}} = \sqrt{\frac{K + \frac{4}{3}\mu}{\rho}}, \quad (4)$$

$$V_{\text{s}} = \sqrt{\frac{\mu}{\rho}}. \quad (5)$$

When the bulk and shear moduli are given in GPa and the density is given in g/cm^3, the unit of the P- and S-wave velocities are km/s. The Poisson's ratio ν is the ratio of the transverse to the axial strain for a medium exposed to a uniaxial stress. For an isotropic material we have

$$\nu = \frac{3K - 2\mu}{2(3K + \mu)}. \quad (6)$$

The P-wave modulus M, Young's modulus E and Lamé's modulus λ have the same unit as the bulk and shear moduli, and are given by

$$M = K + \frac{4}{3}\mu \ , \tag{7}$$

$$E = \frac{9K\mu}{3K + \mu} \ , \tag{8}$$

$$\lambda = K - \frac{2}{3}\mu \ . \tag{9}$$

Even though some of these elastic properties respond more to certain reservoir parameters than others, we shall see that the actual sensitivity of the various physical properties depend on the applied rock physics model.

INVERSE ROCK PHYSICS MODELLING

The inverse rock physics modelling of Johansen *et al.* (2011) make use of forward modelled constraints of elastic and electrical properties from varying reservoir parameters. When studying the sensitivity of the three reservoir properties porosity, lithology and fluid saturation (PLF), these constraints can be presented as 3D cubes, which we denote constraint cubes. Figure 1 shows an example of a density constraint cube with the PLF parameters defining the coordinate axes. In the following we limit the PLF domain to the most relevant range for porosity [0, 0.4] and from [0, 1.0] for lithology and fluid saturation. Each point in the cube has a specific density value which is represented by a colour. In our example one cube is created by defining a 26x26x26 grid of equidistant values for the PLF parameters. For each node in the grid the density is calculated according to equation 3. We interpolate to calculate the values between the nodes. Similarly, constraint cubes for the other elastic and electrical properties can be created. The constraint cubes can be interpreted as a three dimensional scalar field $D_{li}(\phi,C,S)$, where indices l and i identify the specific rock physics model and the various elastic and electrical parameters, respectively.

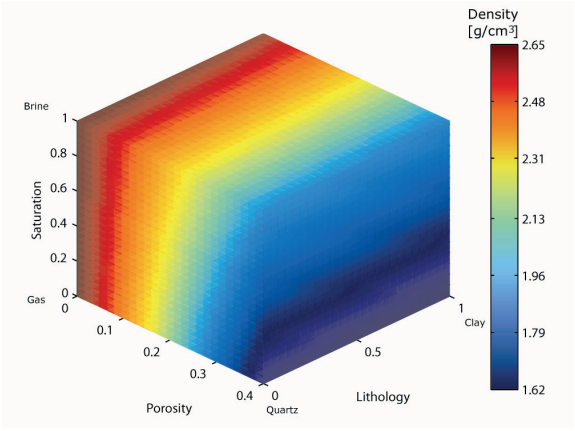

Figure 1 Density constraint cube for a mixture of quartz, clay, gas and brine.

In the inverse rock physics

modelling scheme, the scalar field of elastic or electrical parameters, i.e. the constraint cubes, are numerically resampled into a set of correlation functions $F_l(\hat{d}_i)$. For a specific value of parameter $\hat{d}_i$ of the *i*-th parameter, $F_l(\hat{d}_i)$ now defines all reservoir parameter combinations associated with this value. In our 3D example, this set of values make up a surface in the PLF domain, which we hereafter denote an isosurface because all points on that surface have the same property value $\hat{d}_i$. We denote $F_l(\hat{d}_i)$ the isosurface relation, and it can be found e.g. by using a marching cubes algorithm (Lorensen and Cline 1987) or in MATLAB using the native isosurface function.

The isosurface relation provides the solution to an inverse rock physics modelling considering only one elastic or electrical parameter as input (see Figure 2). Using only one parameter thus only weakly constrains the possible PLF values, However, usually we have two and sometimes three parameters which we can use. With two parameters, the possible PLF solutions are constrained to the intersecting line between the two respective isosurfaces (see Figure 3), i.e.

$$F_l(\hat{d}_i) \cap F_l(\hat{d}_j). \tag{4}$$

where $\hat{d}_j$ is the value of the *j*-th property. Using a measurement $\hat{d}_k$ of a third property identified with the index *k*, reduces the domain for the PLF solutions even further to where all three isosurfaces intersect (see Figure 4), i.e.

$$F_l(\hat{d}_i) \cap F_l(\hat{d}_j) \cap F_l(\hat{d}_k). \tag{5}$$

The inverse modelling results in either no solution, solutions forming one or more sub volumes, surfaces, lines or individual points in the PLF domain, depending on the applied rock physics model, the number of data parameters used as input in the modelling and their respective values with or without taking uncertainties into consideration.

No solutions implies that the applied rock physics model is not consistent with the data, while a solution means the model can relate reservoir properties to the input data. Some models might give similar while others give different predictions of the model parameters. Not all of them can be correct; hence, it is important to remember a particular solution is probably not the only possible solution and might not be the correct solution. Finally, finding several solutions does not necessarily mean that any of them are correct.

Uncertainty can be handled in the inverse rock physics modelling by perturbing the elastic and electrical properties, i.e. not only considering the given data value, but repeating the intersection seeking procedure for values close to it.

CONDITIONING OF PARAMETER SET

The solutions of an inverse rock physics modelling are often non-unique because of the imbalance between the number of parameters derived from measurements and the number of reservoir parameters to be estimated, the number of possible rock physics models and their non-linear relations between the various parameters. Our aim is to reduce the ambiguity in the porosity, lithology and fluid saturation (PLF) estimations to acquire as precise and robust predictions as possible. This can be achieved if we manage to reduce the number of solutions, the range of PLF values in the solutions and the number of unstable

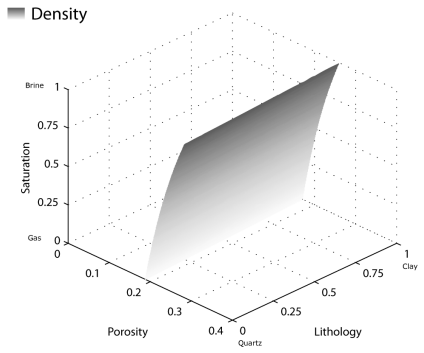

Figure 2 Isosurface for a particular density value which constrains the porosity more than the lithology and fluid saturation.

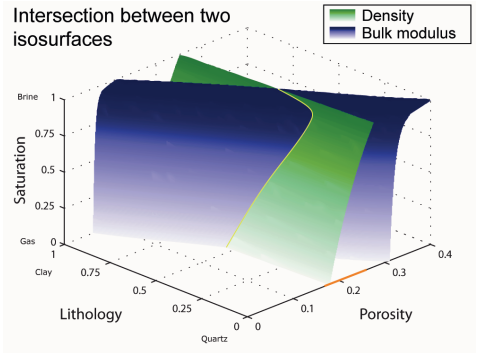

Figure 3 Porosity, lithology and fluid saturation constrained to the intersecting line (highlighted in yellow) between isosurfaces for a particular value of the density and bulk modulus. The porosity interval for the solution is highlighted in orange on the porosity axis.

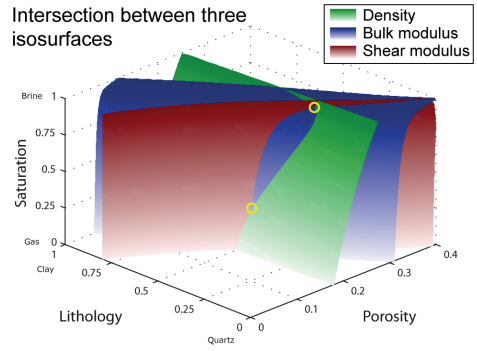

Figure 4 Porosity, lithology and fluid saturation constrained to the intersecting points (highlighted by yellow circles) between isosurfaces for a particular value of the density, bulk and shear moduli.

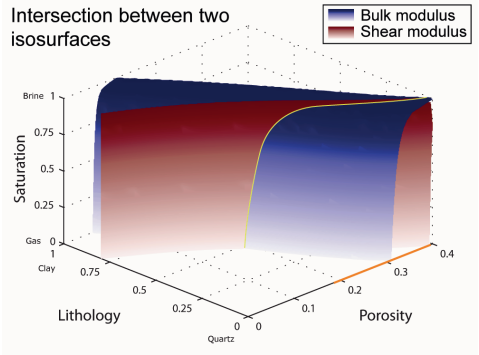

Figure 5 Porosity, lithology and fluid saturation constrained to the intersecting line (highlighted in yellow) between isosurfaces for a particular value of the bulk and shear moduli. The porosity interval for the solution is highlighted in orange on the porosity axis.

solutions. The latter is important because we are dealing with uncertain observations, and we want to avoid a situation where a small perturbation in the elastic or electrical parameters results in a significant change in the estimated PLF values. We are limited by the parameters at our disposal and their PLF sensitivities, but some parameter combinations give more precise and robust solutions than others.

Compare the porosity solution range marked in orange on the porosity axis in Figure 5 with the one in Figure 3. Individually, the bulk and shear moduli in Figure 5 do practically not constrain the porosity at all which in this case results in a wide range of possible porosities. In Figure 3, we see that the imposed constraints of the density on the porosity results in a smaller range of values for this reservoir parameter when combined with the same bulk moduli as in Figure 5.

Figure 6 illustrates the problem with solution stability. The isosurfaces for two values of the P-wave velocity V_p is plotted together with the isosurface for a density value (Figure 6a) and an S-wave velocity value (Figure 6b). The density isosurface intersects the V_p isosurfaces at an angle closer to 90° than the V_s isosurface does. Hence, in Figure 6a the small change of less than 3% in the V_p value results in a very small change in the PLF solution, while a significant deviation in predicted PLF values can be observed in Figure 6b.

Examining the topology of the isosurfaces in the constraint cubes confirms some of our previous statements regarding sensitivity. Figure 7 shows the V_p/V_s velocity ratio constraint cubes for an inclusion based and an unconsolidated model. The unconsolidated model displays a clear reduction in the velocity ratio with porosity due to the softening of the rock and reduced P-wave velocity. The inclusion based model does not exhibit similar sensitivity to the porosity. For a particular rock physics model, the sensitivity can change within the PLF domain. This is illustrated for the inclusion based model in Figure 8 where we have plotted the isosurfaces for two different values of the V_p/V_s velocity ratio.

We propose a method for evaluating the conditioning of the elastic and electrical parameters to be used in estimating the PLF parameters. We start by extracting information about the average topology of the isosurfaces in the constraint cubes, i.e. the sensitivity to the PLF parameters, and imposed variances due to differences in the applied rock physics models. Afterwards, we consider the average orientation of the isosurfaces to help choose combinations of elastic and electrical properties which give the most stable solutions.

Reservoir property sensitivities

For each elastic and electrical parameter, denoted data parameter, we calculate an average PLF sensitivity value. The values range from 0 to 1, where a more sensitive parameter will have a higher value than a less sensitive parameter. Hence, a porosity sensitivity value close to 1 means that the normal vectors of every point on the isosurfaces

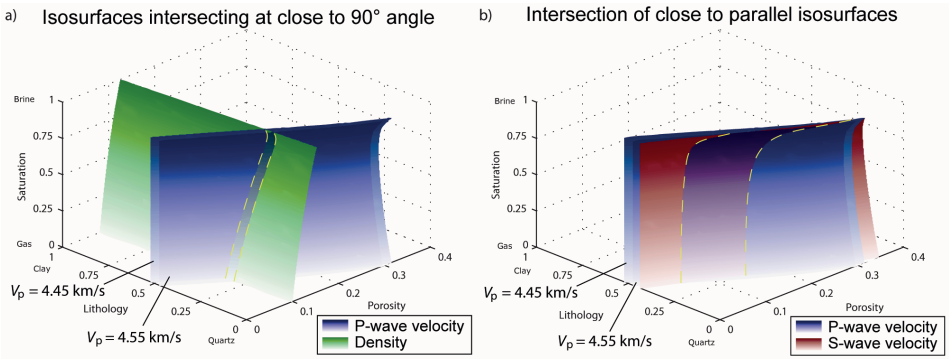

Figure 6 Illustration of solution stability due to angle between intersecting (yellow stippled lines) property isosurfaces. An intersection at (a) an angle closer to 90° displays more stable solutions than intersection of (b) more parallel surfaces.

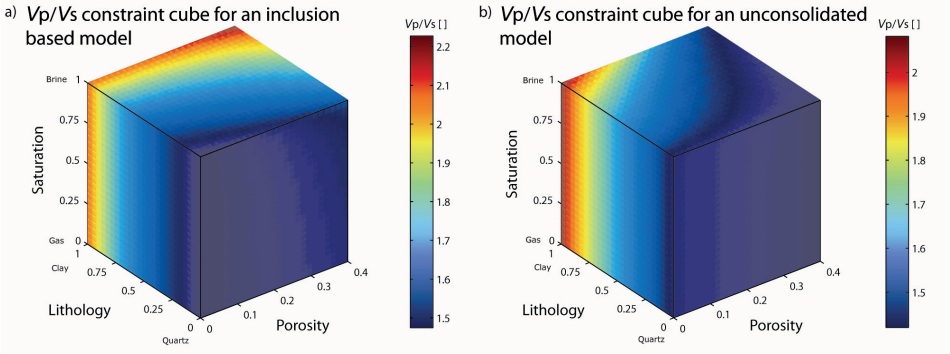

Figure 7 V_p/V_s velocity ratio constraint cubes for (a) an inclusion based model and (b) a model of an unconsolidated rock.

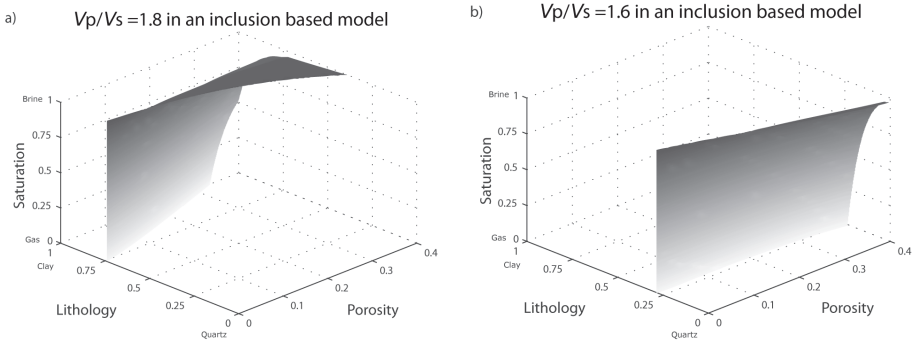

Figure 8 V_p/V_s velocity ratio isosurfaces for an inclusion based model for (a) V_p/V_s = 1.8 and (b) V_p/V_s = 1.6.

making up the porosity constraint cube, are close to parallel with the porosity axis. This implies that the isosurfaces must exhibit quite flat topologies and form an angle close to 90° with the porosity axis.

The sensitivity value ξ_{mi} for a PLF parameter *m* of data parameter *i* is a measure of the average PLF dispersion and we define it as

$$\xi_{mi} = 1 - \overline{\sigma}_{mi} \ , \tag{6}$$

where $\overline{\sigma}_{mi}$ is the mean normalised standard deviation for this PLF and data parameter, averaged over the various rock physics models we are testing. Considering a total of *Q* models, we have that

$$\overline{\sigma}_{mi} = \frac{1}{Q}\sum_{l=1}^{Q}\overline{\sigma}_{lmi} \ , \tag{7}$$

where $\overline{\sigma}_{lmi}$ is the mean normalised standard deviation for rock physics model *l*. We calculate $\overline{\sigma}_{lmi}$ by sampling through a total of *P* equidistant values between the minimum and maximum data parameter values of the corresponding scalar field $D_{li}(\phi,C,S)$, where the PLF parameters ϕ, *C* and *S* are the porosity, lithology and fluid saturation, respectively. Next, we calculate the PLF parameter values correlating to the *P* data values using the isosurface relation $F_l\left(\hat{d}_i\right)$. From a geometrical perspective, this means we approximate the constraint cubes to be made up of *P* isosurfaces, where *P* must be large enough to capture local variations of the PLF and data parameter dependencies in the scalar field. In this paper we use *P* = 76. We define the mean normalised standard deviation for rock physics model *l* to be

$$\overline{\sigma}_{lmi} = \frac{1}{P}\sum_{p=1}^{P}\sigma_{lmip} \ , \tag{8}$$

where σ_{lmip} is the normalised standard deviation for isosurface *p*. It is found by considering the isosurface being made up of N_{lip} discrete sets of data points and calculating the dispersion of the PLF parameter values defining those points. It is given by

$$\sigma_{lmip} = \frac{1}{\delta_m}\sqrt{\frac{1}{N_{lip}}\sum_{q=1}^{N_{lip}}\left(M_{lmipq} - \overline{M}_{lmip}\right)^2} \ , \tag{9}$$

where M_{lmipq} and $\overline{M}_{lmip}$ are the PLF parameter value in point q and the average of the PLF parameter values of all the data points on surface p, respectively. The PLF parameter normalising constant δ_m, is given by

$$\delta_m = \sigma_{\text{full}}\left(m_{\max} - m_{\min}\right) , \tag{10}$$

where $m_{\max}$ and $m_{\min}$ are maximum and minimum values for that PLF parameter, respectively. The factor σ_{full}, is the standard deviation representing a case with full dispersion, i.e. where the data points are evenly distributed between the minimum and maximum values. It depends on the number of data points, but it rapidly converges towards 0.2887. We use $\sigma_{\text{full}} = 0.3$, because for some calculations we have very few data points. By including the minimum and maximum values in the normalising constant we can compare the final results of the three PLF parameters even though they span different ranges.

We take the variance in sensitivity due to differences in the various rock physics models, into consideration by calculating the standard deviation ς_{mi} for model parameter m and data parameter i of $\overline{\sigma}_{lmi}$. It is given by

$$\varsigma_{mi} = \sqrt{\frac{1}{Q}\sum_{l=1}^{Q}\left(\overline{\sigma}_{lmi} - \overline{\sigma}_{mi}\right)^2} . \tag{11}$$

Combining sensitivities

Choosing combinations of data parameters with isosurfaces which on average are more parallel to a respective side in the constraint cubes will lead to the most stable solutions because they will then intersect at a close to normal angle. We calculate what we call a combined sensitivity, to help evaluate the average orientation of the isosurfaces in the constraint cubes. For PLF parameter m and data parameter i, we define the combined sensitivity value Ξ_{mi} as the sensitivity value for this PLF parameter subtracted the average sensitivity value of the other PLF parameters, i.e.

$$\Xi_{mi} = \left(1 + \frac{1}{\hat{M}-1}\right)\xi_{mi} - \left(\frac{1}{\hat{M}-1}\right)\sum_{\hat{m}=1}^{\hat{M}}\xi_{\hat{m}i} , \tag{12}$$

where $\hat{M}$ is the total number of PLF parameters and $\hat{m}$ is a summation index for the model parameters.

If we attempt to estimate the three PLF parameters using only two data parameters as input, we get an underdetermined problem. Because we will not be able to make precise

predictions for all three parameters we focus on two of them. For estimating the combined sensitivity value, we achieve this by excluding the sensitivity value in equation 12 for the PLF parameter we are ignoring.

We can select the data parameters with isosurfaces which on average have the flattest topology and are most normal to a respective PLF parameter axis, by choosing those with combined sensitivity values closest to 1 for each of the PLF parameters. This will in general lead to the smallest solution ranges and most stable solutions of the reservoir properties.

EXAMPLES

We demonstrate the conditioning evaluation method on two examples. In the first example we use a synthetic data set so that we have full control over the various parameters and to be able to test the performance of our evaluations. In the second example, we evaluate the conditioning of elastic and electrical parameters for eleven rock physics models. These models have been calibrated by Jensen *et al.* (2011) based on joint elastic-electrical laboratory measurements on compacting reservoir sandstone core plugs published by Han *et al.* (2011).

Example 1

The nine rock physics models we test in this study are summarised in Table 1. The solid components are mixed using the Hill model (Hill 1963), and the fluid components using Wood's equation (Wood 1955). The constituent properties are presented in Table 2. In the inclusion based models, we are testing three different pore geometries; 1) only spherical pores, 2) 50-50 spherical and ellipsoidal pores and 3) pores with various aspect ratios. (All non-spherical pores are oblate). The pore model details are listed in Table 3.

Models one through six are various realisations of the differential effective medium (DEM) theory (Bruggeman 1935), where the pore space is gradually introduced as inclusions into the solid host medium. The first three models are for the three chosen pore geometries when the pore space is modelled as fluid saturated when using the DEM theory. The next three are for the three pore geometries when we introduce vacuous pores using the DEM model and then perform a Gassmann fluid substitution (Gassmann 1951) to calculate the effective elastic properties of the saturated rock.

In models seven and eight we calculate the bulk and shear moduli of the solid matrix using the modified Hashin-Shtrikman upper- and lower-bounds, respectively; also known as Hashin-Shtrikman-Walpole bounds (Walpole 1966a,b). We use the mineral value, when the rock has no porosity, and the highest porosity point (ϕ_{max} = 40%) as end members in the modelling. We calculate the elastic moduli of the high porosity point using the Hertz-

Mindlin model (Mindlin 1949). Again, we perform a Gassmann fluid substitution (Gassmann 1951) to calculate the effective elastic moduli of the saturated rock.

Model nine is based on Dvorkin and Nur's (1996) contact cement model (CCT). This theory is applicable for cemented granular rocks. We use CCT to calculate the effective dry rock bulk and shear moduli from the high porosity point down to a porosity of 15.25%.

Table 1 Rock physics models applied in example 1.

Model number	Short description
1	Differential effective medium with spherical pores.
2	Differential effective medium with spherical and ellipsoidal pores.
3	Differential effective medium with pores having various aspect ratios.
4	Differential effective medium with spherical pores and introducing the fluid phase through Gassmann fluid substitution.
5	Differential effective medium with spherical and ellipsoidal pores and introducing the fluid phase through Gassmann fluid substitution.
6	Differential effective medium with pores having various aspect ratios and introducing the fluid phase through Gassmann fluid substitution.
7	Hashin-Shtrikman-Walpole upper bound between mineral and Hertz-Mindlin modelled end-members and introducing the fluid phase through Gassmann fluid substitution.
8	Hashin-Shtrikman-Walpole lower bound between mineral and Hertz-Mindlin modelled end-members and introducing the fluid phase through Gassmann fluid substitution.
9	Hashin-Shtrikman-Walpole upper bound between mineral and contact cement modelled end-members.

Table 2 Rock physics properties of the constituents used in example 1.

Constituent	Density [g/cm^3]	Bulk modulus [GPa]	Shear modulus [GPa]
Quartz	2.65	37	44
Clay	2.60	21	7
Brine	1.02	2.62	0
Gas	0.1466	0.042	0

Table 3 Pore geometries we use in example 1.

Pore geometries	Aspect ratios	Corresponding aspect ratio concentrations
Spherical	1.0	1.0
50-50 spherical and ellipsoidal	1.0	0.5
	0.1	0.5
Various aspect ratios	1.0	0.6419
	0.5	0.3205
	0.1	0.03205
	0.01	0.005
	0.001	0.0005
	0.0001	0.00005

Between this porosity and the mineral point we use the Hashin-Shtrikman-Walpole (Walpole 1966a,b) lower bound to calculate the elastic moduli. We apply Gassmann fluid substitution (Gassmann 1951) to find the effective elastic moduli of the saturated rock.

Models one through six and nine are appropriate for modelling consolidated rocks, and model seven and eight are typically used for modelling unconsolidated rocks. See Appendix A for more details about the various models.

We generate a synthetic data log by calculating elastic properties for 27 different combinations of porosity, lithology and fluid saturation (PLF), using rock physics model number 3. The PLF combinations are shown in Figure 9.

After evaluating the conditioning of the elastic properties we will use the inverse rock physics modelling of Johansen *et al.* (2011) on various combinations of the elastic parameters to test the performance of our evaluation. Furthermore, in this example we choose to only combine two elastic parameters to demonstrate the consequence of having such an under-determined problem.

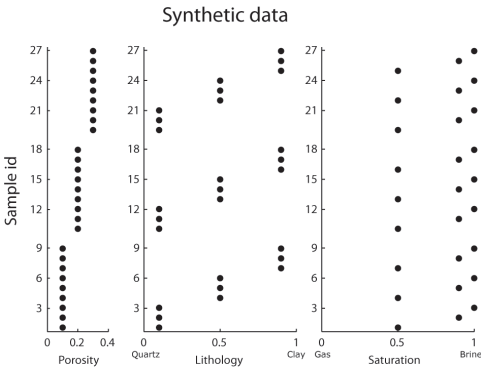

Figure 9 Porosity, lithology and fluid saturation for the synthetic data set.

Example 2

Here we assume to be in a pre-inverse modelling phase. We evaluate various combinations of elastic and electrical properties which can be suitable for doing reservoir characterization based on data from a seismic and possibly controlled-source electromagnetic survey. The rock physics models we test have been calibrated (Jensen *et al.* 2011) against joint elastic-electrical compaction measurements on reservoir sandstones (Han *et al.* 2011). The measurements were done on brine saturated core plugs mainly composed of quartz and kaolinite. We have no specific information about the reservoir itself, but in the following we assume it to be at about 2 km depth. Furthermore, in anticipation of locating oil, the fluid saturation S is now the volume fraction of brine versus oil with $S = 1$ still meaning fully brine saturated. The constituent properties used in this modelling are listed in Table 4.

We use differential effective medium theory (Mukerji *et al.* 1995; Gelius and Wang 2008) on eleven models. For consistency, the mineral constituents are used as inclusion material in both the elastic and electric modelling (Jensen *et al.* 2011). The electric

modelling has the fluid phase as the host material and the elastic modelling uses the bulk and shear moduli for the rock at a critical porosity as host material. We use the calibrated values of Jensen *et al.* (2011) for the critical porosity with corresponding elastic moduli and the elastic moduli of the clay mineral (see Table 5).

Table 4 Rock physics properties of the constituents used in example 2.

Constituent	Density [g/cm^3]	Bulk modulus [GPa]	Shear modulus [GPa]	Conductivity [S/m]
Quartz	2.65	37	44	0
Clay	2.60	20.6	8.46	0.02
Brine	1.02	2.67	0	9.43
Oil	0.79	1.31	0	0

Table 5 Model properties used in example 2.

Model	Clay aspect ratio	Properties at critical porosity		
		Porosity [%]	Bulk modulus [GPa]	Shear modulus [GPa]
SX1	0.087	36.0	3.086	3.086
SX2	0.034	36.0	4.450	4.450
SX3	0.105	36.0	4.810	4.809
SX4	0.081	42.6	4.990	3.483
SX5	0.108	49.3	7.888	2.561
SX6	0.153	36.2	5.698	5.689
SX7	0.145	50.0	8.000	2.957
SX8	0.052	50.0	8.000	3.446
SX9	0.072	45.2	7.061	5.517
SX10	0.032	36.0	4.552	4.552
SX11	0.095	36.0	6.548	6.548

RESULTS

Example 1

Table 6 lists the results of the sensitivity analysis for the sixteen tested elastic parameters. The entries are sorted in descending order according to the combined sensitivity value for the porosity. Focusing on the porosity, the density ρ is clearly the most and the Poisson's ratio the least sensitive. Furthermore, as can be expected, there is no variation in the sensitivity for the density, while the P- over S-wave velocity ratio (V_p/V_s) and Lamé's modulus λ divided with the shear modulus μ are the parameters with largest variation in sensitivity with respect to porosity. Considering the lithology, $\lambda\rho$-$\mu\rho$ is the

most and the density the least sensitive. Poisson's ratio displays the largest variation in sensitivity with respect to lithology.

The combined sensitivity values singles out the density to be best suited for conditioning the porosity. It has a significantly higher value of 0.77 than the second best parameter which is $\lambda\rho$ with a value of 0.62. Considering the lithology, there are three parameters which are almost equally good, namely Poisson's ratio, λ/μ and the V_p/V_s ratio with combined sensitivity values of 0.40, 0.37 and 0.37, respectively. All of them exhibit large variations in sensitivity.

Based on these results, we expect the density to be best for making porosity predictions and Poisson's ratio, λ/μ and V_p/V_s are good candidates for lithology predictions. But the S-wave velocity and $\lambda\rho$-$\mu\rho$ might be equally good as their combined sensitivity value for the lithology are close to the same as for the other three when taking the variance into consideration.

Table 7 shows the parameter combinations we choose to test in the inverse rock physics modelling and a brief reasoning for each of them. For the uncertainty analysis, perturbation is applied to the elastic parameter which is most sensitive to the lithology.

Figure 10a shows the normalised average dispersion of the model parameter predictions for the various property combinations, considering all the rock physics models, data samples and perturbations; i.e. solution ranges. We see low dispersions for the combinations we expected to do well and high for those we expected to do badly. Figure 10b shows the average dispersion in mean model parameter prediction for the various property perturbations, considering the tested rock physics models and data samples; i.e. the stability of the solutions. The density versus the S-wave velocity and versus $\lambda\rho$-$\mu\rho$ give the most stable solutions.

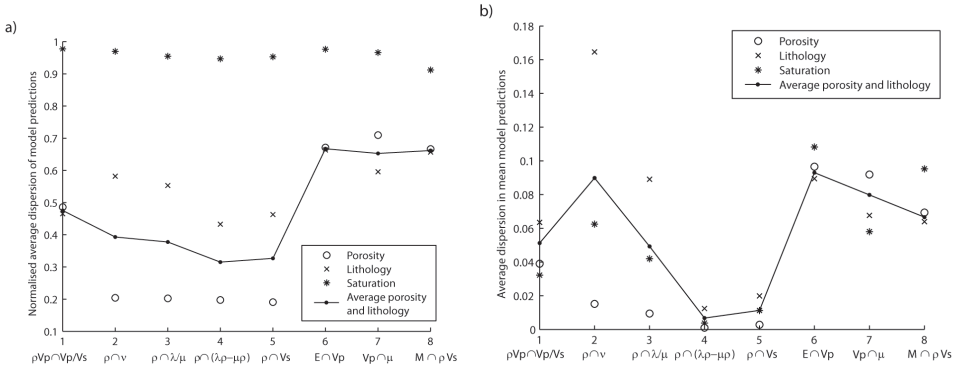

Figure 10 Average (a) solution ranges and (b) solution stability for various combinations of the elastic properties, based on the results of the inverse rock physics modelling.

Table 6 Results of sensitivity analysis for example 1. The parameters are the bulk modulus (K), density (ρ), Lamé's modulus (λ), P-wave modulus (M), P-wave velocity (V_p), Poisson's ratio (ν), shear modulus (μ), S-wave velocity (V_s), Young's modulus (E). The sensitivity, model variance in sensitivity and combined sensitivity values are respectively ξ, ς, Ξ indexed by the porosity ϕ and lithology C.

Parameters	$\xi_\phi \pm \varsigma_\phi$	$\xi_C \pm \varsigma_C$	Ξ_ϕ	Ξ_C
ρ	0.82 ± 0.00	0.05 ± 0.00	0.77	-0.77
$\lambda\rho$	0.73 ± 0.03	0.11 ± 0.01	0.62	-0.62
λ	0.69 ± 0.05	0.13 ± 0.02	0.56	-0.56
K	0.65 ± 0.03	0.33 ± 0.03	0.32	-0.32
ρV_p	0.63 ± 0.04	0.40 ± 0.04	0.23	-0.23
M	0.61 ± 0.05	0.51 ± 0.03	0.10	-0.10
ρV_s	0.58 ± 0.05	0.50 ± 0.04	0.08	-0.08
$\mu\rho$	0.63 ± 0.05	0.59 ± 0.02	0.04	-0.04
E	0.58 ± 0.06	0.57 ± 0.03	0.01	-0.01
V_p	0.51 ± 0.06	0.50 ± 0.06	0.01	-0.01
μ	0.57 ± 0.06	0.61 ± 0.03	-0.04	0.04
V_s	0.46 ± 0.07	0.59 ± 0.06	-0.13	0.13
$\lambda\rho - \mu\rho$	0.55 ± 0.05	0.77 ± 0.03	-0.22	0.22
V_p / V_s	0.29 ± 0.12	0.66 ± 0.10	-0.37	0.37
λ/μ	0.32 ± 0.13	0.69 ± 0.08	-0.37	0.37
ν	0.18 ± 0.03	0.58 ± 0.14	-0.40	0.40

Table 7 Combination of properties we test in the inversion in example 1. The perturbations are applied to the parameters we associate with the lithology prediction.

Label	**Parameter for prediction of**		**Reasoning for the various combinations**
	Porosity	**Lithology**	
1	$\rho\, V_p$	(V_p / V_s)	Often used combination, e.g. in rock physics template.
Examples of combinations we expect to give good results.			
2	ρ	ν	Parameters with highest combined sensitivity values.
3	ρ	(λ/μ)	λ/μ has almost as high combined sensitivity value for lithology as ν, and lower dispersion.
4	ρ	$(\lambda\rho–\mu\rho)$	$\lambda\rho–\mu\rho$ does not have as high combined sensitivity value for lithology as ν and λ/μ, but much lower dispersion.
5	ρ	V_s	V_s has even lower combined sensitivity value for lithology as $\lambda\rho–\mu\rho$, but close to the same dispersion.
Examples of combinations we expect to give bad results.			
6	E	V_p	Combined sensitivity values closest to zero.
7	V_p	μ	Similar situation as E combined with V_p.
8	M	ρV_s	Sensitivity values for porosity and lithology are almost the same for M as they are for ρV_s.

Figure 11 shows the porosity, lithology and fluid saturation solutions for parameter combination 1, 4, 5 and 8, and for the rock physics model which we used to generate the synthetic data (i.e. the correct model). Combination 1, which is the often used combination, has on average slightly larger solution ranges than combination 4 and 5, which our parameter analysis favoured. Combination 8 was predicted to give bad results, and we can see it clearly has the largest solution ranges for porosity and lithology. However, it does have smaller solution ranges for saturation which we decided to ignore in our evaluation. Also, this combination displays a larger difference in solution ranges between those for the main and perturbed data values than the other combinations. Finally, note the stippled lines for two of the perturbations, showing that no solution could be found for these ill-conditioned elastic properties.

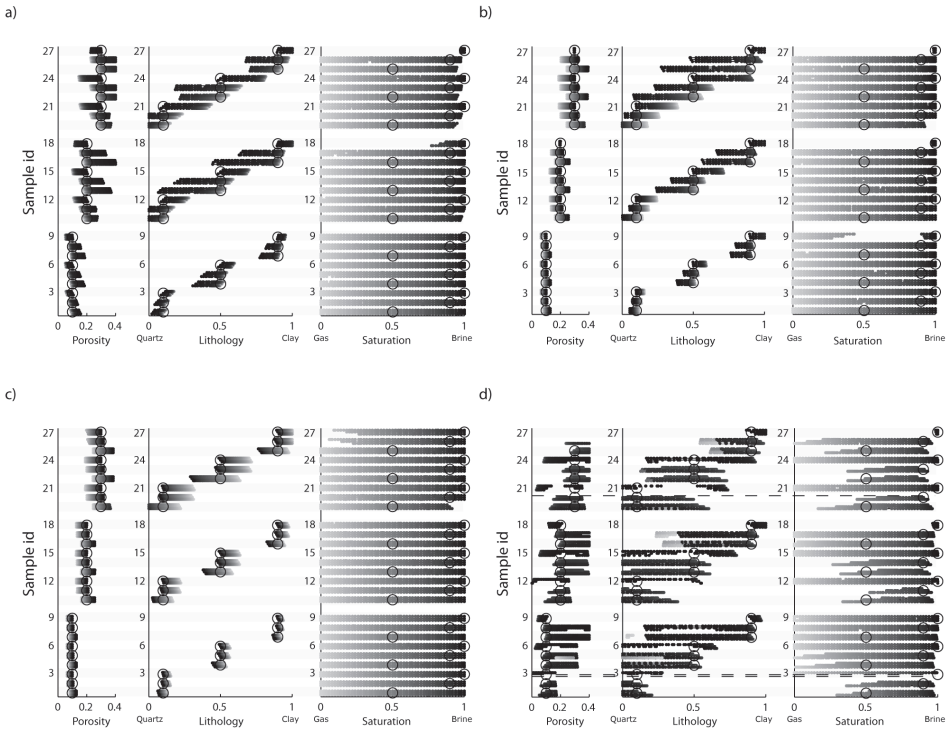

Figure 11 Porosity, lithology and fluid saturation solutions for using various combinations of the elastic properties in the inverse modelling; (a) ρV_p versus V_p/V_s, (b) ρ versus $\lambda\rho-\mu\rho$, (c) ρ versus V_s and (d) M versus ρV_s. The correct model parameters are plotted as circles and the modelled solutions as dots where the gray gradient corresponds to fluid saturation. The solutions from the perturbations are plotted above and below the main data values for positive and negative perturbations, respectively. The dimmed zebra stripes on the background separate the various data samples.

Example 2

Table 8 lists the results of the evaluation procedure for the five best candidates for each of the reservoir parameters, and sorted in descending order according to their respective combined sensitivity values. Because the eleven tested models are very homogeneous, the variance in the sensitivity values, i.e. average standard deviation over all models, is zero or close to zero for all studied properties.

Table 8 Results of sensitivity analysis for example 2. The parameters are the conductivity (σ), bulk modulus (K), density (ρ), Lamé's modulus (λ), P-wave velocity (V_p), Poisson's ratio (ν), shear modulus (μ), and S-wave velocity (V_s). The sensitivity, model variance in sensitivity and combined sensitivity values are respectively ξ, ς, Ξ indexed by the porosity ϕ, lithology C and saturation S.

		Parameters	ξ_ϕ	ς_ϕ	ξ_C	ς_C	ξ_S	ς_S	Ξ_ϕ	Ξ_C	Ξ_S
Prediction of	Porosity, ϕ	ρ	0.92	0.00	0.07	0	0.09	0	0.84	-0.43	-0.4
		$\lambda\rho$	0.77	0.03	0.12	0	0.07	0	0.68	-0.3	-0.37
		K	0.78	0.02	0.34	0.01	0.04	0	0.59	-0.07	-0.52
		λ	0.67	0.08	0.12	0.01	0.07	0.01	0.57	-0.25	-0.32
		ρV_p	0.78	0.01	0.38	0.01	0.04	0	0.56	-0.02	-0.54
	Lithology, C	$\lambda\rho - \mu\rho$	0.77	0.01	0.73	0.01	0.02	0	0.39	0.34	-0.73
		ν	0.59	0.02	0.58	0.03	0.04	0.01	0.28	0.27	-0.55
		V_p/V_s	0.53	0.03	0.5	0.06	0.06	0.03	0.25	0.21	-0.45
		μ	0.76	0.02	0.58	0.01	0.01	0	0.47	0.19	-0.66
		λ/μ	0.53	0.03	0.49	0.07	0.07	0.03	0.24	0.19	-0.44
	Saturation, S	σ	0.63	0.00	0.74	0.03	0.63	0	-0.06	0.11	-0.06
		λ	0.67	0.08	0.12	0.01	0.07	0.01	0.57	-0.25	-0.32
		$\lambda\rho$	0.77	0.03	0.12	0	0.07	0	0.68	-0.3	-0.37
		ρ	0.92	0.00	0.07	0	0.09	0	0.84	-0.43	-0.4
		λ/μ	0.53	0.03	0.49	0.07	0.07	0.03	0.24	0.19	-0.44

Again the density ρ singles out as the best property for predicting the porosity. But density estimates from seismic data are typically not very reliable. Therefore, $\lambda\rho$ (λ being Lamé's modulus) is a more likely candidate.

The combined sensitivity values with respect to lithology are quite close for the listed parameters in Table 8. But the sensitivity values display some differences. The two highest ranked parameters seem to be the best choices, namely $\lambda\rho - \mu\rho$ and ν (where μ is the shear modulus and ν is Poisson's ratio).

For the fluid saturation the conductivity is the best candidate followed by Lamé's modulus. However, the combined sensitivity value for the conductivity is negative because it is also very sensitive to the porosity and lithology.

Based on these results and a closer inspection of the relevant constraint cubes, we determine the best combination for predicting the porosity, lithology and fluid saturation under the assumed reservoir conditions, to be $\lambda\rho$, $\lambda\rho - \mu\rho$ and σ.

If a controlled-source electromagnetic survey is not an option, then due to the topology in the constraint cubes for the possible candidates, the bulk modulus K, ν and λ (or $\lambda\rho$) seems to be the best choice.

DISCUSSION

It is important to remember that the porosity, lithology and fluid saturation (PLF) sensitivity is modelled dependent. Hence, the results of the evaluation are not general which can be confirmed by inspecting the variance in sensitivity in example 1. One might of course see some general trends which can be applied in some qualitative studies, but will not necessarily apply to all possible cases and which might not satisfy the level of precision required in quantitative studies.

The combined sensitivity values can become negative due to the way we have defined them in equation 12. A negative value means it is equally sensitive to the other PLF parameter values as the one being studied. Alternatively, multiplication of sensitivity values could be used to calculate the combined sensitivity value, e.g. in example 1 where we have only two input elastic parameters, we could define it as

$$\Xi_{\text{porosity}}\left(\xi_{\text{porosity}}, \xi_{\text{lithology}}\right) = \xi_{\text{porosity}}\left(1 - \xi_{\text{lithology}}\right), \tag{23}$$

where ξ and Ξ are the sensitivity and combined sensitivity values, respectively. A disadvantage with this definition is that we will not as easily be able to determine the relative strength in sensitivity with respect to the two reservoir parameters. Also, the

combined sensitivity value would then give some possibly undesired results; e.g. $\Xi_{\text{porosity}}(0.9,0.9) = \Xi_{\text{porosity}}(0.1,0.1) < \Xi_{\text{porosity}}(0.5,0.5)$, $\Xi_{\text{porosity}}(0.9,0.6) = \Xi_{\text{porosity}}(0.6,0.4)$ and $\Xi_{\text{porosity}}(0.2,0.1) = \Xi_{\text{porosity}}(0.3,0.4)$.

Our parameter evaluation procedure can fail to identify good parameter combinations. Consider for example two hypothetical properties insensitive to the fluid saturation which gives completely vertical isosurfaces in the PLF domain (assuming the z-axis is associated with the saturation). If these surfaces intersect at a normal angle the solution would be a straight vertical line, i.e. one single porosity and lithology value. If in addition they are normal to a respective porosity and lithology axis, the parameter evaluation procedure would correctly identify them as a good combination for predicting these two reservoir properties. If we rotate both isosurfaces 45 degrees in the porosity-lithology plane about the intersecting line, we get a less trivial porosity and lithology dependency for the data parameters. Now, the evaluation procedure would wrongly identify this combination as badly conditioned. Hence, there is a chance of under predicting the conditioning of some combinations. This can be addressed by manual inspection of the respective constraint cubes or extending the procedure to find an average unit normal vector for each of the constraint cubes and evaluate the dot product between them.

Because the sensitivity and combined sensitivity values are averages over several models and the whole PLF domain, they might be misleading for specific solutions due to possible large variance in the sensitivity as shown in Figure 8. Therefore, it is important to consider the variance in sensitivity calculated in equation 11. We can see this in example 1 comparing the variation in sensitivity values for the four property combinations we expected to give good results. Number 2 and 3 were looking most promising based on the combined sensitivity values. But they displayed significantly higher variances than combination 4 and 5, which in our inverse modelling produced significantly better results than 2 and 3.

Another factor for the solution stability is the gradient of the data property in the PLF domain; how much are solutions displaced due to a change in a data property value, i.e. displacement of an isosurface. The evaluation procedure does not consider this factor; it only considers displacement of solutions due to the angle at the intersection between the respective isosurfaces. It is not included in the procedure because it is not so easy to give an average value for this. But a small difference between the maximum and minimum data parameter values in a constraint cube compared to uncertainties means this parameter is not well suited for reliable quantitative predictions of the reservoir parameters. However, most parameters have large enough difference between the minimum and maximum values, making them possible candidates. Because the properties often exhibit local variations in the gradient the stability of solutions is increased in certain parts, at the

expense of other parts in the PLF domain. An average of the gradient would typically cancel out these variations. Instead we suggest including information about the gradient as part of the sensitivity analysis when presenting the solutions of a particular inverse rock physics modelling.

In example 1 we confirmed the results of the elastic parameter conditioning evaluation by doing an inverse rock physics modelling. We predicted combinations **2**, **3**, **4** and **5** to give the best results, 6, 7 and 8 to give the worst and combination 1, the often used P-wave acoustic impedance versus V_p/V_s ratio, to be somewhere in between (see Table 7). Arranging these combinations with respect to having the narrowest PLF solution ranges from the inverse modelling, gives the following order (from smallest to largest): **4**, **5**, **3**, **2**, 1, 7, 6 and 8 (Figure 10a). Arranging them according to smallest variation of average solutions with respect to perturbing one of the properties, gives the following order (from smallest to largest): **4**, **5**, **3**, 1, 8, 7, **2** and 6 (Figure 10b).

The ambiguity of an underdetermined problem is clearly illustrated in the synthetic case study. Figure 11 shows the results of the inverse modelling using the correct rock physics model. We are not only presented with non-unique solutions, but no sensible prediction of fluid saturation can be done based on these results.

The lack of solutions for some of the perturbed values shown in Figure 11d illustrates the pitfall in choosing a badly conditioned elastic parameter combination. Here, the P-wave modulus combined with P-wave acoustic impedance could fail to identify the correct solution if one did not take uncertainties into consideration in the inverse modelling.

In example 2 we found the conductivity to be almost equally sensitive to the porosity and lithology as the fluid saturation. The reason for this is the applied rock physics model, which reflects the properties of the studied reservoir rock. It is obvious that the conductivity should exhibit comparable sensitivity to the porosity and fluid saturation; replacing a conductive fluid with a non conductive material, being fluid or solid will have an insulating effect on the rock. What might be less obvious is the large sensitivity towards lithology. The reason for this is that the clay is here modelled to be pore filling, i.e. replacing the fluid phase. And even though it is modelled with a conductivity of 0.02 S/m, it is much less conductive than brine.

A very homogeneous set of models were considered in the real data case study, giving rock physical descriptions of one of the expected facies in the reservoir. For a full analysis, this study should be extended to include relevant models for other facies expected to be found in the target reservoir and surrounding area. The presented parameter evaluation procedure can then for example be used to help select which combination of elastic and electrical parameters is best suited to identify the various facies.

CONCLUSIONS

We propose a procedure for evaluating the conditioning of elastic and electrical parameters to use in reservoir characterization. We demonstrate a good correlation between the results of the evaluation compared with the results from an inverse rock physics modelling for various data parameter combinations and models. In particular, we were able to identify which combinations give the most precise and robust predictions of the reservoir parameters. Also, we illustrate the ambiguity when predicting reservoir properties with respect to non-unique solutions, especially when dealing with uncertainties and an underdetermined problem. The method was demonstrated on both a controlled synthetic data set and on models calibrated against joint elastic-electrical laboratory measurements on core plugs.

In the synthetic data case study we find the density ρ and $\lambda\rho$-$\mu\rho$ (where λ and μ are the Lamé and shear modulus) to be the best combination for predicting the porosity and lithology. In the real data case study we predict $\lambda\rho$, $\lambda\rho-\mu\rho$ and the conductivity σ to give the most accurate predictions of the porosity, lithology and fluid saturation. Both results are model dependent and must not blindly be used as general truths.

ACKNOWLEDGEMENT

We thank the Norwegian Research Council (Petromaks program) and Statoil for financial support of the doctoral program of Erling Hugo Jensen.

APPENDIX A
ROCK PHYSICS MODELS

Hashin-Shtrikman-Walpole bounds

The Hashin-Shtrikman-Walpole bounds (Walpole, 1966a,b) is a more general form of the Hashin-Shtrikman bounds (Hashin and Shtrikman, 1963), and the bulk (K) and shear (μ) moduli are given by

$$K = K_1 + \frac{V_2}{(K_2 - K_1)^{-1} + V_1\left(K_1 + \frac{4}{3}\mu_m\right)^{-1}}, \qquad \text{(A-1)}$$

$$\mu = \mu_1 + \frac{V_2}{(\mu_2 - \mu_1)^{-1} + V_1\left[\mu_1 + \frac{\mu_m}{6}\left(\frac{9K_m + 8\mu_m}{K_m + 2\mu_m}\right)\right]^{-1}}, \quad \text{(A-2)}$$

where V is the volume fraction, index 1 and 2 refers to the two components, and the upper bound is found when K_m and μ_m are the maximum bulk and shear moduli of the two components. The lower bound is found when they are the minimum moduli of the two components.

Hertz-Mindlin model

In the Hertz-Mindlin (HM) model (Mindlin 1949) the effective elastic moduli of a dry, random packing of spherical grains is given by

$$K_{HM} = \left[\frac{C^2(1-\phi)^2\mu^2}{18\pi^2(1-\nu)^2}P\right]^{1/3}, \quad \text{(A-3)}$$

$$\mu_{HM} = K_{HM}\frac{3(5-4\nu)}{5(2-\nu)}, \quad \text{(A-4)}$$

where ϕ is the porosity, μ and ν are the shear modulus and Poisson's ratio for the mixed mineral, respectively. In this study we used a confining pressure P = 40 MPa, and the coordination number $C \approx 8.3147$ we interpolated from data compiled by Murphy (1982).

Contact cement theory

The contact cement theory (CCT) of Dvorkin and Nur's (1996) is used for calculating the effective dry rock elastic moduli of cemented granular rocks according to

$$K_{CCT} = \frac{1}{6}C(1-\phi_0)M_c S_n, \quad \text{(A-5)}$$

$$\mu_{CCT} = \frac{3}{5}K_{DN} + \frac{3}{20}C(1-\phi_0)\mu_c S_\tau, \quad \text{(A-6)}$$

$$M_c = \rho_c V_{pc}^2, \quad \text{(A-7)}$$

$$\mu_c = \rho_c V_{sc}^2, \quad \text{(A-8)}$$

where ϕ_0 is porosity of the starting framework, ρ_c, V_{pc} V_{sc} are the density, P- and S-wave velocities of the cement material, respectively. The S_n and S_τ parameters are proportional to

the normal and shear stiffnesses, respectively, and they depend on the cement and grain properties as well as the amount of contact cement.

Differential effective medium theory

The differential effective medium (DEM) theory (Bruggeman 1935) is an inclusion based theory taking into account higher order interaction. Here, one of the constituents is considered the host medium while the remaining components are embedded as inclusions. This is an asymmetric model because given the same volume fractions of the constituents, interchanging the host with one of the embedding components results in different elastic moduli. For a two phase composition the elastic moduli can, according to the differential effective medium theory, be solved from the coupled differential equations

$$(1-y)\frac{d}{dy}\left[K^*(y)\right] = \left(K_2 - K^*(y)\right)P_2^*(y), \tag{A-9}$$

$$(1-y)\frac{d}{dy}\left[\mu^*(y)\right] = \left(\mu_2 - \mu^*(y)\right)Q_2^*(y). \tag{A-10}$$

Phase one acts as the host material with bulk moduli $K_1 = K^*(y=0)$ and shear moduli $\mu_1 = \mu^*(y=0)$, while the bulk and shear moduli of phase two is K_2 and μ_2, respectively, and y is the volume fraction of phase two. The geometrical factors $P_2^*(y)$ and $Q_2^*(y)$ are calculated having phase two as the inclusion material in a host with effective moduli K^* and μ^*.

In the real data case study where we have chosen the minerals as the inclusion material, we use the modified differential effective medium theory (Mukerji *et al.* 1995) where the high porous end member is redefined to a chosen critical porosity.

For the conductivity σ, we use the differential effective medium of Gelius and Wang (2008)

$$\sigma(T,\phi,s,S_w) = \sigma_w S_w^m \phi^m \left(\frac{B(s,T) + lB(s,T)\sigma_K(s,T)/\sigma(s,T,S_w)}{B(s,T) + lB(s,T)\sigma_K(s,T)/\sigma_w} \right)^n, \tag{A-11}$$

where T, ϕ, s, S_w, σ_w, σ_K are the temperature, porosity, brine salinity, water saturation, water and kaolinite conductivities, respectively. The ease of which cations move along the clay surface is given by the equivalent electrical conductance parameter B. The geometrical parameters l, m and n are functions of the porosity, water saturation and volume fraction of kaolinite, as well as the quartz and clay grain alignment factors m_Q and m_K, respectively. In our modelling, m_Q is set to 1.5 because we assume spherical quartz grains. The clay grains are modelled as disperse in the pore space. It is also assumed a polarization effect where

the clay particles are aligned with their major axis parallel with the electric field. If the depolarization factor of the major axis is $A_{a,}$ this implies that the clay alignment factor m_K is set to $1/A_a$. More details can be found in Gelius and Wang (2008).

REFERENCES

Aki K. and Richards P.G. 2002. *Quantitative seismology*. University Science Books, ISBN 9780935702965.

Avseth P., Mukerji T. and Mavko G. 2005. *Quantitative Seismic Interpretation. Applying Rock Physics Tools to Reduce Interpretation Risk*. Cambridge University Press, ISBN 9780521151351.

Berryman J.G. 1992. Single-scattering approximations for coefficients in Biot's equations of poroelasticity. *J. Acoust. Soc. Am*. **91**, 551-571.

Bruggeman D.A.G. 1935. Berechnung verschiedener physikalischer Konstanten von heterogenen Substanzen. *Ann. Physik (Leipzig)* **24**, 636-679.

Digby P.J. 1981. The Effective Elastic Moduli of Porous Granular Rocks. *Journal of Applied Mechanics* **48**, 803-808.

Dvorkin J. and Nur A. 1996. Elasticity of high-porosity sandstones: theory for two North Sea datasets. *Geophysics* **61**, 1363-1370.

Gassmann F. 1951. Über die Elastizität poröser Medien. *Vierteljahrsschrift der Naturforschenden Gesellschaft in Zürich* **96**, 1-23.

Gelius L.-J. and Wang Z. 2008. Modelling production caused changes in conductivity for a siliciclastic reservoir: a differential effective medium approach. *Geophysical Prospecting* **56**, 677-691.

Goodway B., Chen T. and Downton J. 1997. Improved AVO fluid detection and lithology discrimination using Lamé petrophysical parameters. *Expanded Abstracts*. CSEG, 1997 Convention.

Gray D. 2002. Elastic inversion for Lamé parameters. *72nd Annual International Meeting*, SEG, Expanded Abstract, 213-216.

Gray F.D. and Andersen E.A. 2000. The Application of AVO and Inversion to Formation Properties. *World Oil* **221**.

Gray D., Goodway B. and Chen T. 1999. Bridging the gap: Using AVO to detect changes in fundamental elastic constants. *69th Annual Internat. Mtg.,* SEG Expanded Abstract **18**, 852-855.

Han T., Best A.I., Sothcott J. and MacGregor L.M. 2011. Joint elastic-electrical properties of reservoir sandstones and their relationships with petrophysical parameters. *Geophysical Prospecting* **59**, 518-535.

Hill R. 1963. Elastic properties of reinforced solids: Some theoretical principles. *Journal of the Mechanics and Physics of Solids* **11**, 357-372.

Jensen E.H., Gelius L.-J., Johansen T.A. and Wang Z. 2011. Consistent joint elastic-electrical differential effective medium modelling of compacting reservoir sandstones. *Submitted to Geophysical Prospecting.*

Hashin Z. and Shtrikman S. 1963. A variational approach to the theory of the elastic behaviour of multiphase materials. *Journal of the Mechanics and Physics of Solids* **11**, 127-140.

Johansen S., Amundsen H.F., Røsten T., Ellingsrud S., Eidesmo T. and Bhuyian A. 2005. Subsurface hydrocarbons detected by electromagnetic sounding. *First Break* **23**, 31-36.

Johansen T.A., Jensen E.H., Mavko G. and Dvorkin J. 2011. Inverse rock physics modelling. *In preparation to be submitted to Geophysics*.

Kuster G.T. and Toksoz M.N. 1974. Velocity and attenuation of seismic waves in two-phase media: Part I. Theoretical formulations. *Geophysics* **39**, 587-606.

Liliana V.-M., Megchún J. and Vázquez G. 2004. Petrophysical properties estimation by integrating AVO, seismic inversion and multiattribute analysis in a 3-D volume of Playuela, Veracruz. *Extended abstract for AAPG International Conference*, Cancun, Mexico.

Lorensen W.E. and Cline H.E. 1987. Marching cubes: A high resolution 3D surface construction algorithm. *SIGGRAPH Comput. Graph*. **21**, 163-169.

Mindlin R.D. 1949. Compliance of elastic bodies in contact. *J. Appl. Mech*. **16**, 259-268.

Mukerji T., Berryman J.G., Mavko G. and Berge P.A. 1995. Differential effective medium modelling of rock elastic moduli with critical porosity constraints. *Geophys. Res. Lett*. **22**, 555-558.

Murphy W.F. III. 1982. Effects of Microstructure and Pore Fluids on the Acoustic Properties of Granular Sedimentary Materials. *Ph.D. dissertation, Stanford University*.

Ødegaard E. and Avseth. P. 2004. Well log and seismic data analysis using rock physics templates. *First Break* **22**, 37–43.

Reuss A. 1929. Berechnung der Fließgrenze von Mischkristallen auf Grund der Plastizitätsbedingung für Einkristalle. *ZAMM - Journal of Applied Mathematics and Mechanics / Zeitschrift für Angewandte Mathematik und Mechanik* **9**, 49-58.

Sheng P. 1990. Effective-medium theory of sedimentary rocks. *Physical Review B* **41**, 4507.

Voigt W. 1928. *Lehrbuch der Kristallphysik (mit Ausschluss der Kristalloptik).* B.G. Teubner J.W. Edwards.

Walpole L.J. 1966a. On bounds for the overall elastic moduli of inhomogeneous systems—I. *Journal of the Mechanics and Physics of Solids* **14**, 151-162.

Walpole L.J. 1966b. On bounds for the overall elastic moduli of inhomogeneous systems—II. *Journal of the Mechanics and Physics of Solids* **14**, 289-301.

Walton K. 1987. The effective elastic moduli of a random packing of spheres. *Journal of the Mechanics and Physics of Solids* **35**, 213-226.

Wood A.W. 1955. *A Textbook of Sound. New York: McMillan Co*.

" The major difference between a thing that might go wrong and a thing that cannot possibly go wrong is that when a thing that cannot possibly go wrong goes wrong it usually turns out to be impossible to get at or repair."

Douglas Adams, *'Mostly Harmless'*

English humorist & science fiction novelist (1952 - 2001)

APPENDIX VI: ERRATA

VI

APPENDIX VI: ERRATA

Below is a list of changes made in this final print compared to the thesis which was submitted on July 22, 2011.

- Table of Contents, page vii: The errata have been added to the table of contents.
- Appendix II Paper 2, page 69, Equation 5: Two different weight factors were assigned to $n = 7$. This has been corrected to only be one, namely 0.6.
- Appendix II Paper 2, page 75, line 31: The word "united" has been replaced with "unified" in the title of the reference by Wang and Gelius 2010.
- Appendix III: Paper 3, page 92, line 20: "1 %" has been replaced with "1 unit".
- Appendix III: Paper 3, page 92, line 31: The word "results" has been replaced with "result".
- Appendix III: Paper 3, page 93, Figure 9: Units have been added to the values in the plot headings, and in Figure 9 a) the words "density modulus" has been replaced with "density".
- Appendix III: Paper 3, page 94, Figure 10: The plotted bulk and shear moduli were in fact the P-wave and bulk moduli. This has been corrected.
- Appendix III: Paper 3, page 94: Figure 11: The title of a) should have been the one for b) and vice versa. They have now been correctly interchanged and the caption has been updated accordingly.
- Appendix V: Paper 5, page 149, Table 6: The symbol "ξ_L" has been replaced with "ξ_C".
- Appendix V: Paper 5, page 151, Table 8: The symbol "ξ_L" has been replaced with "ξ_C".

"What we think, or what we know, or what we believe is, in the end,

of little consequence. The only consequence is what we do."

John Ruskin

English critic, essayist, & reformer (1819 – 1900)